LECTURE NOTES ON

AERODYNAMICS

B TECH IV SEMESTER
(IARE - R18)

AERONAUTICAL ENGINEERING

Prepared by

Dr. Maruthupandiyan K

Professor, Department of Aeronautical Engineering

Dr. P K Mohanta

Associate Professor, Department of Aeronautical Engineering

INSTITUTE OF AERONAUTICAL ENGINEERING
(Autonomous)
Dundigal, Hyderabad – 500 043

UNIT-I

INTRODUCTORY TOPICS FOR AERODYNAMICS

Potential flow

In fluid dynamics, potential flow describes the velocity field as the gradient of a scalar function: the velocity potential. As a result, a potential flow is characterized by an irrotational velocity field, which is a valid approximation for several applications. The irrotationality of a potential flow is due to the curl of the gradient of a scalar always being equal to zero.In the case of an incompressible flow the velocity potential satisfies Laplace's equation, and potential theory is applicable. However, potential flows also have been used to describe compressible flows. The potential flow approach occurs in the modeling of both stationary as well as no stationary flows.

Figure 1.1: Elementary flows like Uniform flow and Doublet

Velocity potential

In fluid dynamics, a potential flow is described by means of a velocity potential φ, being a function of space and time. The flow velocity v is a vector field equal to the gradient, ∇, of the velocity potential φ:

$$v = \nabla \varphi \ .$$

Sometimes, also the definition $v = -\nabla\varphi$, with a minus sign, is used. But here we will use the definition above, without the minus sign. From vector calculus it is known, that the curl of a gradient is equal to zero

$$\nabla \times \nabla \varphi = 0$$

and consequently the vorticity, the curl of the velocity field v, is zero

$$\nabla \times v = 0 .$$

This implies that a potential flow is an irrotational flow. This has direct consequences for the applicability of potential flow. In flow regions where vorticity is known to be important, such as wakes and boundary layers, potential flow theory is not able to provide reasonable predictions of the flow. Fortunately, there are often large regions of a flow where the assumption of irrotationality is valid.

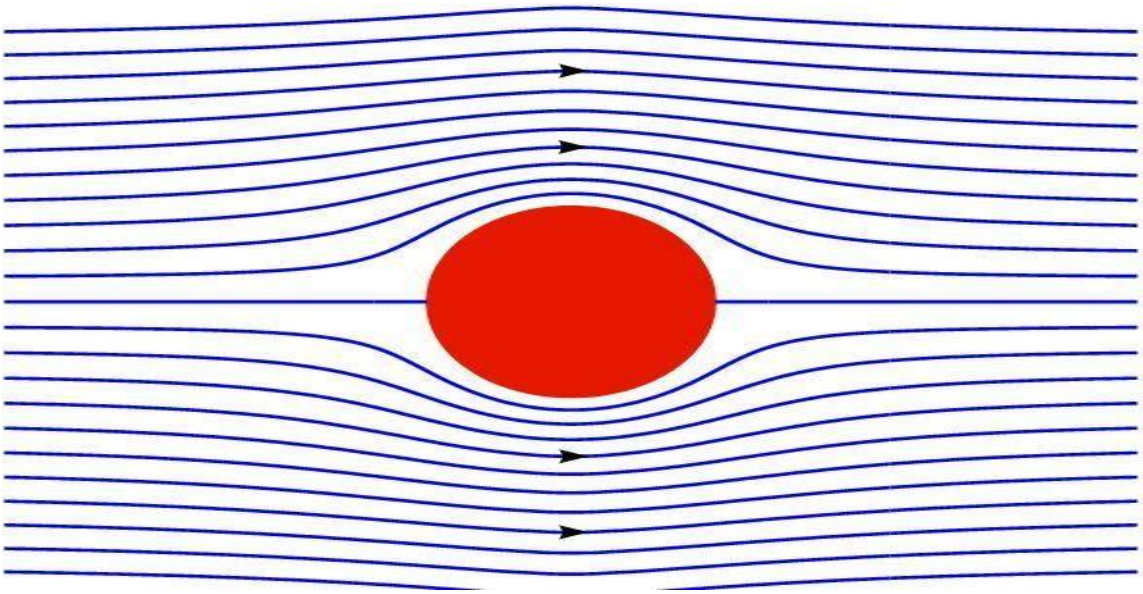

Figure 1.2: Streamlines for inviscid flow over an oval

STREAMLINE

Consider an unsteady flow with a velocity field given by V = V(x, y, z, t).Also, consider an infinitesimal fluid element moving through the flow field, say, element A as shown in Figure.

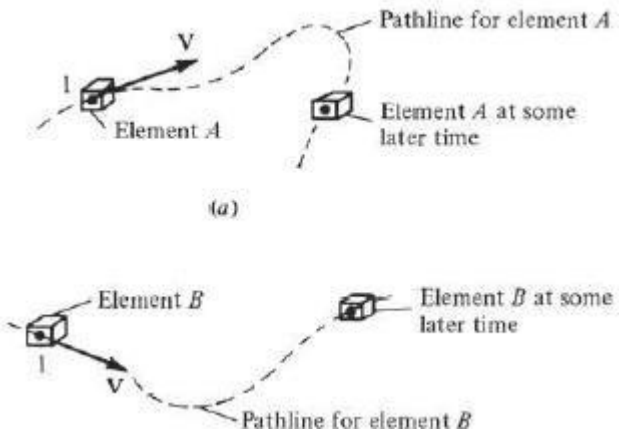

trace the path of element A as it moves downstream from point 1, as given by the dashed line in Figure . Such a path is defined as the pathline for element A. Now, trace the path of another fluid element, say, element B as shown in Figure. Assume that element B also passes through point 1, but at some different time from element A. The pathline of element B is given by the dashed line in Figure 2.27b. Because the flow is unsteady, the velocity at point 1 (and at all other points of the flow) changes with time. Hence, the pathlines of elements A and B are different curves in Figure. In general, for unsteady flow, the pathlines for different fluid elements passing through the same point are not the same.

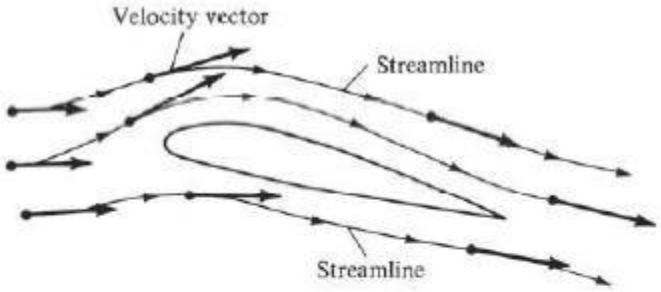

Figure 2.28 Streamlines.

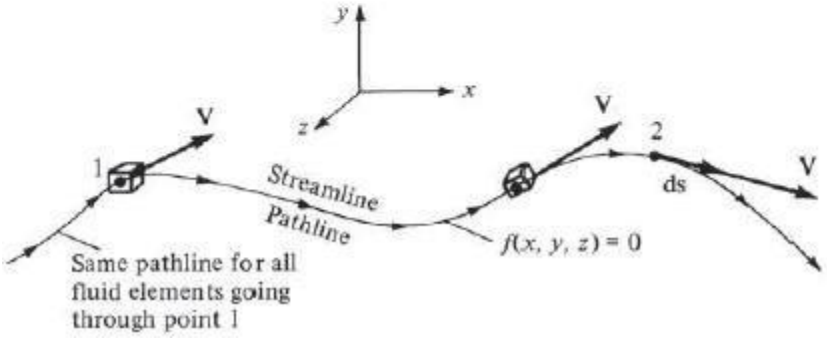

Angular Velocity, Vorticity

Consider an infinitesimal fluid element moving in a flow field. As it translates along a streamline, it may also *rotate,* and in addition its shape may become *distorted*as sketched in Figure. The amount of rotation and distortion depends on the velocity field; the purpose of this section is to quantify this dependency.

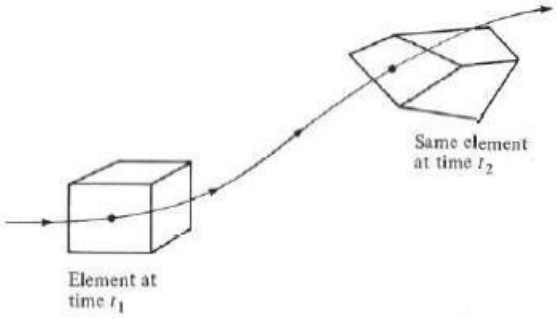

Consider a two-dimensional flowin the *xy* plane. Also, consider an infinitesimal fluid element in this flow. Assume that at time *t* the shape of this fluid element is rectangular, as shown at the left of Figure 2.33. Assume that the fluid element is moving upward and to the right; its position and shape at time *t* + _*t* are shown at the right in Figure 2.33. Note that during the time increment _*t*, the sides *AB* and *AC* have rotated through the angular displacements−_*θ*1 and _*θ*2, respectively. (Counterclockwise rotations by convention are considered positive;

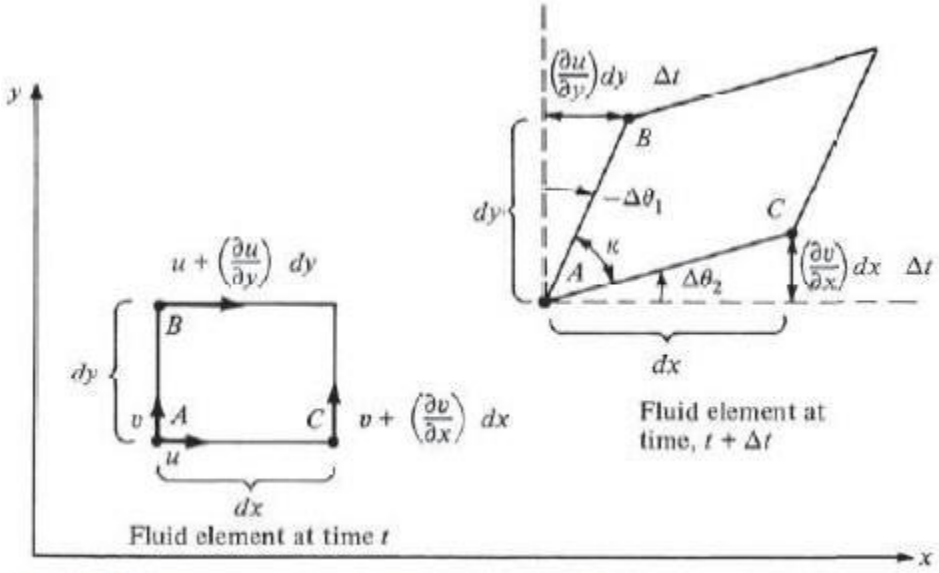

Figure 2.33 Rotation and distortion of a fluid element.

$$\text{Distance in } y \text{ direction that } A \text{ moves during time increment } \Delta t = v\Delta t$$

$$\text{Distance in } y \text{ direction that } C \text{ moves during time increment } \Delta t = \left(v + \frac{\partial v}{\partial x}dx\right)\Delta t$$

$$\text{Net displacement in } y \text{ direction of } C \text{ relative to } A = \left(v + \frac{\partial v}{\partial x}dx\right)\Delta t - v\Delta t$$

$$= \left(\frac{\partial v}{\partial x}dx\right)\Delta t$$

$$\boxed{\omega = \frac{1}{2}\left[\left(\frac{\partial w}{\partial y} - \frac{\partial v}{\partial z}\right)\mathbf{i} + \left(\frac{\partial u}{\partial z} - \frac{\partial w}{\partial x}\right)\mathbf{j} + \left(\frac{\partial v}{\partial x} - \frac{\partial u}{\partial y}\right)\mathbf{k}\right]}$$

$$\boxed{\xi = \left(\frac{\partial w}{\partial y} - \frac{\partial v}{\partial z}\right)\mathbf{i} + \left(\frac{\partial u}{\partial z} - \frac{\partial w}{\partial x}\right)\mathbf{j} + \left(\frac{\partial v}{\partial x} - \frac{\partial u}{\partial y}\right)\mathbf{k}}$$

$$\boxed{\xi = \nabla \times \mathbf{V}}$$

In a velocity field, the curl of the velocity is equal to the vorticity.

The above leads to two important definitions:

1. If $\nabla \times V = 0$ at every point in a flow, the flow is called rotational. This implies that the fluid elements have a finite angular velocity.

2. If $\nabla \times V = 0$ at every point in a flow, the flow is called irrotational. This implies that the fluid elements have no angular velocity; rather, their motion through space is a pure translation.

Stream function

In this section, we consider two-dimensional steady flow. Recall from Section 2.11that the differential equation for a streamline in such a flow is given by Equation(2.118), repeated below

$$\frac{dy}{dx} = \frac{v}{u}$$

The function $\bar{\psi}\ (x, y)$ is called the *stream function*. From Equation (2.140) we see that the equation for a streamline is given by *setting the stream function equalto a constant* (i.e., $c1$, $c2$, $c3$, etc.). Two different streamlines are illustrated in Figure 2.40; streamlines *ab* and *cd* are given by $\bar{\psi} = c1$ and $\bar{\psi} = c2$, respectively. There is a certain arbitrariness in Equations (2.139) and (2.140) via the arbitrary constant of integration *c*. Let us define

the stream function more precisely in order to reduce this arbitrariness. Referring to Figure 2.40, let us define thenumerical value of $\bar{\psi}$ such that the *difference* $\Delta\bar{\psi}$ between $\bar{\psi} = c2$ for streamline *cd* and $\bar{\psi} = c1$ for streamline *ab* is equal to the *mass* flow between the two streamlines. Since Figure 2.40 is a two-dimensional flow, the mass flow between two streamlines is defined *per unit depth perpendicular to the page*. That is, in Figure 2.40 we are considering the mass flow inside a streamtube bounded by streamlines *ab* and *cd*, with a rectangular cross-sectional area equal to Δn times a unit depth perpendicular to the page. Here, Δn is the normal distance between *ab* and *cd*, as shown in Figure 2.40. Hence, mass flow between streamlines *ab*and *cd* per unit depth perpendicular to the page is

$$\Delta\bar{\psi} = c_2 - c_1$$

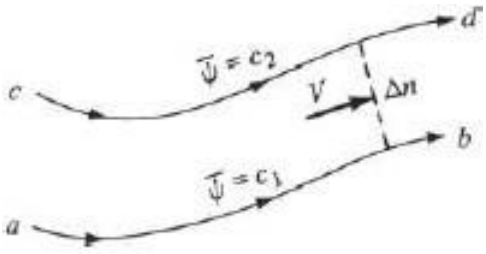

Figure 2.40 Different streamlines

The above definition does not completely remove the arbitrariness of the constant of integration in Equations (2.139) and (2.140), but it does make things a bit more precise. For example, consider a given two-dimensional flow field. Choose one streamline of the flow, and give it an arbitrary value of the stream function, say, $\psi = c1$. Then, the value of the stream function for any other streamline in the flow, say, $\psi = c2$, is fixed by the definition given in Equation (2.141). Which streamline you choose to designate as $\psi = c1$ and what numerical value you give $c1$ usually depend on the geometry of the given flow field,

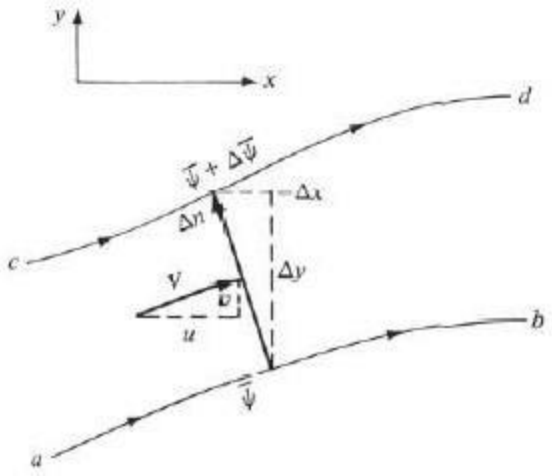

Figure 2.41 Mass flow through Δn is the sum of the mass flows through Δy and $-\Delta x$.

The equivalence between ψ = constant designating a streamline, and _ $\bar{\psi}$equaling mass flow (per unit depth) between streamlines, is natural. For a steadyflow, the mass flow inside a given streamtube is constant along the tube; the massflow across any cross section of the tube is the same. Since by definition _ $\bar{\psi}$
is equal to this mass flow, then _ $\bar{\psi}$ itself is constant for a given streamtube. In Figure 2.40, if $\bar{\psi}$ 1 = c1 designates the streamline on the bottom of the streamtube, then $\bar{\psi}$ 2 = c2 = c1+_ $\bar{\psi}$ is also constant along the top of the streamtube. Since by definition of a streamtube (see Section 2.11) the upper boundary of the streamtube is a streamline itself, then ψ2 = c2 = constant must designate this streamline.

We have yet to develop the most important property of the stream function, namely, derivatives of $\bar{\psi}$ yield the flow-field velocities. To obtain this relationship, consider again the streamlines *ab* and *cd* in Figure 2.40. Assume that these streamlines are close together (i.e., assume_n is small), such that the flowvelocity V is a constant value across _n. The mass flow through the streamtube per unit depth perpendicular to the page is

$$\Delta\bar{\psi} \equiv \rho V \, \Delta n \quad (1)$$

$$\frac{\Delta\bar{\psi}}{\Delta n} = \rho V$$

Circulation

Consider a closed curve *C* in a flow field, as sketched in Figure 2.38. Let **V** and **ds** be the velocity and directed line segment, respectively, at a point on *C*.The circulation, denoted by _, is defined as

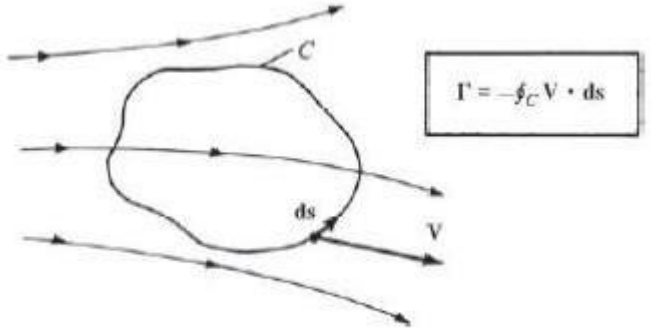

Figure 2.38 Definition of circulation.

The circulation is simply the negative of the line integral of velocity around aclosed curve in the flow; it is a kinematic property depending only on the velocity field and the choice of the curve *C*. As discussed in Section 2.2.8, LineIntegrals, by mathematical convention the positive sense of the line integral is counterclockwise. However, in aerodynamics, it is convenient to consider a positive circulation as being clockwise. Hence, a minus sign appears in the definition given by Equation (2.136) to account for the positive-counterclockwise sense of the integral and the positive-clockwise sense of circulation

$$\Gamma \equiv -\oint_C \mathbf{V} \cdot \mathbf{ds} = -\iint_S (\nabla \times \mathbf{V}) \cdot \mathbf{dS}$$

Laplace's equation

Laplace's equation and Poisson's equation are the simplest examples of elliptic partial differential equations. The general theory of solutions to Laplace's equation is known as potential theory. The solutions of Laplace's equation are the harmonic functions, which are important in many fields of science, notably the fields of electromagnetism, astronomy, and fluid dynamics, because they can be used to accurately describe the behavior of electric, gravitational, and fluid potentials. In the study of heat conduction, the Laplace equation is the steady-stateheat equation. In mathematics, Laplace's equation is a second-order partial differential equation named after Pierre-Simon Laplace who first studied its properties. This is often written as:

$$\nabla^2 \varphi = 0 \text{ or } \Delta \varphi = 0$$

Where $\nabla^2 \varphi = 0$ is the Laplace operator and φ is a scalar function.

Flow singularities-Uniform flow (source, sink, doublet, Vortex)

A uniform flow consists of a velocity field where $V = u\hat{\imath} + v\hat{}$ is a constant. In 2-D, this velocity field is specified either by the freestream velocity components u_∞, v_∞, or by the freestream speed V_∞ and flow angle α.

$$u = u_\infty = V_\infty \cos \alpha$$
$$v = v_\infty = V_\infty \sin \alpha$$

Note also that $V^2 = u^2 + v^2$. The corresponding potential and stream functions are

$$\varphi(x, y) = u_\infty x + v_\infty y = V_\infty (x \cos \alpha + y \sin \alpha)$$
$$\psi(x, y) = u_\infty y - v_\infty x = V_\infty (y \cos \alpha - x \sin \alpha)$$

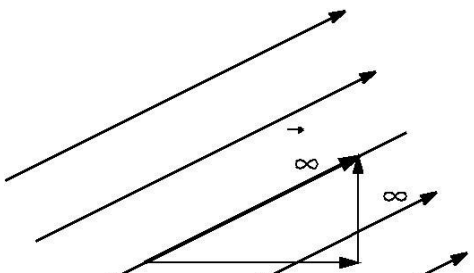

Figure 1.3: Velocity potential and stream function for uniform flow

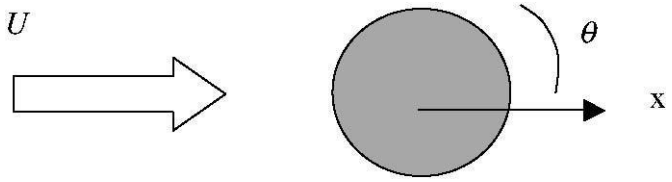

Figure 1.4: Uniform flow over a cylinder

A uniform flow, *U*, impinges on a cylinder of radius *R*. The polar coordinate frame is shown.

The problem posed by the flow configuration in Figure, assuming that the motion is incompressible and irrotational, is to find a solution of Laplace‘s equation that has zero radial flow on the surface of the cylinder and approaches the uniform, oncoming flow as *r* goes to infinity. The uniform flow has a velocity potential,

$\varphi = Ux$ so that, in polar coordinates, the problem is,

$$\frac{1}{r}\frac{\partial}{\partial r}\left(r\frac{\partial \varphi}{\partial r}\right)+\frac{1}{r^2}\frac{\partial^2 \varphi}{\partial \theta^2}=0,$$

$$\frac{\partial \varphi}{\partial r}=0, \qquad r=R,$$

$$\varphi \to Ur\cos\theta, \qquad r\to\infty$$

It is a simple matter to check that a the solution satisfying the equation and all the boundary conditions is,

$$\varphi = U\cos\theta\left(r+\frac{R^2}{r}\right), \qquad r\geq R$$

so that the velocity components are,

$$u_{(r)}=\frac{\partial \varphi}{\partial r}=U\cos\theta\left(1-\frac{R^2}{r^2}\right)$$

$$u_{(\theta)}=\frac{1}{r}\frac{\partial \varphi}{\partial \theta}=-U\sin\theta\left(1+\frac{R^2}{r^2}\right)$$

Recall that the azimuthal velocity is reckoned positive if it is anticlockwise. Note that the tangential velocity is a maximum at $\theta = \pm\pi/2$.

It is left as an exercise for the student to show from the velocity fields that the streamfunction for the flow is given by,

$$\psi = -U\sin\theta\left(r-\frac{R^2}{r}\right)$$

The streamlines of the floware shown in Figure 5.

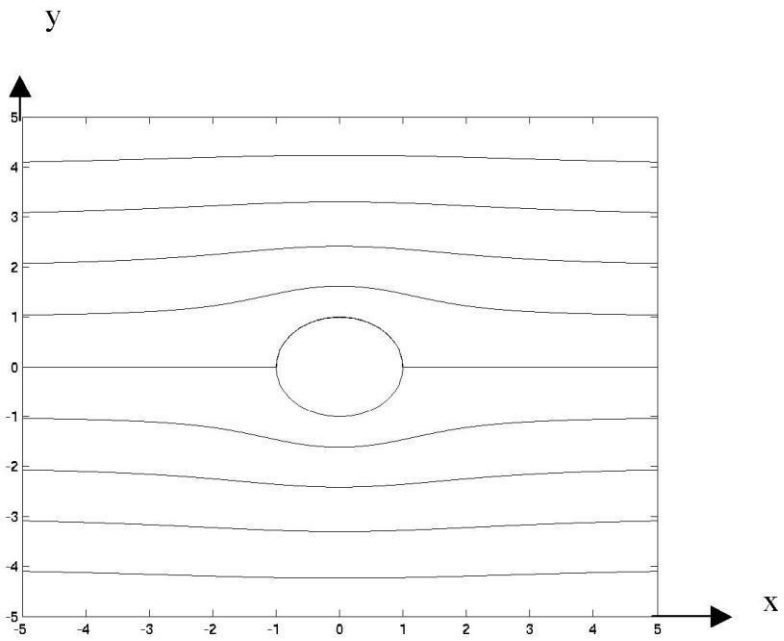

Figure 1.5: Streamlines in potential flow over a cylinder

One notices immediately the artificial character of the flow, in particular the fore-aft complete symmetry. One never sees this is real life situations. When the flow approaches a blunt body like the cylinder the flow typically separates from the body leaving a turbulent wake behind the cylinder as shown in Figure 5, which is a reproduction of a figure from Prandtl and Tietjens, 1934 , Applied Hydro-and Aeromechanics, *Dover* pp.311 (Dover edition1957).

PLATE 1.[1]

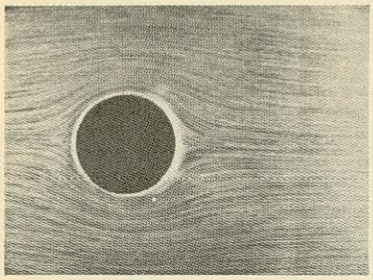

FIG. 1.—Flow round cylinder immediately after starting (potential flow).

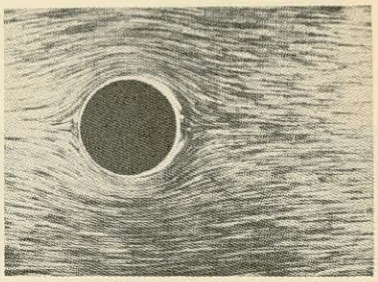

FIG. 2.—Backward flow in the boundary layer behind the cylinder; accumulation of boundary layer material.

PLATE 2.

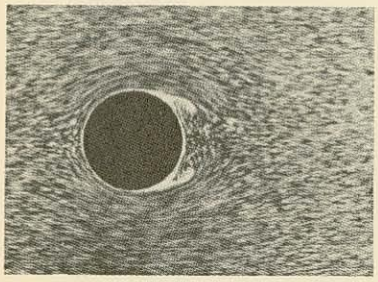

FIG. 3.—Formation of two vortices; flow breaking loose from cylinder.

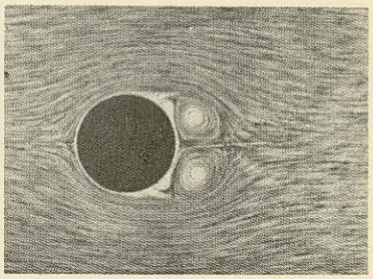

FIG. 4.—The eddies increase in size.

PLATE 3.

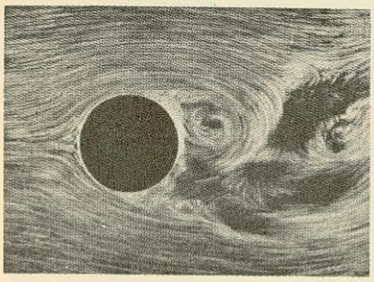

FIG. 5.—The eddies grow still more; finally the picture becomes unsymmetrical and disintegrates.

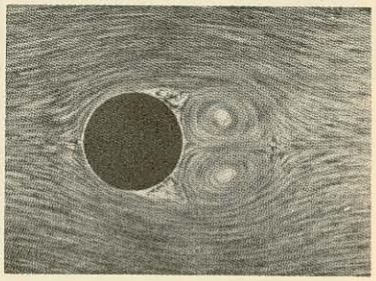

FIG. 6.—Final picture obtained a long time after starting.

[1] The direction of flow in all photographs is from left to right.

279

Figure 1.6: Streamlines in real flow over a cylinder

The reason for the artificiality can be traced to the predicted pressure distribution on

the surface of the cylinder. Using the Bernoulli equation we can obtain the pressure field from the velocity . Let the pressure at infinity be the uniform value p_0 . We can ignore the role of the gravitational potential by imagining the cylinder oriented with its axis vertical so that the motion takes place in a plane of constant *z*. The total Bernoulli function, which is a constant, is then

$$B = p_0 + \frac{\rho U^2}{2}$$

Elsewhere in the field of motion the pressure is obtained from

$$\frac{p}{\rho} + \frac{u_{(r)}^{\ 2}}{2} + \frac{u_{(\theta)}^{\ 2}}{2} = \frac{p_0}{\rho} + \frac{U^2}{2}$$

Consider the motion of the fluid element on the center line approaching the cylinder along y=0. On this line the component

$u_{(\theta)}$ is zero so that the pressure is, from

$$p = p_0 + \frac{\rho U^2}{2} - \frac{\rho U^2}{2}\left[1 - \frac{R^2}{x^2}\right]$$

Doublet Flow

There is a special, degenerate case of a source-sink pair that leads to a singularity called a *doublet*. The doublet is frequently used in the theory of incompressible flow; the purpose of this section is to describe its properties.

Consider a source of strength _ and a sink of equal (but opposite) strength −_ separated by a distance *l*, as shown in Figure 3.24*a*. At any point *P* in the flow, the stream function is

$$\psi = \frac{\Lambda}{2\pi}(\theta_1 - \theta_2) = -\frac{\Lambda}{2\pi}\Delta\theta$$

$$\psi = \lim_{\substack{l \to 0 \\ \kappa = l\Lambda = \text{const}}} \left(-\frac{\Lambda}{2\pi} d\theta \right)$$

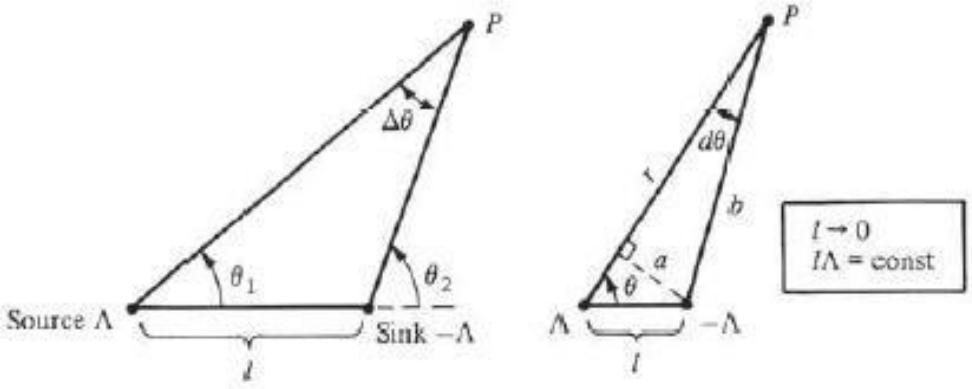

(a) Source-sink pair (b) Limiting case for a doublet

Figure 3.24 How a source-sink pair approaches a doublet in the limiting case.

$$a = l \sin\theta$$

$$b = r - l\cos\theta$$

$$d\theta = \frac{a}{b}$$

Hence,

$$d\theta = \frac{a}{b} = \frac{l\sin\theta}{r - l\cos\theta}$$

Substituting Equation (3.86) into (3.85), we have

$$\psi = \lim_{\substack{l \to 0 \\ \kappa = \text{const}}} \left(-\frac{\Lambda}{2\pi} \frac{l\sin\theta}{r - l\cos\theta} \right)$$

or

$$\psi = \lim_{\substack{l \to 0 \\ \kappa = \text{const}}} \left(-\frac{\kappa}{2\pi} \frac{\sin\theta}{r - l\cos\theta} \right)$$

or

$$\boxed{\psi = -\frac{\kappa}{2\pi} \frac{\sin\theta}{r}}$$

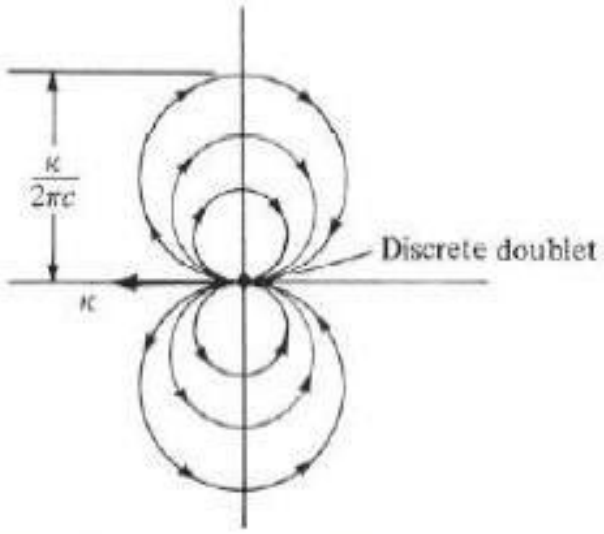

Figure 3.25 Doublet flow with strength κ.

Nonlifting Flow Over A Circular Cylinder

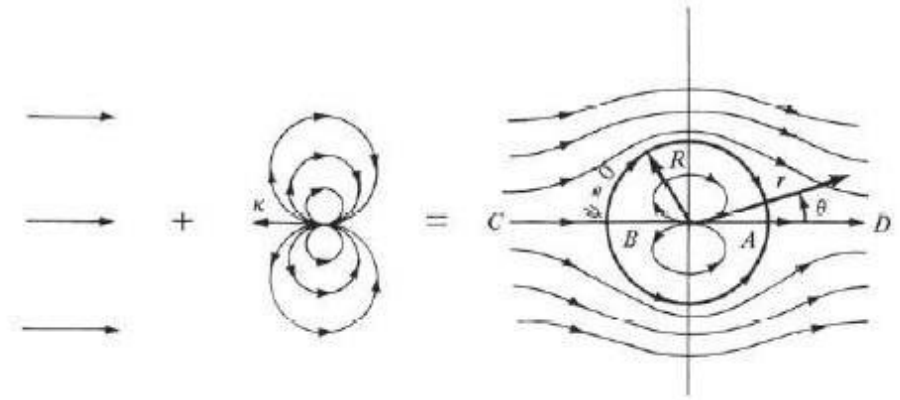

Figure 3.26 Superposition of a uniform flow and a doublet; nonlifting flow over a circular cylinder.

Consider the addition of a uniform flow with velocity V∞ and a doublet of strength κ, as shown in Figure 3.26. The direction of the doublet is upstream, facing into the uniform flow. From Equations (3.57) and (3.87), the stream function for the combined flow is

$$\psi = V_\infty r \sin\theta - \frac{\kappa}{2\pi}\frac{\sin\theta}{r}$$

$$\psi = V_\infty r \sin\theta \left(1 - \frac{\kappa}{2\pi V_\infty r^2}\right)$$

The velocity field is obtained by differentiating

$$V_r = \frac{1}{r}\frac{\partial\psi}{\partial\theta} = \frac{1}{r}(V_\infty r\cos\theta)\left(1 - \frac{R^2}{r^2}\right)$$

$$V_r = \left(1 - \frac{R^2}{r^2}\right) V_\infty \cos\theta$$

$$V_\theta = -\frac{\partial\psi}{\partial r} = -\left[(V_\infty r\sin\theta)\frac{2R^2}{r^3} + \left(1 - \frac{R^2}{r^2}\right)(V_\infty \sin\theta)\right]$$

$$V_\theta = -\left(1 + \frac{R^2}{r^2}\right) V_\infty \sin\theta$$

the pressure distribution is also symmetrical about both axes. As a result, the pressure distribution over the top of the cylinder is exactly balanced by the pressure distribution over the bottom of the cylinder (i.e., there is no net lift). Similarly, the pressuredistribution over the front of the cylinder is exactly balanced by the pressure distribution over the back of the cylinder (i.e., there is no net drag). In real life, the result of zero lift is easy to accept, but the result of zero drag makes no sense.Weknow that any aerodynamic body immersed in a real flow will experience a drag. This paradox between the theoretical result of zero drag, and the knowledge that in real life the drag is finite, was encountered in the year 1744 by the Frenchman Jean Le Rond d‘Alembert—and it has been known as d‘Alembert‘s paradox ever since. For d‘Alembert and other fluid dynamic researchers during the eighteenth and nineteenth centuries, this paradoxwas unexplained and perplexing. Of course, today we know that the drag is due to viscous

effects which generate frictional shear stress at the body surface and which cause the flow to separate from the surface on the back of the body, thus creating a large wake downstream of the body and destroying the symmetry of the flow about the vertical axis through the cylinder.

Non lifting and lifting flow over a cylinder Kutta-Joukowski theorem

The Kutta–Joukowski theorem is a fundamental theorem of aerodynamics used for the calculation of the lift of an airfoil and any two-dimensional bodies including circular cylinders translating in a uniform fluid at a constant speed large enough so that the flow seen in the body-fixed frame is steady and unseparated. The theorem relates the lift generated by an airfoil to the speed of the airfoil through the fluid, the density of the fluid and the circulation around the airfoil. The circulation is defined as the line integral around a closed loop enclosing the airfoil of the component of the velocity of the fluid tangent to the loop.[1] It is named after the GermanMartin Wilhelm Kutta and the RussianNikolai Zhukovsky (or Joukowski) who first developed its key ideas in the early 20th century. Kutta–Joukowski theorem is an inviscid theory, but it is a good approximation for real viscous flow in typical aerodynamic applications.

Kutta–Joukowski theorem relates lift to circulation much like the Magnus effect relates side force (called Magnus force) to rotation.[2] However, the circulation here is not induced by rotation of the airfoil. The fluid flow in the presence of the airfoil can be considered to be the superposition of a translational flow and a rotating flow. This rotating flow is induced by the effects of camber, angle of attack and a sharp trailing edge of the airfoil. It should not be confused with a vortex like a tornado encircling the airfoil. At a large distance from the airfoil, the rotating flow may be regarded as induced by a line vortex (with the rotating line perpendicular to the two-dimensional plane). In the derivation of the Kutta–Joukowski theorem the airfoil is usually mapped onto a circular cylinder. The theorem is proved in many text books for a circular cylinder and the Joukowski airfoil, but it holds true for general airfoils.

The theorem applies to two-dimensional flow around a fixed airfoil (or any shape of infinite span). The lift per unit span L' of the airfoil is given by[3]

$$L' = -\rho_\infty V_\infty \Gamma$$

where ρ_∞ and V_∞ are the fluid density and the fluid velocity far upstream of the airfoil, and Γ is the circulation defined as the line integral

$$\Gamma = \oint_C \mathbf{V} \cdot d\mathbf{s} = \oint_C V \cos\theta \, ds$$

around a closed contour C enclosing the airfoil and followed in the positive (anti-clockwise) direction. As explained below, this path must be in a region of potential flow and not in theboundary layer of the cylinder. The integrand $V \cos\theta$ is the component of the local fluid velocity in the direction tangent to the curve C and $d s$ is an infinitesimal length on the curve, C . Equation (1) is a form of the Kutta–Joukowski theorem.The force per unit length acting on a right cylinder of any cross section whatsoever is equal to $-\rho_\infty V_\infty \Gamma$ and is perpendicular to the direction of V_∞ .

Lifting Flow Over A Cylinder

we superimposed a uniform flow and a doublet to synthesize the flow over a circular cylinder, as shown in Figure 3.26. In addition, we proved that both the lift and drag were zero for such a flow. However, the streamline pattern shown at the right of Figure 3.26 is not the only flow that is theoretically possible around a circular cylinder. It is the only flow that is consistent with zero lift. However, there are other possible flow patterns around a circular cylinder— different flow patterns that result in a nonzero lift on the cylinder. Such lifting flows are discussed in this section.

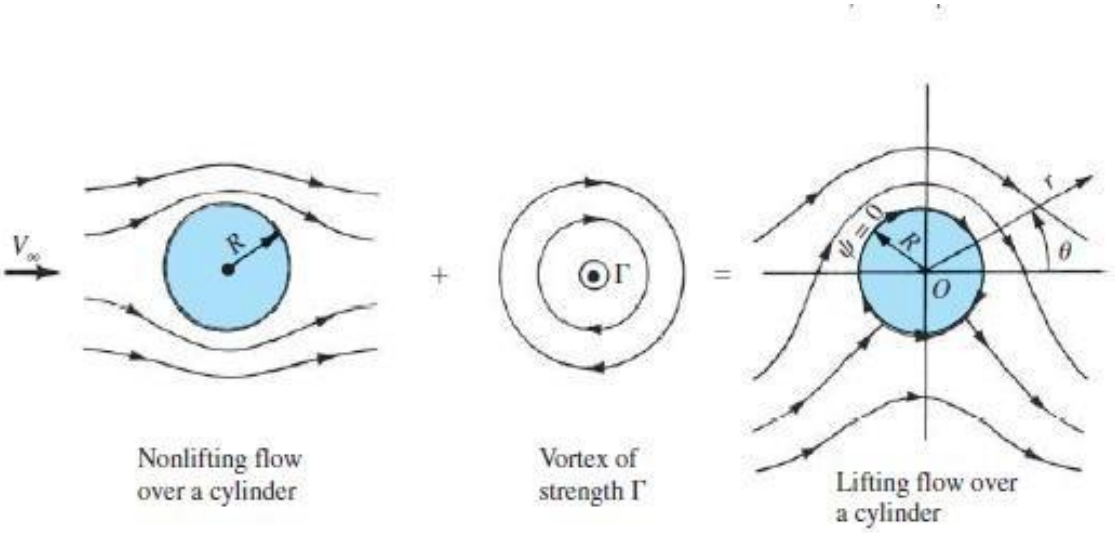

Consider the flow synthesized by the addition of the nonlifting flow over a cylinder and a vortex of strength , as shown in figure . The stream function for nonlifting flowover a circular cylinder of radius R is given by

$$\psi_1 = (V_\infty r \sin\theta)\left(1 - \frac{R^2}{r^2}\right)$$

The stream function for a vortex of strength is given by above equation.Recall that the stream function is determined within an arbitrary constant; hence,

$$\psi_2 = \frac{\Gamma}{2\pi} \ln r + \text{const}$$

$$\text{Const} = -\frac{\Gamma}{2\pi} \ln R$$

The resulting stream function for the flow shown at the right of Figure

$$\psi = (V_\infty r \sin\theta)\left(1 - \frac{R^2}{r^2}\right) + \frac{\Gamma}{2\pi} \ln \frac{r}{R}$$

for the lifting flow over a cylinder of radius R

$$V_r = \left(1 - \frac{R^2}{r^2}\right) V_\infty \cos\theta$$

$$V_\theta = -\left(1 + \frac{R^2}{r^2}\right) V_\infty \sin\theta - \frac{\Gamma}{2\pi r}$$

,

To locate the stagnation points in the flow, set $Vr = V\theta = 0$

$$V_r = \left(1 - \frac{R^2}{r^2}\right) V_\infty \cos\theta = 0$$

$$V_\theta = -\left(1 + \frac{R^2}{r^2}\right) V_\infty \sin\theta - \frac{\Gamma}{2\pi r} = 0$$

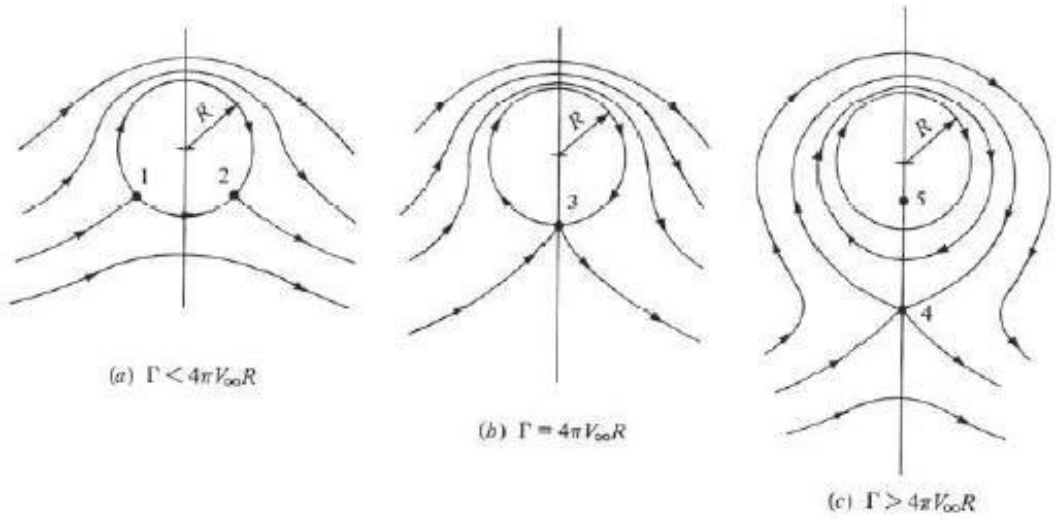

(a) $\Gamma < 4\pi V_\infty R$

(b) $\Gamma = 4\pi V_\infty R$

(c) $\Gamma > 4\pi V_\infty R$

$$\theta = \arcsin\left(-\frac{\Gamma}{4\pi V_\infty R}\right)$$

$$r = \frac{\Gamma}{4\pi V_\infty} \pm \sqrt{\left(\frac{\Gamma}{4\pi V_\infty}\right)^2 - R^2}$$

$$V = V_\theta = -2V_\infty \sin\theta - \frac{\Gamma}{2\pi R}$$

$$C_p = 1 - \left(\frac{V}{V_\infty}\right)^2 = 1 - \left(-2\sin\theta - \frac{\Gamma}{2\pi R V_\infty}\right)^2$$

$$C_p = 1 - \left[4\sin^2\theta + \frac{2\Gamma\sin\theta}{\pi R V_\infty} + \left(\frac{\Gamma}{2\pi R V_\infty}\right)^2\right]$$

$$c_d = c_a = \frac{1}{c}\int_{\text{LE}}^{\text{TE}} (C_{p,u} - C_{p,l})\, dy$$

$$c_d = \frac{1}{c}\int_{\text{LE}}^{\text{TE}} C_{p,u}\, dy - \frac{1}{c}\int_{\text{LE}}^{\text{TE}} C_{p,l}\, dy$$

$$c_d = -\frac{1}{2}\int_0^{\pi} C_p \cos\theta\, d\theta - \frac{1}{2}\int_{\pi}^{2\pi} C_p \cos\theta\, d\theta$$

$$c_d = -\frac{1}{2}\int_0^{2\pi} C_p \cos\theta\, d\theta$$

$$\int_0^{2\pi} \cos\theta\, d\theta = 0$$

$$\int_0^{2\pi} \sin^2\theta \cos\theta\, d\theta = 0$$

$$\int_0^{2\pi} \sin\theta \cos\theta\, d\theta = 0$$

$$c_l = -\frac{1}{2}\int_{\pi}^{2\pi} C_{p,l} \sin\theta\, d\theta + \frac{1}{2}\int_{\pi}^{0} C_{p,u} \sin\theta\, d\theta$$

$$\int_0^{2\pi} \sin\theta\, d\theta = 0$$

$$\int_0^{2\pi} \sin^3\theta\, d\theta = 0$$

$$\int_0^{2\pi} \sin^2\theta\, d\theta = \pi$$

$$c_l = \frac{\Gamma}{RV_\infty}$$

$$L' = \frac{1}{2}\rho_\infty V_\infty^2 2R\frac{\Gamma}{RV_\infty}$$

$$\boxed{L' = \rho_\infty V_\infty \Gamma}$$

The above equation gives the lift per unit span for a circular cylinder with circulation . It is a remarkably simple result, and it states that *the lift per unit span is directlyproportional to circulation*. Equation (3.140) is a powerful relation in theoretical aerodynamics. It is called the *Kutta-Joukowski theorem.*

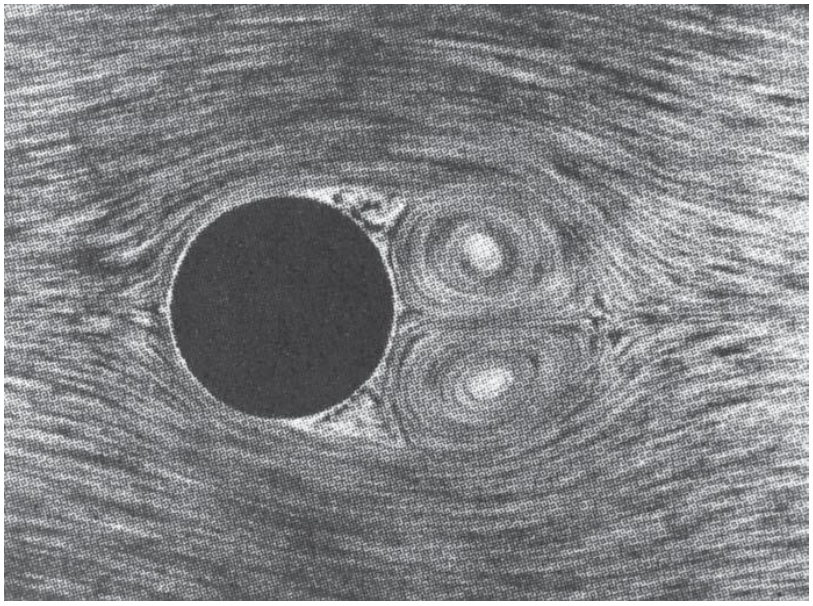

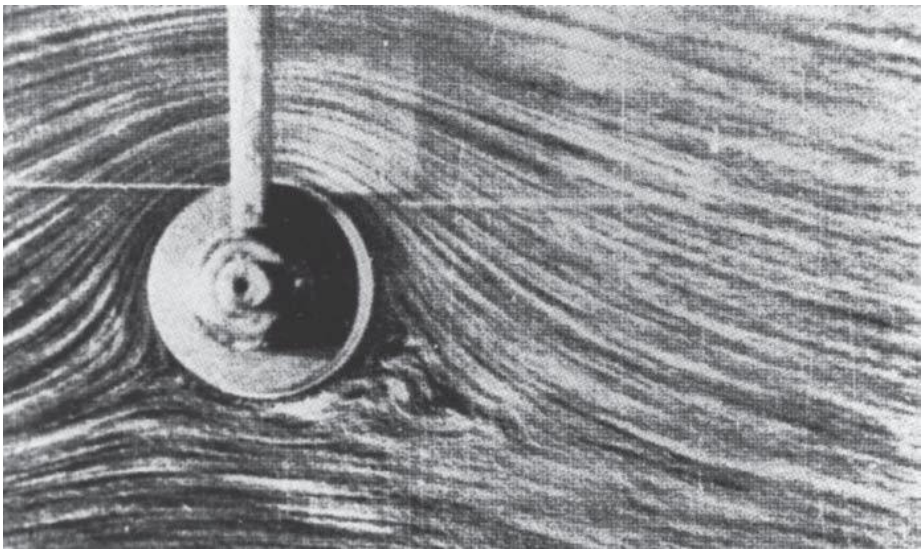

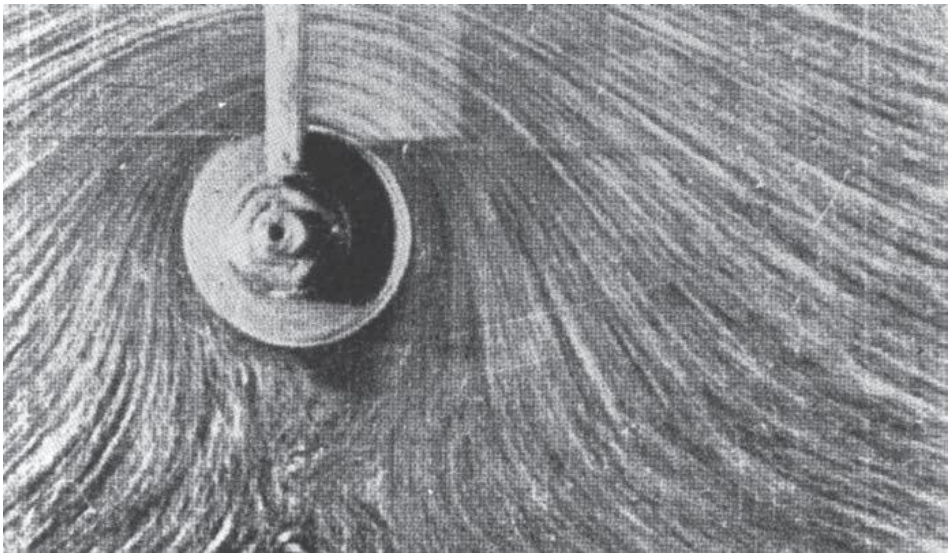

UNIT-II

THIN AEROFOIL THEORY

Airfoil nomenclature

Airfoil‖ means –shape of a section of a wing.‖ It is a two-dimensional concept.

Airfoils cannot fly: wings fly.

Airfoil properties are used to calculate and design wing properties.

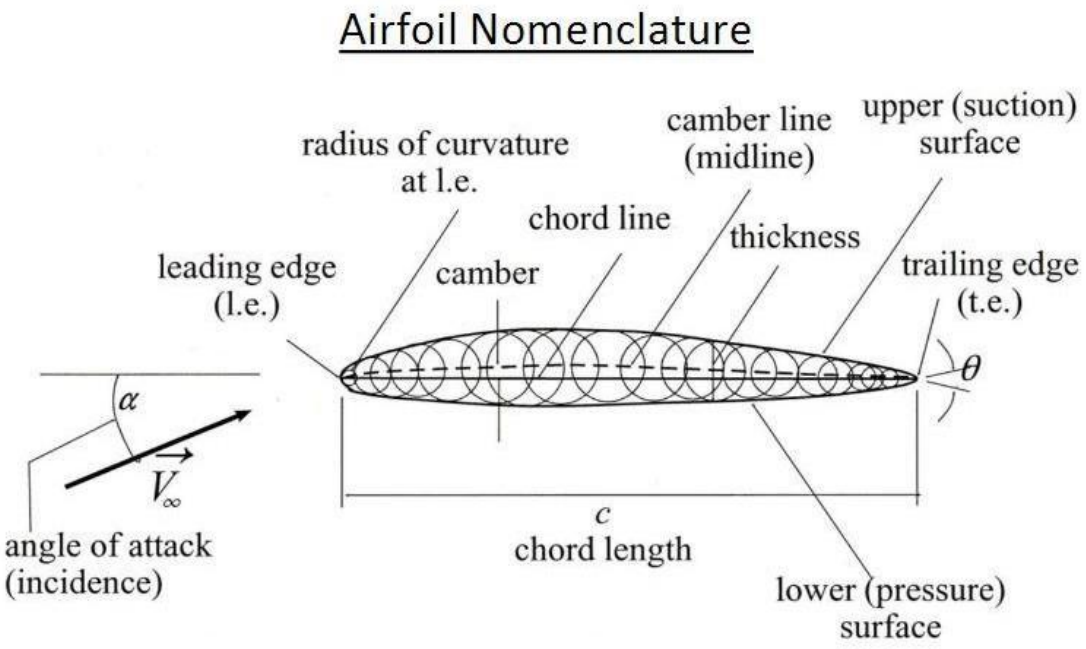

Figure 2.1: Airfoil nomenclature

An airfoil or aerofoil is the shape of a wing, blade (of a propeller, rotor, or turbine), or sail (as seen in cross-section).An airfoil-shaped body moved through a fluid produces an aerodynamic force. The component of this force perpendicular to the direction of motion

is called lift. The component parallel to the direction of motion is called drag. Subsonic flight airfoils have a characteristic shape with a rounded leading edge, followed by a sharp trailing edge, often with a symmetric curvature of upper and lower surfaces. Foils of similar function designed with water as the working fluid are called hydrofoils.

The lift on an airfoil is primarily the result of its angle of attack and shape. When oriented at a suitable angle, the airfoil deflects the oncoming air (for fixed-wing aircraft, a downward force), resulting in a force on the airfoil in the direction opposite to the deflection. This force is known as aerodynamic force and can be resolved into two components: lift and drag. Most foil shapes require a positive angle of attack to generate lift, but cambered airfoils can generate lift at zero angle of attack. This "turning" of the air in the vicinity of the airfoil creates curved streamlines, resulting in lower pressure on one side and higher pressure on the other. This pressure difference is accompanied by a velocity difference, via Bernoulli's principle, so the resulting flow field about the airfoil has a higher average velocity on the upper surface than on the lower surface. The lift force can be related directly to the average top/bottom velocity.

The various terms related to airfoils are defined as

- The upper surface is generally associated with higher velocity and lower static pressure.
- The pressure surface lower surface has a comparatively higher static pressure than the suction surface. The pressure gradient between these two surfaces contributes to the lift force generated for a given airfoil.

The geometry of the airfoil is described with a variety of terms:

- The leading edge is the point at the front of the airfoil that has maximum curvature (minimum radius)

- The trailing edge is defined similarly as the point of minimum curvature at the rear of the airfoil.
- The chord line is the straight line connecting leading and trailing edges.

The shape of the airfoil is defined using the following geometrical parameters:

- The mean camber line or mean line is the locus of points midway between the upper and lower surfaces. Its shape depends on the thickness distribution along the chord;
- The thickness of an airfoil varies along the chord. It may be measured in either of two ways:
- Thickness measured perpendicular to the camber line.
- Thickness measured perpendicular to the chord line. This is sometimes described as the "British convention".

Finally, important concepts used to describe the airfoil's behaviour when moving through a fluid are:

- The aerodynamic center, which is the chord-wise length about which the pitching moment is independent of the lift coefficient and the angle of attack.
- The center of pressure, which is the chord-wise location about which the pitching moment is zero.

The NACA identified different airfoil shapes with a logical numbering system.For example, the first family of NACA airfoils, developed in the 1930s, was the ‒four-digit‖ series, such as the NACA 2412 airfoil. Here, the first digit is the maximum camber in hundredths of chord, the second digit is the location of maximum camber along the chord from the leading edge in tenths of chord, and thelast two digits give the maximum thickness in hundredths of chord. For theNACA2412 airfoil, the maximum camber is 0.02c located at 0.4c from the leading edge,and the maximum thickness is 0.12c. It is common practice to state these numbers in percent of chord, that is, 2 percent camber at

40 percent chord, with 12 percent thickness. An airfoil with no camber, that is, with the camber line and chord line coincident, is called a symmetric airfoil. Clearly, the shape of a symmetric airfoil is the same above and below the chord line. For exaThe second family of NACA airfoils was the ―five-digit‖ series, such as the

NACA 23012 airfoil. Here, the first digit when multiplied by 3 2 gives the design lift coefficient1 in tenths, the next two digits when divided by 2 give the location of maximum camber along the chord from the leading edge in hundredths of chord, and the final two digits give the maximum thickness in hundredths of chord. For the NACA23012 airfoil, the design lift coefficient is 0.3, the location of maximum camber is at 0.15*c*, and the airfoil has 12 percent maximum thickness. mple, the NACA 0012 airfoil is a symmetric airfoil with a maximum thickness of 12 percent.

One of the most widely used family ofNACAairfoils is the ―6-series‖ laminar flow airfoils, developed during World War II. An example is the NACA 65-218. Here, the first digit simply identifies the series, the second gives the location of minimum pressure in tenths of chord from the leading edge (for the basic symmetric thickness distribution at zero lift), the third digit is the design lift coefficient in tenths, and the last two digits give the maximum thickness in hundredths of chord. For the NACA 65-218 airfoil, the 6 is the series designation, the minimum pressure occurs at 0.5c for the basic symmetric thickness distribution at zero lift, the design lift coefficient is 0.2, and the airfoil is 18 percent thick.

AIRFOIL CHARACTERISTICS

The typical variation of lift coefficient with angle of attack for an airfoil is sketched in Figure. At low-to-moderate angles of attack, cl varies linearly with α; the slope of this straight line is denoted by a0 and is called the lift slope. In this region, the flow moves smoothly over the airfoil and is attached over most of the surface, as shown in the streamline picture at the left of Figure However, as α becomes large, the flow tends to separate from the top surface of the airfoil, creating a large wake of relatively ―dead air‖

behind the airfoil as shown at the right of Figure .Inside this separated region, the flow is recirculating, and part of the flow is actually moving in a direction opposite to the freestream—so-called reversed flow. The consequence of this separated flow at high α is a precipitous decrease in lift and a large increase in drag; under such conditions the airfoil is said to be stalled. The maximumvalue of cl , which occurs just prior to the stall, is denoted by cl,max; it is one of the most important aspects of airfoil performance, because it determines the stalling speed of an airplane. The higher is cl,max, the lower is the stalling speed. A great deal of modern airfoil research has been directed toward increasing cl,max. Again examining Figure, we see that cl increases linearly with α until flow separation begins to have an effect. Then the curve becomes nonlinear, cl reaches a maximum value, and finally the airfoil stalls. At the other extreme of the curve, noting Figure, the lift at α = 0 is finite; indeed, the lift goes to zero only when the airfoil is pitched to some negative angle of attack. The value of α when lift equals zero is called the zero-lift angle of attack and is denoted by αL=0. For a symmetric airfoil, αL=0 = 0, whereas for all airfoils with positive camber (camber above the chord line), αL=0 is a negative value, usually on the order of−2 or −3◦.

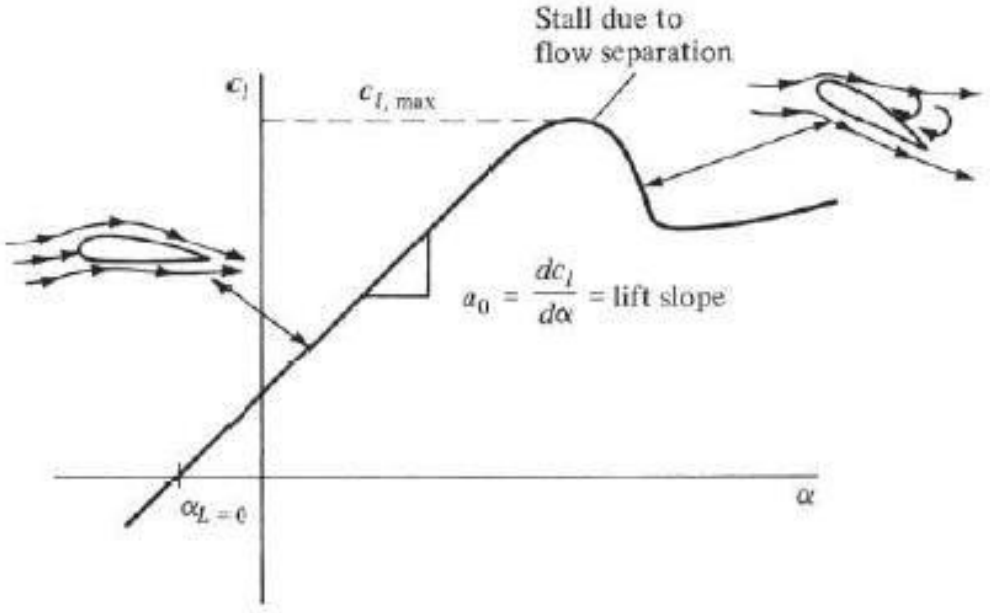

Wing of infinite aspect ratio

All real wings are finite in span (airfoils are considered as infinite in the span). The lift coefficient differs from that of an airfoil because there are strong vortices produced at the wing tips of the finite wing, which trail downstream. These vortices are analogous to mini-tornadoes, and like a tornado, they reach out in the flow field and induce changes in the velocity and pressure fields around the wing. Imagine that you are standing on top of the wing you will feel a downward component of velocity over the span of the wing, induced by the vortices trailing downstream from both tips. This downward component of velocity is called downwash.

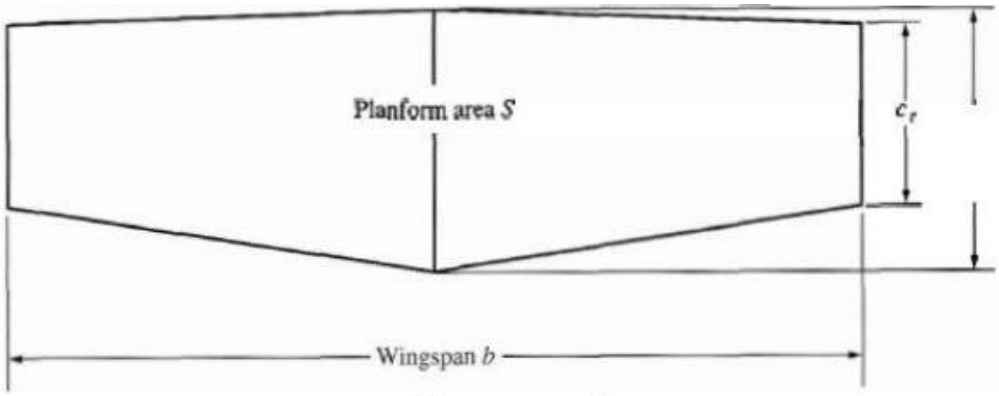

Aspect ratio AR $\equiv \frac{b^2}{S}$; Taper ratio $\equiv \frac{c_t}{c_r}$

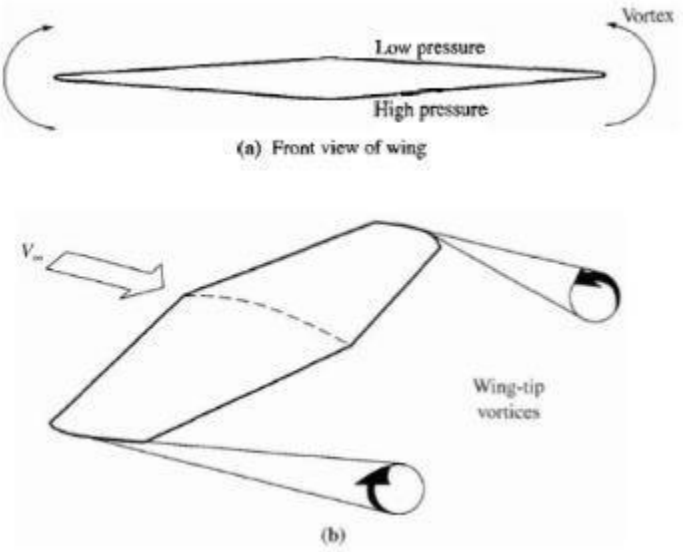

Figure 2.2: Vortex formation around wings

The local downwash at your location combines with the free-stream relative wind to produce a local relative wind. This local relative wind is inclined below the free- stream direction through the induced angle of attack. Hence, you are effectively feeling an angle of attack different from the actual geometric angle of attack of the wing relative to the free stream; you are sensing a smaller angle of attack. For Example if the wing is at a geometric angle of attack of 5°, you are feeling an effective angle of attack which is smaller. Hence, the lift coefficient for the wing is going to be smaller than the lift coefficient for the airfoil. The lift slope for a finite wing decreases as the aspect ratio decreases. At any given angle of attack larger than the value of CL becomes smaller as the aspect ratio is decreased. When applied to straight wings at AR < 4, the equations for high AR do not apply because are derived from a theoretical model which represents the finite wing with a single lifting line across the span of the wing.

$$a = \frac{a_0}{1 + a_0/(\pi e_1 \mathrm{AR})}$$

$a_0 = \frac{dc_l}{d\alpha}$ airfoil

$a = \frac{dC_L}{d\alpha}$ wing

lift slope per *radian* and **e1** is a factor that depends on the geometric shape of the wing, including the aspect ratio and taper ratio.

$$AR = \frac{b^2}{S}$$

Prandtl's lifting line theory does not apply to low-aspect-ratio wings. It holds for aspect ratios of about 4 or larger.

CL-α- diagram for a wing of infinite aspect ratio

The fact that a wing is of finite length has considerable effect on its aerodynamic properties. The primary effect is due to the span-wise lift distribution (it is no longer constant), caused by the flow about the wing tips. In normal operating conditions, the wing will have high pressure on it lower surface and a low pressure on its upper surface. This pressure difference is what generates the lift. However, this same pressure difference causes flow from the underside of the wing to the upper side of the wing around the wing tips.

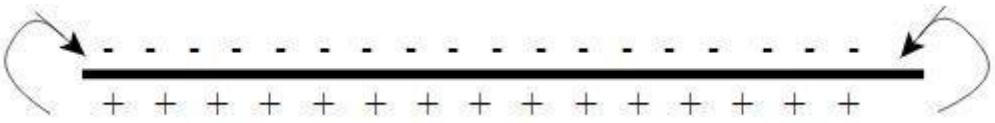

Figure 2.3: Vortex distribution on a wing

This type of flow swirls off the tips of the wing in the form of vortices. In fact there is a vortex distribution across the entire span of the wing with the strongest vortices at the wing tips. These
vortices trail downstream behind the wing and rotate in the direction shown in the figure. Vortices on the right hand side of the wing (looking from the rear) rotate counter clockwise, and
those on the left hand side of the wing rotate clockwise. The general result is that the vortices induce a downward flow at the wing interior. This downward flow is called downwash, and it influences the flow in front of, at, and behind the wing. This downward flow causes a change in
the local wing angle-of-attack such that the wing sees a different angle-of-attack then the one that it sees with respect to the free stream

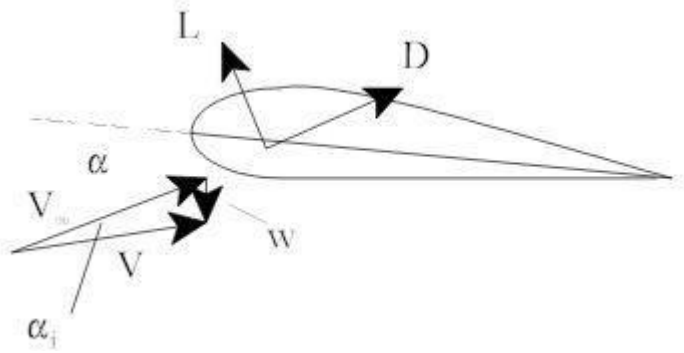

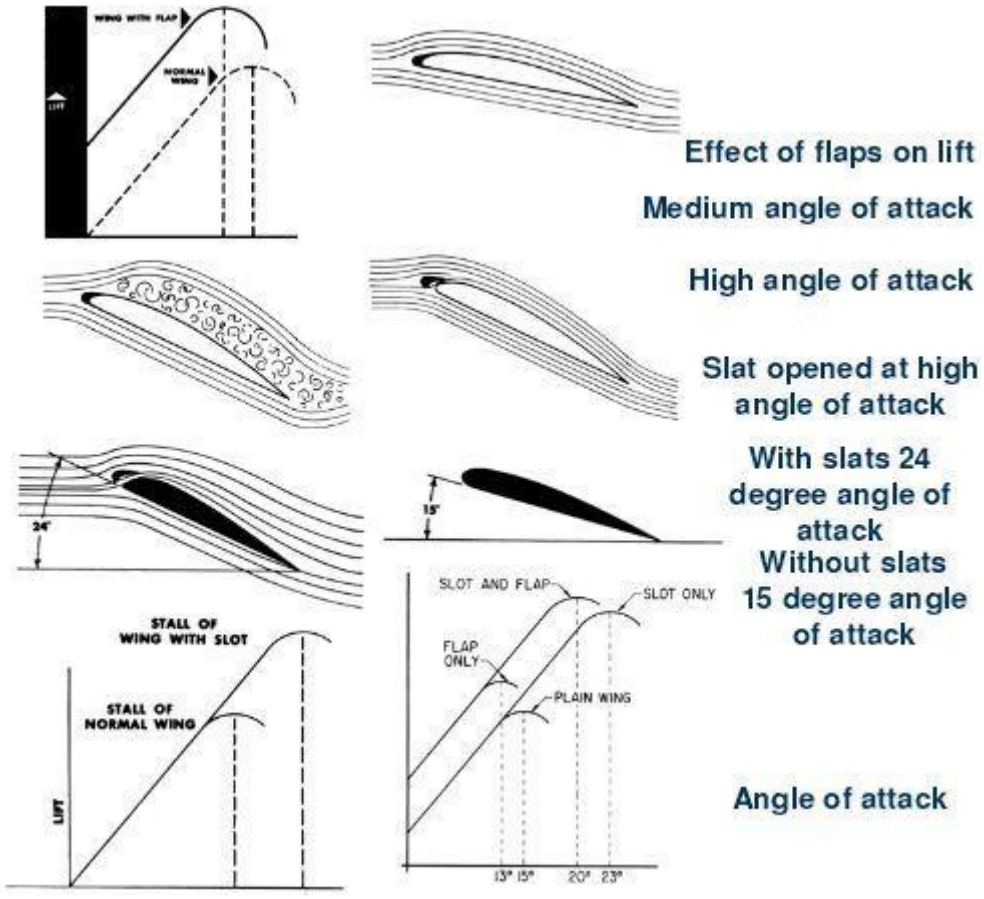

Figure 2.4: Effect of high-lift devices on flow over airfoil

Kutta's trailing edge condition

The Kutta condition is a principle in steady-flow fluid dynamics, especially aerodynamics, that is applicable to solid bodies with sharp corners, such as the trailing edges of airfoils. A body with a sharp trailing edge which is moving through a fluid will create about itself a circulation of sufficient strength to hold the rear stagnation point at the trailing edge. In fluid flow around a body with a sharp corner, the Kutta condition refers to the flow pattern in which fluid approaches the corner from both directions, meets at the corner, and then flows away from the body. None of the fluid flows around the corner, remaining attached to the body. When a smooth symmetric body, such as a cylinder with oval cross-section, moves with zero angle of attack through a fluid it generates no lift. There are two stagnation points on the body - one at the front and the

other at the back. If the oval cylinder moves with a non-zero angle of attack through the fluid there are still two stagnation points on the body - one on the underside of the cylinder, near the front edge; and the other on the topside of the cylinder, near the back edge. The circulation around this smooth cylinder is zero and no lift is generated, despite the positive angle of attack.

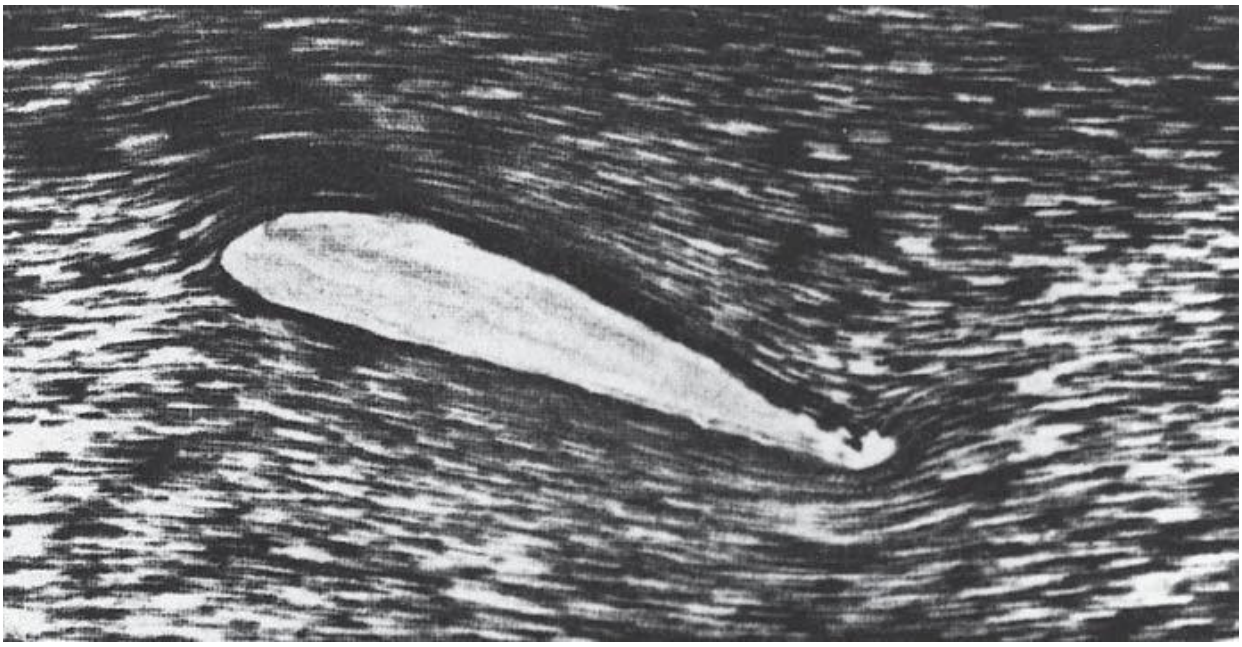

The Kutta condition allows an aerodynamicist to incorporate a significant effect of viscosity while neglecting viscous effects in the underlying conservation of momentum equation. It is important in the practical calculation of lift on a wing. The equations of conservation of mass and conservation of momentum applied to an inviscid fluid flow, such as a potential flow, around a solid body result in an infinite number of valid solutions. One way to choose the correct solution would be to apply the viscous equations, in the form of the Navier–Stokes equations. However, these normally do not result in a closed-form solution. The Kutta condition is an alternative method of incorporating some aspects of viscous effects, while neglecting others, such as skin friction and some other boundary layer effects. The condition can be expressed in a number of ways. One is that there cannot be an infinite change in velocity at the trailing edge. Although an inviscid fluid can have abrupt changes in velocity, in reality

viscositysmooths out sharp velocity changes. If the trailing edge has a non-zero angle, the flow velocity there must be zero. At a cusped trailing edge, however, the velocity can be non-zero although it must still be identical above and below the airfoil. Another formulation is that the pressure must be continuous at the trailing edge. The Kutta condition does not apply to unsteady flow. Experimental observations show that the stagnation point (one of two points on the surface of an airfoil where the flow speed is zero) begins on the top surface of an airfoil (assuming positive effective angle of attack) as flow accelerates from zero, and moves backwards as the flow

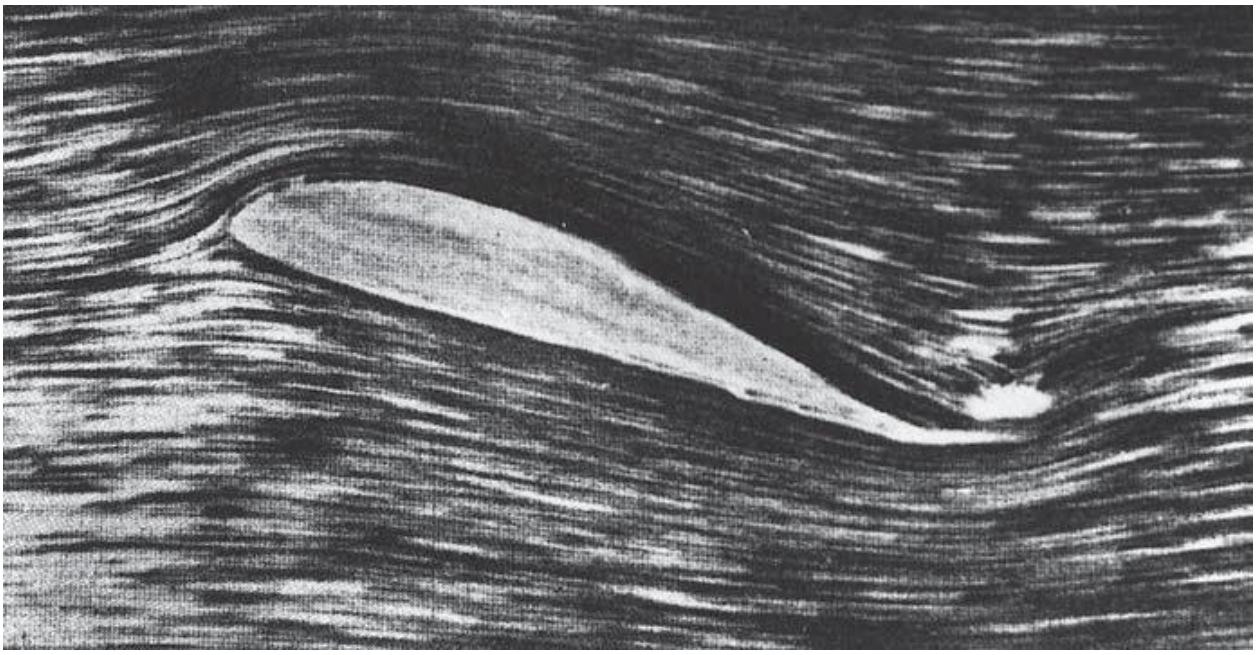

accelerates. Once the initial transient effects have died out, the stagnation point is at the trailing edge as required by the Kutta condition.

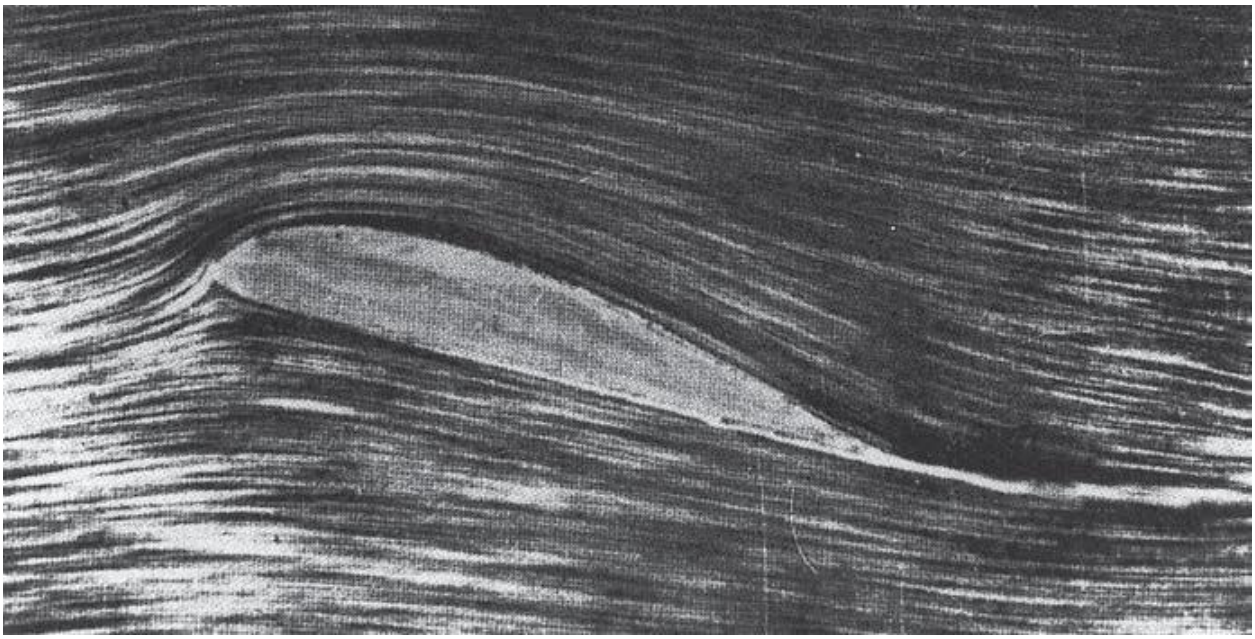

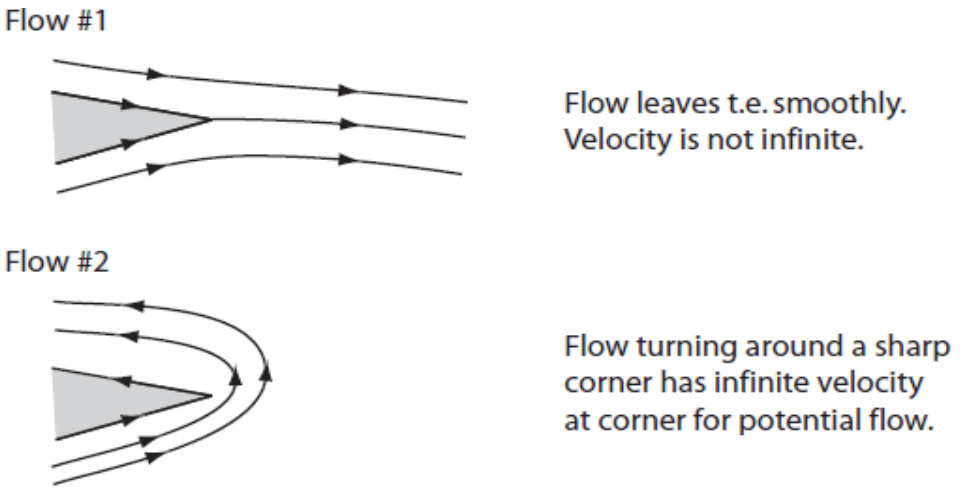

Figure 2.5: Kutta condition for circulation at the T.E. of the airfoil

Generation of lift

A fluid flowing past the surface of a body exerts a force on it. Lift is the component of this force that is perpendicular to the oncoming flow direction. It contrasts with the drag force, which is the component of the surface force parallel to the flow direction. If the fluid is air, the force is called an aerodynamic force.

Lift is also exploited in the animal world, and even in the plant world by the seeds of certain trees. While the common meaning of the word "lift" assumes that lift opposes weight, lift in the technical sense used in this article can be in any direction with respect to gravity, since it is defined with respect to the direction of flow rather than to the direction of gravity. When an aircraft is flying straight and level (cruise) most of the lift opposes gravity. However, when an aircraft is climbing, descending, or banking in a turn the lift is tilted with respect to the vertical. Lift may also be entirely downwards in some aerobatic manoeuvres, or on the wing on a racing car. In this last case, the term downforce is often used. Lift may also be largely horizontal, for instance on a sail on a sailboat. Aerodynamic/hydrodynamic lift is distinguished from other kinds of lift in fluids. It requires relative motion of the fluid which distinguishes it from aerostatic lift or buoyancy lift as used by balloons, blimps, dirigibles, boats and submarines. It also usually refers to situations in which the body is completely immersed in the fluid, and is thus distinguished from planing lift as used by motorboats, surfboards, and water-skis, in which only a lower portion of the body is immersed in the lifting fluid flow.

Kelvin's Circulation Theorem And The Starting Vortex

Consider an arbitrary inviscid, incompressible flowas sketched in figure. Assume that all body forces f are zero. Choose an arbitrary curve C1 and identify the fluid elements that are on this curve at a given instant in time t1. Also, by definition the circulation around curve C1 is 1 = −C1 V· ds. Now let these specific fluid elements move downstream. At some later time, t2, these same fluid elements will form another curve C2, around which the circulation is 2 =

————————————C2V· ds. For the conditions stated above, we can readily show that 1 = 2.In fact, since we are following a set of specific fluid elements, we can state that circulation around a closed curve formed by a set of contiguous fluid elements remains constant as the fluid elements move throughout the flow. Hence, a mathematical statement of the above discussion is simply

$$\boxed{\frac{D\Gamma}{Dt} = 0}$$

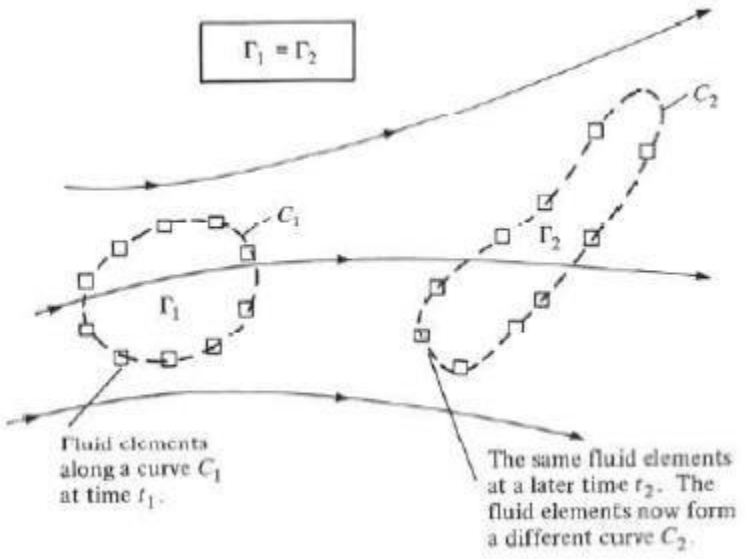

The starting vortex is a vortex which forms in the air adjacent to the trailing edge of an airfoil as it is accelerated from rest in a fluid. It leaves the airfoil (which now has an equal but opposite "bound vortex" around it), and remains (nearly) stationary in the flow. It rapidly decays through the action of viscosity. Whenever the speed or angle of attack of an airfoil changes there is a corresponding amount of vorticity deposited in the wake behind the airfoil, joining the two trailing vortices. This vorticity is a continuum of mini-starting-vortexes. The wake behind an aircraft is a continuous sheet of weak vorticity, between the two trailing vortices, and this accounts for the changes in strength of the trailing vortices as the airspeed of the aircraft and angle of attack on the wing change during flight. (The strength of a vortex cannot change within the fluid except by the dissipative action of viscosity. Vortices either form continuous loops of constant strength, or they terminate at the boundary of the fluid - usually a solid surface such as the ground.)The starting vortex is significant to an understanding of the Kutta condition and its role in the circulation around any airfoil generating lift.

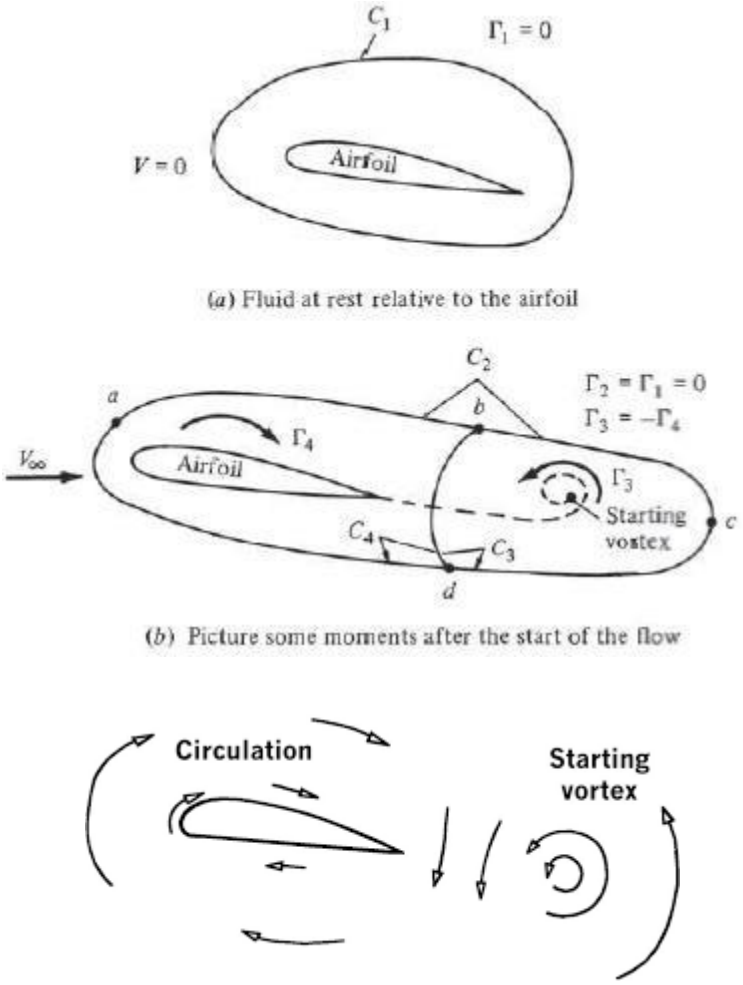

Figure 2.6: Starting vortex

Thin aerofoil theory

simple solution for general two-dimensional aerofoil sections can be obtained by neglecting thickness effects and using a mean-line only section model. For incompressible, inviscid flow, an aerofoil section can be modelled by a distribution of vortices along the mean line. This is a standard potential flow modelling technique which will give quick and reasonable estimates of lift coefficient and moment coefficient. However, as it models inviscid flow, there will be no estimate of drag coefficient.

The vortex distribution along the mean line forms a continuous vorticity sheet. So rather than considering the strength of point vortices, we consider the strength of the distribution per unit length, γ(s). The distribution function is assumed to take the following form.

gamma (theta) = 2 V_infty left (A_0 tan(frac{theta}{2}) + bigsum_{n=1}^infty A_n sin(n theta) right)

This function is Glauert's approximation and is based on Joukowski transformation results (A0 term) which mainly covers the effect of angle of attack, plus a Fourier series variation (A1 terms) to account for camber. It automatically obeys the Kutta condition with zero vorticity at the trailing edge. It is based on a mapped angular position (θ) rather than an exact surface location (s) to allow for ease of integration. The mapping between s and θ is shown below,

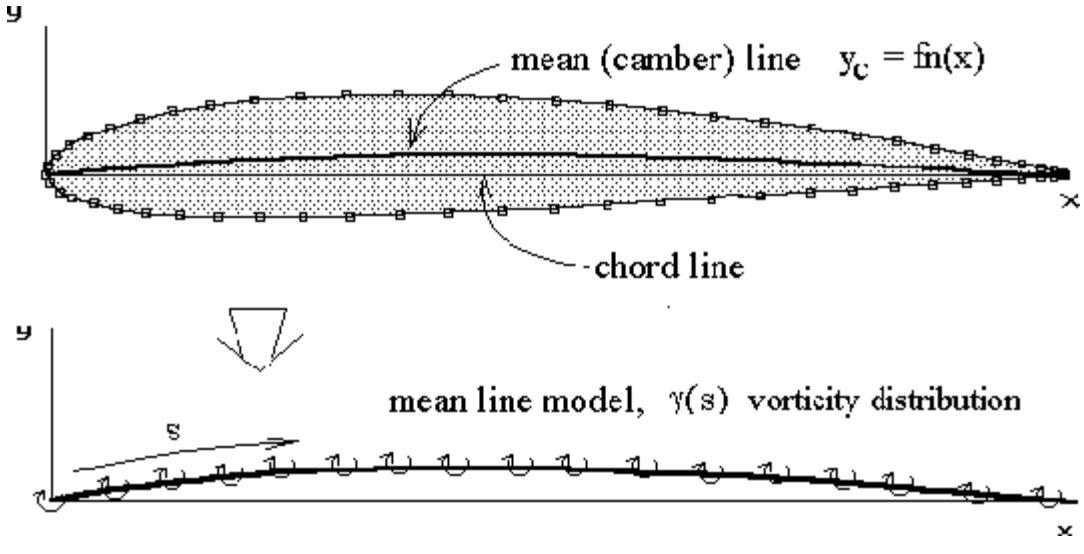

The vorticity distribution is thus given as a function of the angular variable (θ) which is related to chordwise position (x) as follows,

x = frac{c}{2} + frac{c}{2} cos(theta)

where (c) is the chord length. Note that chord-wise position (x) is used instead of distance along the mean line (s) for simplicity and is valid in cases where the camber height is not too large. For typical aerofoils with small camber, the difference between these two distances is negligible. With no camber this model becomes equivalent to the Joukowski mapping of a cylinder to a flat plate aerofoil. The magnitude of the vortex sheet strength must be calculated to complete the mathematical model.

For thin cambered plate models, a boundary condition of zero flow normal to the surface is applied in order to create an equation that can be solved for the required coefficients (A0, A1, A2,) to determine the necessary strength of the vortex sheet.

Given an aerofoil geometry, freestream velocity and angle of incidence, the magnitude of the coefficients (A0, A1, A2) is to be found by solving the boundary condition equation, along the surface. In this case the condition of flow velocity normal to the surface can be more easily formulated in terms of horizontal and vertical velocity components.

text{ If } V_n = 0 text{ then } frac{v}{u} = frac {dy_c}{dx}

The ratio of vertical (v) to horizontal (u) velocity at the surface (mean line) must equal the surface gradient (dyc/dx).

The flow horizontal and vertical velocities are made up of freestream and vortex induced components.v = V_{infty} sin (alpha) + v_i text{ and } u = V_{infty} cos(alpha) + u_i

where ui and vi are the horizontal and vertical velocities induced by the vortex sheet. Both of these components will be much less than the freestream velocity. Also due to the ‖flatness‖ of the section vi will be much larger than ui, so for small angles of incidence, the horizontal vortex induced component can be neglected. If these small angle assumptions are made for the incidence, the boundary condition equation becomes ,

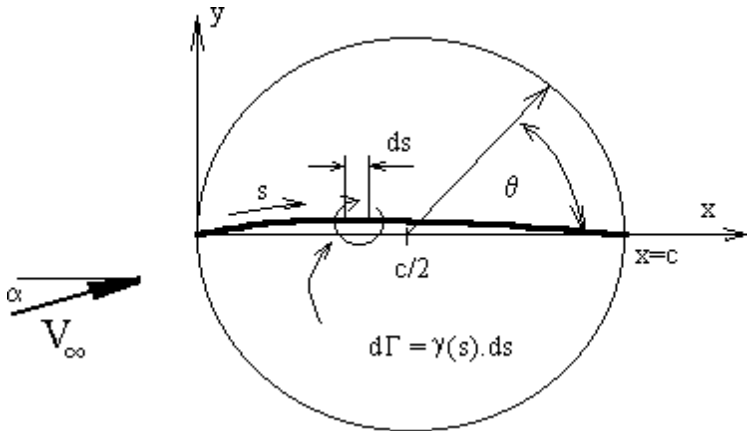

The velocity induced vertically (vi) at any point on the mean line can be found by summing up the effects of small individual segments (ds) of the vorticity distribution. where (x) is the location at which the induced velocity is being calculated and (s) is the chord-wise location of the vortex element. On integration after substitution for s,x and γ this gives,

The solution for coefficients (A0, A1, A2,.) can now be obtained from this equation. The solution is based on Glauert's integral method. The equation is summed (integrated) along the chord line to find initially coefficient A0. It is then scaled by cosine multiples and again summed along the chord. Each scaled integration will yield one higher order coefficient. ∫ (boundary condition equation).dθ along chord line produces,

On a three-dimensional, finite wing, lift over each wing segment (local lift per unit span, or does not correspond simply to what two-dimensional analysis predicts. Instead, this local amount of lift is strongly affected by the lift generated at neighboring wing sections. As such, it is difficult to predict analytically the overall amount of lift that a wing of given geometry will generate. The lifting-line theory yields the lift distribution along the

span-wise direction, based only on the wing geometry (span-wise distribution of chord, airfoil, and twist) and flow conditions.

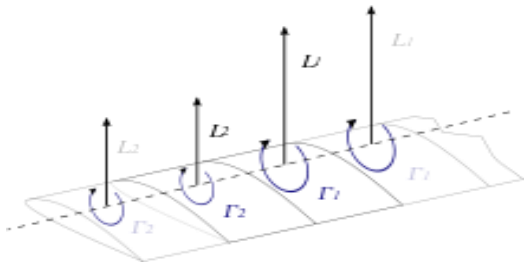

Figure 2.7: Lifting-line for a thin airfoil

Elements of panel method

Panel methods were developed to overcome the disadvantage of an incomplete geometry model. Panel methods also model the blade thickness and include the hub in the numerical model. The development of panel methods for propellers was apparently not an easy task. After the ship hull flow could be treated by panel methods it took another decade until the late 1980s before the first successful panel approaches were established for propellers. The implementation of a robust Kutta condition is a decisive element of each propeller panel code, since it controls torque and thrust. In principle, there exist many possibilities to create panel codes, depending on panel type and the formulation of the problem

The majority of the panel codes used for propellers follows Morino‘s approach (Morino and Kuo 1974, Morino 1975). Morino‘s approach is a direct formulation, i.e. it solves directly for the potential and determines velocities by numerical differentiation. The approach uses exclusively dipole panels, which discretize the surfaces of the propeller blades, the hub, and part of the wakes of each blade. The Kutta condition demands that at the trailing edge the pressure difference between face and back should vanish. This

couples the dipoles on the wake to the dipoles on the propeller. The panels in the wake all have the same strength for steady flow conditions. The pitch of the wake is either specified by largely empirical relations or determined iteratively as part of the solution. The Kutta condition enforcing a vanishing pressure jump at the trailing edge is a non-linear condition requiring an iterative solution. The numerical implementation of the Kutta condition requires great care, since simplifications or conceptual errors in the physical model may strongly affect the computed lift forces.

Aerodynamic potential flow codes or panel codes are used to determine the fluid velocity, and subsequently the pressure distribution, on an object. This may be a simple two-dimensional object, such as a circle or wing, or it may be a three-dimensional vehicle.

These are the various assumptions that go into developing potential flow panel methods:

- Inviscid
- Incompressible $\nabla \cdot V = 0$
- Irrotational $\nabla \times V = 0$
- Steady

However, the incompressible flow assumption may be removed from the potential flow derivation leaving:

- Potential Flow (inviscid, irrotational, steady) $\nabla^2 \phi = 0$.

High lift airfoils

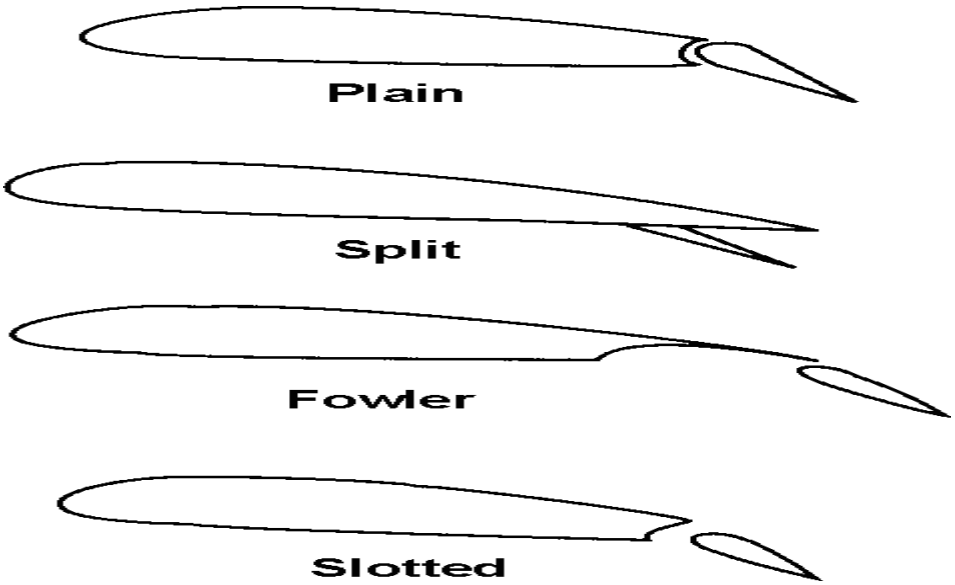

Figure 2.8: High-lift airfoil configurations

a) ‒smooth‖ . Practical-construction wings, when tested in wind tunnels against smooth (sanded-wooden) test specimens, show little resemblance to the smooth specimens. This is exemplified by a later sentence in that same section of the book: ‒the earlier increase of drag coefficient shown by the NACA 66–116 may be caused by surface irregularities because the specimen tested was a practical construction model.‖ Designers must decide how much construction $$ and what materials are selected, in order to impact the end-result smoothness of the wings.

b) Reynolds Number. Since the aircraft speed and altitude are somewhat fixed values, the only detail which the aircraft designer can vary to impact the RN is the wing chord - if you make the wing chord twice as long, you double the RN. This means that short stubby wings are better for high-speed flight. HOWEVER, since that airplane also has to fly

slower when climbing to altitude, a long slender wing would be better there, so the designer must decide which regime is more important.

c) relative extent of the laminar boundary layer. This is where the choice of airfoil section comes in. Chart 65 of that book shows minimum drag coefficients ranging from 0.0056 (NACA 63) to 0.0033 (NACA 66 and NACA 67) The maximum thickness for NACA 63 is at 35 percent; for NACA 66 it is at 45 percent, and for NACA 67 it is at 50 percent. Again, these wings also have to be used when landing the airplane, and during climb to altitude (which involve different lift/drag ratios and different RN), so designers must decide which regime is most important to the mission.

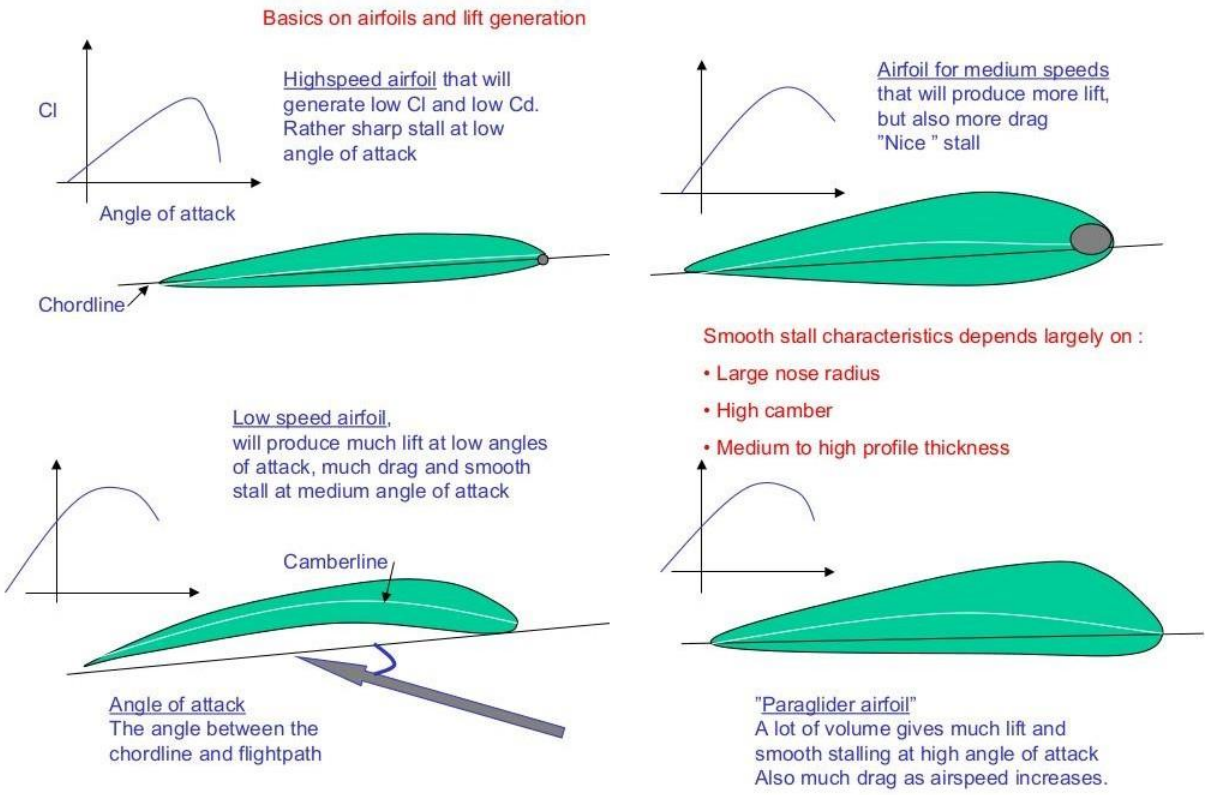

High lift devices

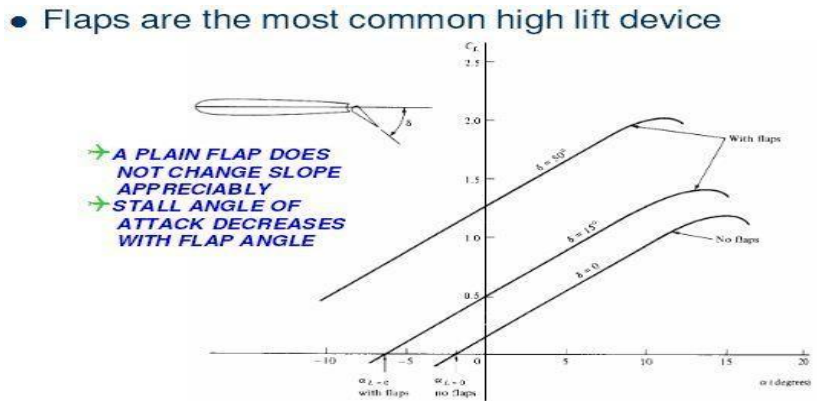

Figure 2.9: Effect of flaps on lift-slope curve

In aircraft design and aerospace engineering, a high-lift device is a component or mechanism on an aircraft's wing that increases the amount of lift produced by the wing. The device may be a fixed component, or a movable mechanism which is deployed when required. Common movable high-lift devices include wing flaps and slats. Fixed devices include leading edge root extensions and boundary layer control systems, which are less commonly used.

Purpose

The size and lifting capacity of a fixed wing is chosen as a compromise between differing requirements. For example, a larger wing will provide more lift and reduce the distance and speeds required for takeoff and landing, but will increase drag, which reduces performance during the cruising portion of flight. Modern passenger jet wing designs are optimized for speed and efficiency during the cruise portion of flight, since this is where the aircraft spends the vast majority of its flight time. High-lift devices compensate for this design trade-off by adding lift at takeoff and landing, reducing the distance and speed

required to safely land the aircraft, and allowing the use of a more efficient wing in flight. The high-lift devices on the Boeing 747-400, for example, increase the wing area by 21% and increase the lift generated by 90%

Flaps

The most common high-lift device is the flap, a movable portion of the wing that can be lowered to produce extra lift. When a flap is lowered this re-shapes the wing section to give it more camber. Flaps are usually located on the trailing edge of a wing, while leading edge flaps are used occasionally. There are many kinds of trailing-edge flap. Simple hinged flaps came into common use in the 1930s, along with the arrival of the modern fast monoplane which had higher landing and takeoff speeds than the old biplanes. In the split flap, the lower surface hinges downwards while the upper surface remains either fixed to the wing or moves independently. Travelling flaps also extend backwards, to increase the wing chord when deployed, increasing the wing area to help produce yet more lift. These began to appear just before World War II due to the efforts of many different individuals and organizations in the 1920s and 30s. Slotted flaps comprise several separate small airfoils which separate apart, hinge and even slide past each other when deployed. Such complex flap arrangements are found on many modern aircraft. Large modern airliners make use of triple-slotted flaps to produce the massive lift required during takeoff.

Slats and slots

Another common high-lift device is the slat, a small aerofoil shaped device attached just in front of the wing leading edge. The slat re-directs the airflow at the front of the wing, allowing it to flow more smoothly over the upper surface when at a high angle of attack. This allows the wing to be operated effectively at the higher angles required to produce more lift. A slot is the gap between the slat and the wing. The slat may be fixed in position, with a slot permanently in place behind it, or it may be retractable so that the

slot is closed when not required. If it is fixed, then it may appear as a normal part of the leading edge of a wing, with the slot buried in the wing surface immediately behind it. Large modern airliners make use of triple-slotted flaps to produce the massive lift required during takeoff.

Boundary layer control and blown flaps

Powered high-lift systems generally use airflow from the engine to shape the flow of air over the wing, replacing or modifying the action of the flaps. Blown flaps take "bleed air" from the jet engine's compressor or engine exhaust and blow it over the rear upper surface of the wing and flap, re-energising the boundary layer and allowing the airflow to remain attached at higher angles of attack. A more advanced version of the blown flap is the circulation control wing, a mechanism that ejects air backwards over a specially designed airfoil to create lift through the Coandă effect.

Another approach is to use the airflow from the engines directly, by placing a flap so that it deploys into the path of the exhaust. Such flaps require greater strength due to the power of modern engines and also greater heat resistance to the hot exhaust. The effect can be significant. Examples include the C-17 Globemaster III.

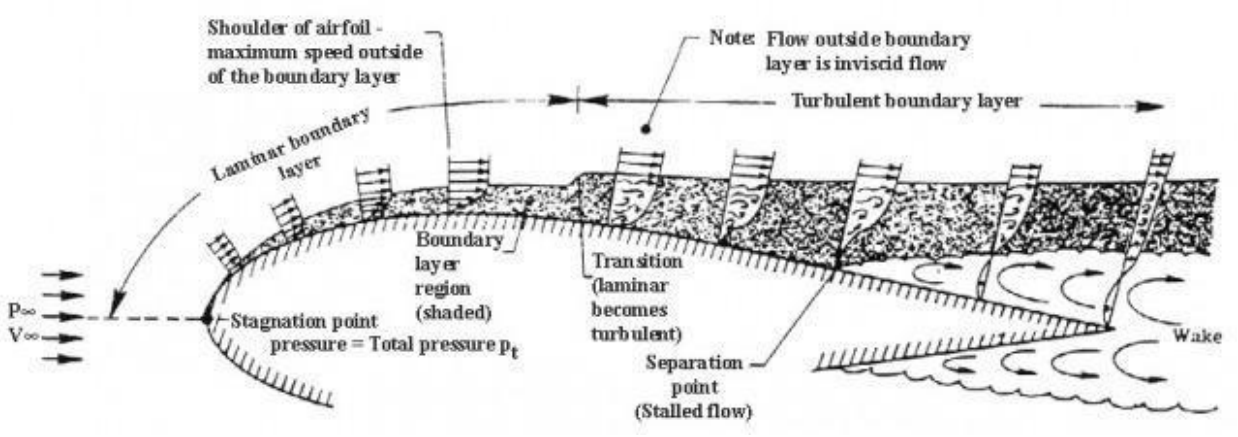

Leading edge root extensions

More common on modern fighter aircraft but also seen on some civil types, is the leading-edge root extension (LERX), sometimes called just a leading edge extension (LEX). A LERX typically consist of a small triangular fillet attached to the wing leading edge root and to the fuselage. In normal flight the LERX generates little lift. At higher angles of attack, however, it generates a vortex that is positioned to lie on the upper surface of the main wing. The swirling action of the vortex increases the speed of airflow over the wing, so reducing the pressure and providing greater lift. LERX systems are notable for the potentially large angles in which they are effective.

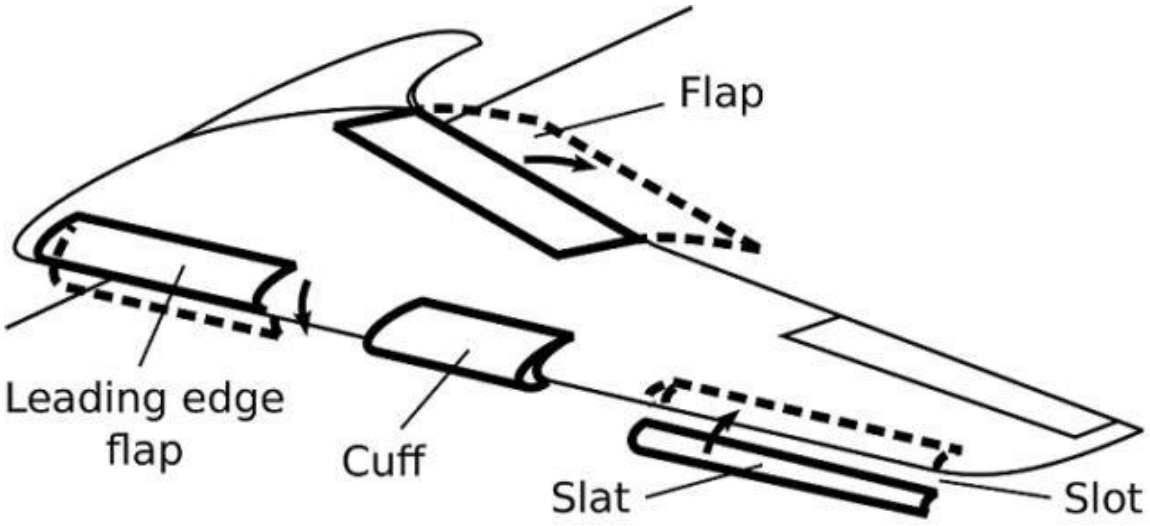

Co-Flow Jet

A Co-Flow Jet (CFJ) wing has an upper surface with an injection slot after the leading edge and a suction slot before the trailing edge, to augment lift, increase the stall margin and reduce drag. CFJ is promoted by the mechanical and aerospace engineering department of the University of Miami. For a hybrid-electric regional aircraft based on

the ATR 72 with the same wing area, size and weight, CFJ improves its cruise lift coefficient for an higher wing loading, allowing more fuel and batteries for longer range.

UNIT-III

FINITE WING THEORY

A very simple model for the flowfield about lifting wing is the superposition of a freestream flow and a horseshoe vortex . The horseshoe vortex consists of three segments: a bound vortex spanning the wing, connected to two trailing vortices at each wing tip. As required by Helmholtz‘s vortex theorems, the circulation Γ is constant along the entire vortex line, and the vortex line extends downstream to infinity. Although this model qualitatively reproduces the observed tip vortices, it is not well suited for accurate prediction of overall wing lift and induced drag. The main deficiency is that its local lift/span $L' = \rho V_\infty \Gamma$ is constant across the span, which is not very realistic. On a real wing, L' always falls gradually to zero at the tips.

Another deficiency is that the induced drag predicted by this model is wildly inaccurate, when compared to more refined models or experimental data. A better flowfield model employs multiple distributed horseshoe vortices as shown in the figure. Each horseshoe vortex has a constant strength along its length and hence obeys Helmholtz‘s theorem. Spreading the trailing vortices across the span rather than all at the tip allows a non-uniform spanwise circulation $\Gamma(y)$ and corresponding loading $L'(y)$ to be represented.

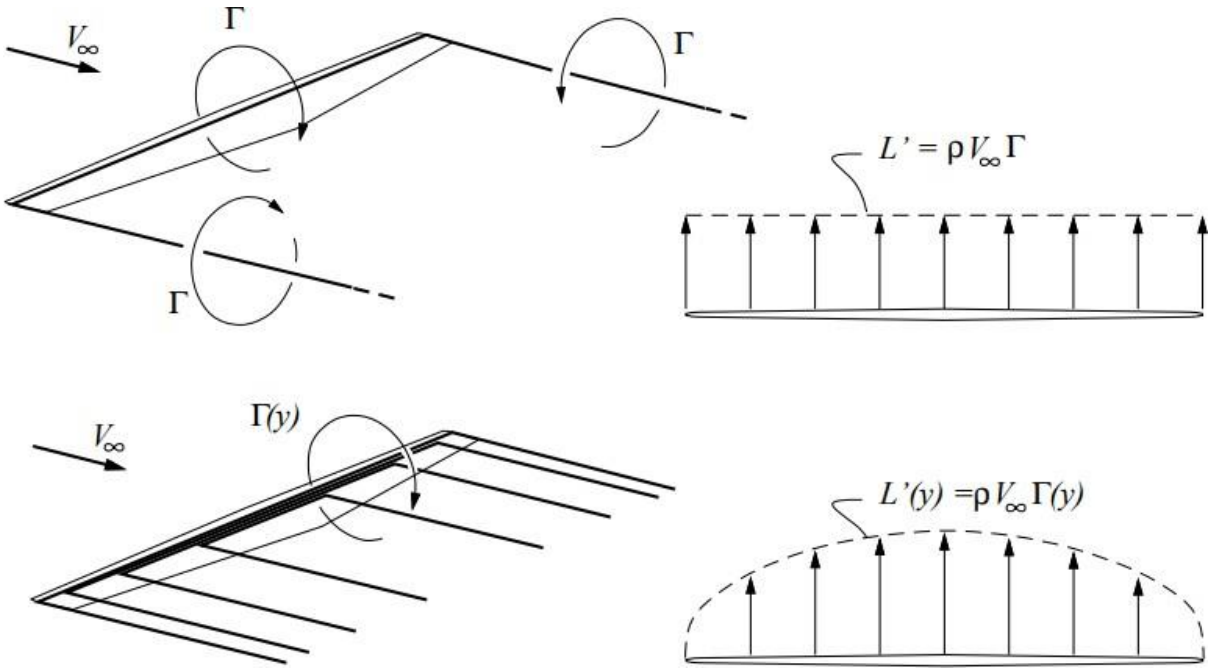

Figure 3.1: Horse-shoe vortex model for a wing

The figure shows only a few horseshoe vortices on the wing, but one can conceptually subdivide these into more and more vortices of decreasing strength, which in the limit become a trailing vortex sheet with strength γ(y). The strength of the sheet can be determined by

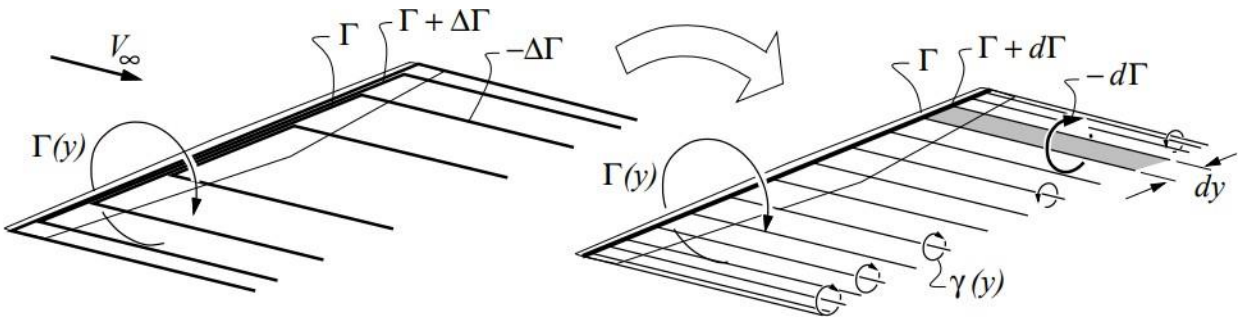

Figure 3.2: Analysis using Horse-shoe vortex model

considering a small change of circulation dΓ between spanwise stations y and y + dy. By Helmholtz's theorem, the dy-wide sheet strip trailing between those two stations must have a circulation −dΓ. This then gives the local sheet strength γ(y).

$$\gamma \ dy = -d\Gamma$$

$$\text{or } \gamma = -\ d\Gamma\ dy$$

Vortex motions

A vortex is the motion of many fluid particles around a common center. The streamlines are concentric circles.

Choose coordinates such that z is perpendicular to flow. In polar coordinates, the vorticity is

$$\Omega_z = \frac{1}{2}\left(\frac{dV}{dr} + \frac{V}{r}\right)$$ (V is function of r, only)

Solid body rotation (forced vortex):

$$V = \omega r$$

or

$$\Omega_z = \omega$$

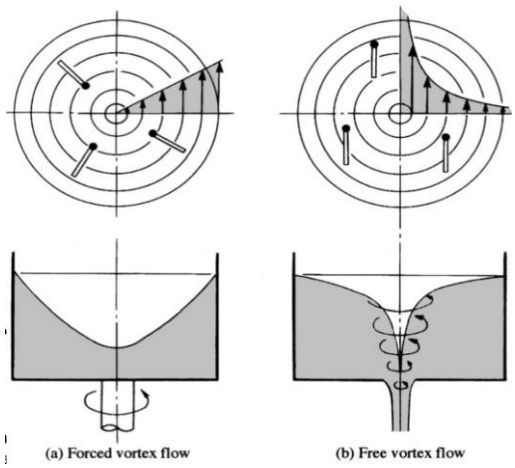

Figure 3.3: Vortex motions

Vortex with irrotational flow (free vortex):

$$\Omega_z = \frac{1}{2}\left(\frac{dV}{dr} + \frac{V}{r}\right) = 0$$

$$\Rightarrow \quad \frac{dV}{V} = -\frac{dr}{r}$$

$$\Rightarrow \quad V = \frac{C}{r}$$

A paddle wheel does not rotate in a free vortex!

Vortex Lines, Vortex Tubes, and Vortex Filaments

The curl of the velocity field of a fluid, which is generally termed *vorticity*, is usually represented by the symbol ω.

A *vortex line* is a line whose tangent is everywhere parallel to the local vorticity vector. The vortex lines drawn through each point of a closed curve constitute the surface of a *vortex tube*. Finally, a *vortex filament* is a vortex tube whose cross-section is of infinitesimal dimensions.

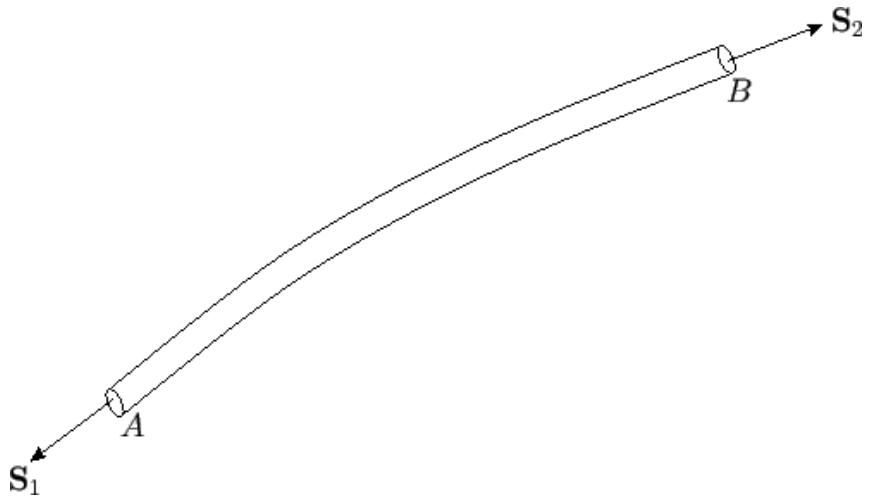

Figure 3.4: A vortex filament

Consider a section AB of a vortex filament. The filament is bounded by the curved surface that forms the filament wall, as well as two plane surfaces, whose vector areas are $\mathbf{S}_1$ and $\mathbf{S}_2$ (say), which form the ends of the section at points A and B, respectively. (See Figure.) Let the plane surfaces have outward pointing normals that are parallel (or anti-parallel) to the vorticity vectors, ω^1 and ω^2, at points A and B, respectively. The divergence theorem, applied to the section, yields

$$\oint \boldsymbol{\omega}\cdot d\mathbf{S} = \int \nabla\cdot\boldsymbol{\omega}\, dV,$$

where $d\mathbf{S}$ is an outward directed surface element, and dV a volume element. However,

$$\nabla\cdot\boldsymbol{\omega} = \nabla\cdot\nabla\times\mathbf{v}\equiv 0$$

implying that

$$\oint \boldsymbol{\omega}\cdot d\mathbf{S} = 0.$$

Now, $\omega\cdot d\mathbf{S} = 0$ on the curved surface of the filament, because ω is, by definition, tangential to this surface. Thus, the only contributions to the surface integral come from the plane areas $\mathbf{S_1}$ and $\mathbf{S_2}$. It follows that

$$\oint \boldsymbol{\omega}\cdot d\mathbf{S} = S_2\,\omega_2 - S_1\,\omega_1 = 0.$$

This result is essentially an equation of continuity for vortex filaments. It implies that the product of the magnitude of the vorticity and the cross-sectional area, which is termed the *vortex intensity*, is constant along the filament. It follows that a vortex filament cannot terminate in the interior of the fluid. For, if it did, the cross-sectional area, S, would have to vanish, and, therefore, the vorticity, ω, would have to become infinite. Thus, a

vortex filament must either form a closed vortex ring, or must terminate at the fluid boundary.

Because a vortex tube can be regarded as a bundle of vortex filaments whose net intensity is the sum of the intensities of the constituent filaments, we conclude that the intensity of a vortex tube remains constant along the tube.

Circulation and Vorticity

Consider a closed curve C situated entirely within a moving fluid. The vector line integral

$$\Gamma_C = \oint_C \mathbf{v} \cdot d\mathbf{r},$$

where $d\mathbf{r}$ is an element of C, and the integral is taken around the whole curve, is termed the *circulation* of the flow around the curve. The sense of circulation (i.e., either clockwise or counter-clockwise) is arbitrary.

Let S be a surface having the closed curve C for a boundary, and let $d\mathbf{S}$ be an element of this surface with that direction of the normal which is related to the chosen sense of circulation around C by the right-hand circulation rule. According to the curl theorem,

$$\Gamma_C = \oint_C \mathbf{v} \cdot d\mathbf{r} = \int_S \boldsymbol{\omega} \cdot d\mathbf{S}.$$

Thus, we conclude that circulation and vorticity are intimately related to one another. In fact, according to the previous expression, the circulation of the fluid around loop C is equal to the net sum of the intensities of the vortex filaments passing through the loop and piercing the surface S (with a filament making a positive, or negative, contribution to the sum depending on whether it pierces the surface in the direction determined by the

chosen sense of circulation around C and the right-hand circulation rule, or in the opposite direction). One important proviso to Equation is that the surface S must lie entirely within the fluid.

Kelvin Circulation Theorem

According to the *Kelvin circulation theorem*, which is named after Lord Kelvin (1824-1907), the circulation around any co-moving loop in an inviscid fluid is independent of time. The proof is as follows. The circulation around a given loop C is defined

$$\Gamma_C = \oint_C \mathbf{v}\cdot d\mathbf{r}. \tag{4.78}$$

$d\mathbf{v} = d(d\mathbf{r}/dt) = d(d\mathbf{r})/dt$

However, for a loop that is co-moving with the fluid, we have . Thus,

$$\frac{d\Gamma_C}{dt} = \oint_C \frac{d\mathbf{v}}{dt}\cdot d\mathbf{r} + \oint_C \mathbf{v}\cdot d\mathbf{v}. \tag{4.79}$$

$d\mathbf{v}/dt = D\mathbf{v}/Dt$

Moreover, the equation of motion of an incompressible inviscid fluid can be written as

$$\frac{D\mathbf{v}}{Dt} = -\nabla\left(\frac{p}{\rho}+\Psi\right), \tag{4.80}$$

Hence,

$$\frac{d\Gamma_C}{dt} = -\oint_C \nabla\left(\frac{p}{\rho}-\frac{1}{2}v^2+\Psi\right)\cdot d\mathbf{r} = 0, \tag{4.81}$$

$\mathbf{v}\cdot d\mathbf{v} = d(v^2/2) = \nabla(v^2/2)\cdot d\mathbf{r}$

$p/\rho - v^2/2 + \Psi$

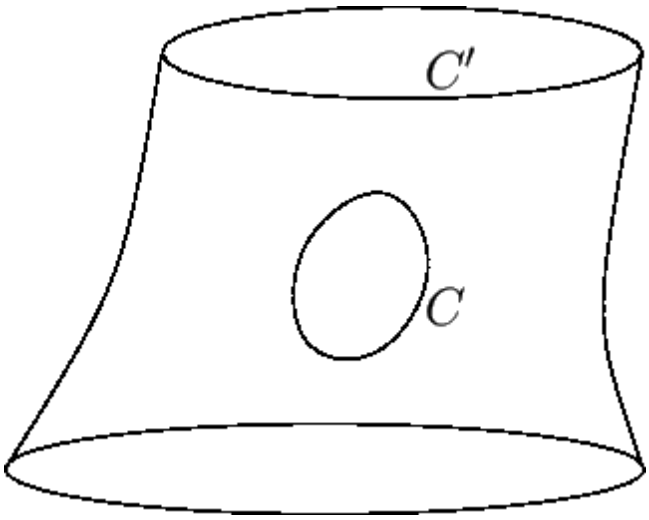

Figure 3.5: A vortex tube

One corollary of the Kelvin circulation theorem is that the fluid particles that form the walls of a vortex tube at a given instance in time continue to form the walls of a vortex tube at all subsequent times. To prove this, imagine a closed loop **C** that is embedded in the wall of a vortex tube but does not circulate around the interior of the tube.

The normal component of the vorticity over the surface enclosed by **C**is zero, because all vorticity vectors are tangential to this surface. Thus, from Equation, the circulation around the loop is zero. By Kelvin's circulation theorem, the circulation around the loop remains zero as the tube is convected by the fluid. In other words, although the surface enclosed by **C** deforms, as it is convected by the fluid, it always remains on the tube wall, because no vortex filaments can pass through it.

Another corollary of the circulation theorem is that the intensity of a vortex tube remains constant as it is convected by the fluid. This can be proved by considering the circulation around the loop C'' pictured in Figure.

Helmholtz’s third theorem:

> *In the absence of rotational external forces, a fluid that is initially irrotational remains irrotational.*

Helmholtz‘s theorems apply to inviscid flows. In observations of vortices in real fluids the strength of the vortices always decays gradually due to the dissipative effect of viscous forces.

Alternative expressions of the three theorems are as follows:

1. The strength of a vortex tube does not vary with time.[2] 2. Fluid elements lying on a vortex line at some instant continue to lie on that vortex line. More simply, vortex lines move with the fluid. Also vortex lines and tubes must appear as a closed loop, extend to infinity or start/end at solid boundaries.
3. Fluid elements initially free of vorticity remain free of vorticity.

Helmholtz’s theorems have application in understanding:

Generation of lift on an airfoil

Starting vortex

Horseshoe vortex

Wingtip vortices.

Helmholtz’s theorems are now generally proven with reference to Kelvin's circulation theorem. However the Helmholtz's theorems were published in 1858, nine years before the 1867 publication of Kelvin's theorem. There was much communication between the two men on the subject of vortex lines, with many references to the application of their theorems to the study of smoke rings.

THE BIOT-SAVART LAW

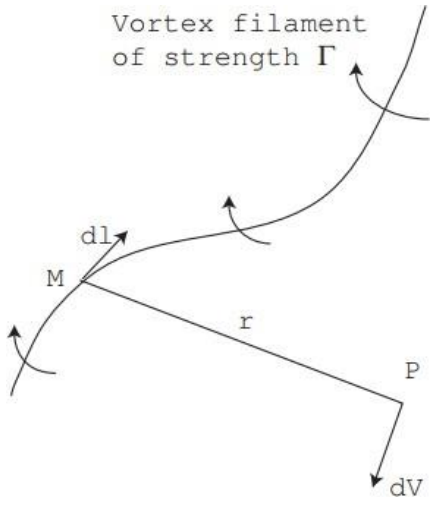

Figure 3.6: Vortex filament and illustration of the Biot-Savart law

Consider a vortex filament with a circulation Γ as shown in Figure 1. An elemental segment d ~l centered at the point M of the vortex filament induces an elemental velocity dV~ = Γ 4π d ~l × ~r |r 3 | , (1)

where ~r = −→ MP, and r = |~r|.

We now apply the Biot-Savart law (1) to a straight vortex filament of infinite length as sketched in Figure 2. The velocity dV~ induced at point P by any elemental segment of the vortex filament d ~l is given by (1). Because the filament is a straight line, dV~ is perpendicular to the plane defined by the filament and the point P. The velocity induced at point P by the entire vortex filament is

$$\vec{V} = \frac{\Gamma}{4\pi} \int_{-\infty}^{+\infty} \frac{d\vec{l} \times \vec{r}}{|r^3|}.$$

The direction of the induced velocity can be obtained from the right-hand screw rule. Its magnitude, V = |V~ |, can be calculated as follows. From the geometry shown in Figure

$$\begin{aligned} r &= \frac{h}{sin\theta} \\ l &= -\frac{h}{tan\theta} \\ dl &= \frac{h}{sin^2\theta}d\theta \end{aligned}$$

Substituting in equation(2), we have

$$V = \frac{\Gamma}{4\pi}\int_{-\infty}^{+\infty}\frac{sin\theta}{r^2}dl = \frac{\Gamma}{4\pi h}\int_0^{\pi} sin\theta d\theta$$

Or

$$V = \frac{\Gamma}{2\pi h}$$

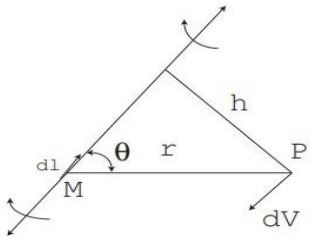

Figure 3.7: Velocity induced at point by an infinite straight vortex filament

Consider the semi-infinite vortex filament shown in Figure 3. The filament extends from O to ∞.

$$V = \frac{\Gamma}{4\pi}\int_0^{+\infty}\frac{sin\theta}{r^2}dl = \frac{\Gamma}{4\pi h}\int_{\frac{\pi}{2}}^{\pi} sin\theta d\theta$$

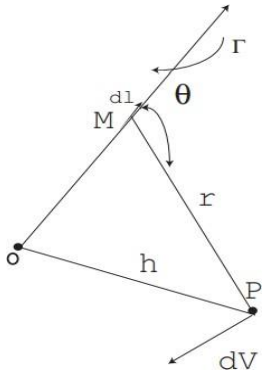

Or

V = Γ 4πh

The velocity induced at P by the semi-infinite vortex filament is half that induced by an infinite vortex filament.

The flow over finite wings

In what respect is the flow around a true wing different from an airfoil (an ‗infinite' wing)?

Airfoil : 2D flow (cl , c d) Real Wing: 3D flow (CL , C D) (1) finite extent (2) variation of sections along the wing span In what respect is the flow around a true wing different from an airfoil (an ‗infinite' wing)?

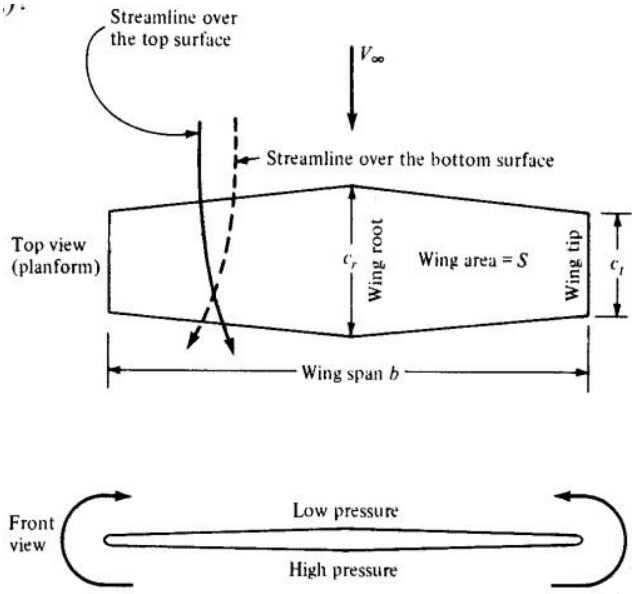

• spanwise flow component due to ‗leakage' flow around the tip

Trailing vortices and downwash

Results: trailing vortices (tip vortices) and downwash (vertical flow component)

Prandtl's Lifting Line Theory, Downwash and Induced Drag

What are the implications of H1, H2 and the Biot–Savart Law on finite wings? How do we model finite wings? • Imagine that all the little γds vortices arrayed along the camber line of a 2D airfoil are collected into a single Γ that's placed at the quarter-chord point. • In 3D, this vortex cannot end so wingtip vortices connect the bound vortex back to the starting vortex that is still sitting on the runway, 1000 miles behind the wing.

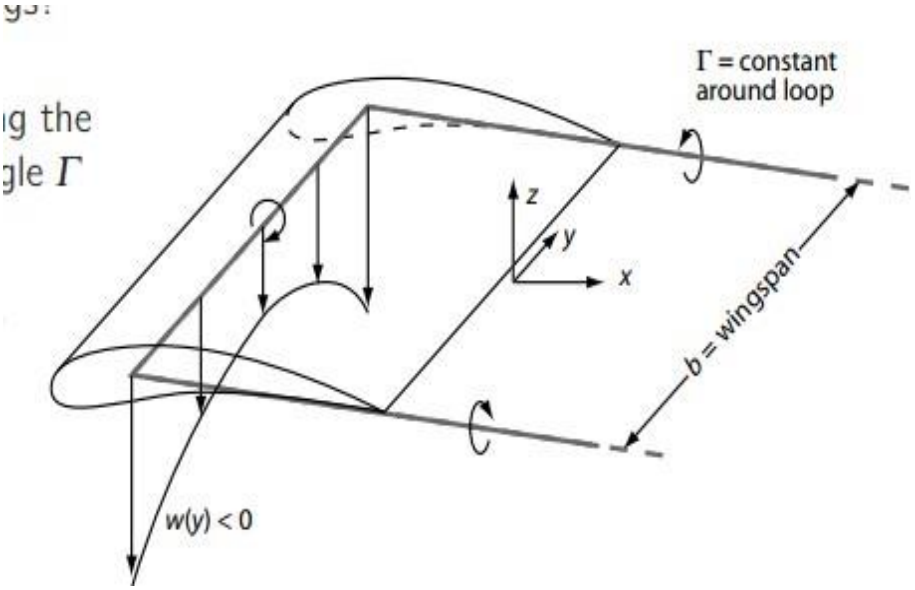

The bound vortex generates lift. • The starting vortex is so far aft, it does not induce any velocity near the wing. • The wingtip vortices generate downwash: w(y) < 0 between themselves, including at the location of the bound vortex. • What is the downwash velocity induced by the pair of wingtip vorices along the bound vortex? Calculate using Biot–Savart. . .

$$w(y) = \frac{-\Gamma}{\pi b\,[1 - (2y/b)^2]}$$

The preceding expression is a bit scary. It implies we have infinite downwash velocities at the wing tips. Even disregarding the impossibility of infinite velocities, we expect our small-angle approximations do not work and that the wingtips are probably stalled. What do we do about this?

• The next level of approximation allows Γ to vary along the wingspan, despite the fact that Γ must be constant along a vortex filament. If we let $\Gamma \to 0$ at the wing tips, maybe we can avoid infinite downwash. How do we have our cake and eat it too?

• Because a single vortex filament must have constant Γ , we simply stack a number of bound vortices along the lifting line but allow them to turn back into trailing vortices at different points along the span. This allows for a varying Γ (y).

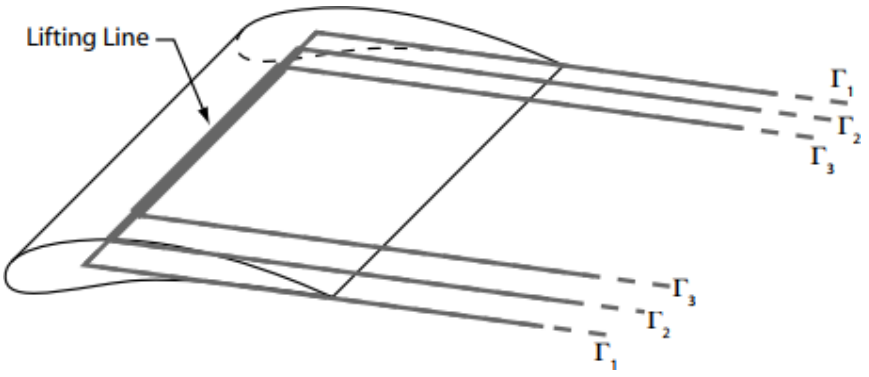

Figure 3.11: Lifting line model for a wing

• Why might Γ vary along the span? All the reasons that L ′ can vary for an airfoil: chord, angle of attack and zero-lift angle can all vary along the span. – Chord variations are called taper: c = c(y) – Angle of attack variations are called twist: α = α(y) – Zero-lift angle variations are called aerodynamic twist: αL = 0 = αL = 0(y) – And, as we will see, there is an induced angle of attack, αi(y) that decreases the effective angle of attack to less than the geometrical angle of attack.

• Now we need to consider what multiple vortices mean for the downwash velocity w(y) along the lifting line.

• Consider the diagram shown to the right that shows the lifting line from directly upstream. The downwash at the point y 0 due to each of the half-infinite vortices is

$$w_n(y_0) = -\frac{1}{2}\frac{\Gamma_n}{2\pi(y_0 - y_n)}$$

where n is an index for each of the half vortices and y n is the y location of each of these. Each of the _A‘ vortices is positive, each of the _B‘ vortices is the negative of the corresponding _A‘.

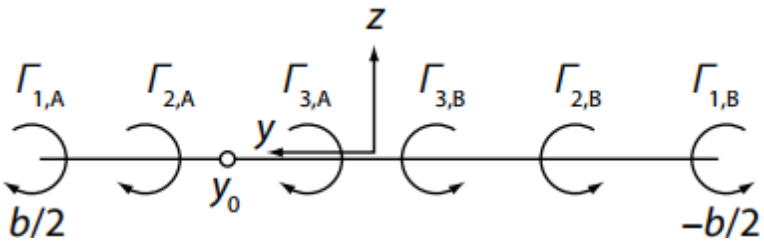

Figure 3.12: Vortex distribution over the wing (side view)

In figure 3.12, the vortices 1A, 2A, 3B, 2B, and 1B induce velocities down; 3A induces a velocity up. The different directions is given by the signs of y 0 − y n and the signs of Γn

• If we have a large number of very weak vortices we can do a little calculus and say

$$dw(y_0,y) = -\frac{d\Gamma(y)}{4\pi(y_0-y)} = -\frac{1}{4\pi(y_0-y)}\left.\frac{d\Gamma}{dy}\right|_y dy$$

and, with this,

$$w(y_0) = -\frac{1}{4\pi}\int_{-b/2}^{b/2}\frac{1}{y_0-y}\left.\frac{d\Gamma}{dy}\right|_y dy.$$

This is the net downwash at y_0 due to all the vortices.

• The net effect of this downwash is to tilt the incoming flow vector down the tilt angle is

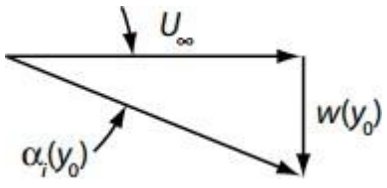

called an induced angle of attack, α_i and, like w(y), this angle depends on y, U_∞ and $w(y_0)$

• We define the induced angle of attack to be positive if w < 0 (as it usually is) so

$$\alpha_i(y_0) \approx -\frac{w(y_0)}{U_\infty} \quad \text{if} \quad w(y) \ll U_\infty$$

• What are the effects of this tilt? 1. The effective angle of attack is less than the geometrical angle of attack (the angle between the chord line and U∞ and this leads to less lift at each station along the blade that you would expect based on the geometrical angle of attack.

2. The aerodynamic force perpendicular to U_∞ at any y_0 is L ′ cos(αi) (i.e., it is decreased slightly because it is tilted back)

3. There is now an aerodynamic force in the direction of U∞ called induced drag: D'_i = L ′sin α_i .

• To sort out the implications of all this, we need a way to determine Γ(y). This function determines L′ and w at each station along the span and needs to correctly reflect all the geometrical features of the wing.

• The strategy for finding Γ (y) is to equate two separate expressions for L ′ for each 2D airfoil section along the wing. First, the Kutta–Joukowski Theorem gives at y 0 L ′ (y) = ρ U∞ Γ (y 0). Second, the 2D airfoil characteristics give L ′ (y) = 2 π [α(y 0)− αi(y 0)− αL = 0(

$$L'(y) = 2\pi\left[\alpha(y_0) - \alpha_i(y_0) - \alpha_{L=0}(y_0)\right] \times \frac{1}{2}\rho U_\infty^2 c(y_0)$$

So, we have two different expressions for L ′ at any y_0. If we set these equal to each other we can solve for the one thing we do not know for a wing we have built, the Γ (y) distribution.

• Setting the two L ′ expressions equal results in the Fundamental Equation of Finite Wing Theory

$$\frac{2\Gamma(y_0)}{U_\infty c(y_0)} = 2\pi \left[\alpha(y_0) - \alpha_{L=0}(y_0) - \frac{1}{4\pi U_\infty} \int_{-b/2}^{b/2} \frac{1}{y_0 - y} \left. \frac{d\Gamma}{dy} \right|_y dy \right]$$

• If we solve this equation for Γ (y_0) we know the lift at each section and, from this, the lift on the wing. • This whole process is very similar to the development of thin-airfoil theory. Equating two expressions for L ′ gives Γ (y_0) and integrating Γ (y_0) over the wingspan gives the overall lift.

• It is difficult to solve this equation (it is another integral equation) so our solution procedure will again include a sine series (this is nice because we would like to have Γ = 0 at the wingtips to avoid infinite downwash.

• What is unfortunate about all this is that for a given wing at a given U∞ more lift requires more Γ (via an increased geometrical angle of attack). We see that increasing Γ also increases the drag. However, increasing Γ also increases α_i so, actually, D_i increases like L_2.

The Elliptical Lift Distribution

Solving the Fundamental Equation of Finite Wing Theory requires us to guess at a Γ (y) distribution and show it‘s a correct guess. (The same approach we used for the γ(x) distribution for thin airfoils.) As a first guess we consider an elliptic distribution:

$$\Gamma(y) = \Gamma_0 \left[1 - \left(\frac{2y}{b}\right)^2\right]^{1/2}$$

This distribution has circulation Γ0 at the root (y = 0) and Γ = 0 at the wingtips (which avoids the infinite downwash problem).

First, let‘s compute the downwash by taking the derivative d Γ /dy and performing the variable transformations: 2y / b = cos θ. With this we obtain

$$w = -\frac{\Gamma_0}{2b}$$

An elliptic Γ distribution produces uniform downwash.

• Is such a Γ distribution possible? Put it into the fundamental equation of finite wing theory to verify. . . • Yep! It works for an elliptic c(y) distribution if there is no twist and no aerodynamic twist (i.e., α and $\alpha_{L=0}$ are constants along the span):

$$c(y) = c_0 \left[1 - \left(\frac{2y}{b}\right)^2\right]^{1/2}$$

• We can integrate this chord distribution to find the planform area, S and the aspect ratio, AR = b 2 / S.

$$S = \frac{\pi c_0 b}{4} \quad \text{and} \quad AR = \frac{4b}{\pi c_0}$$

Twisted wings

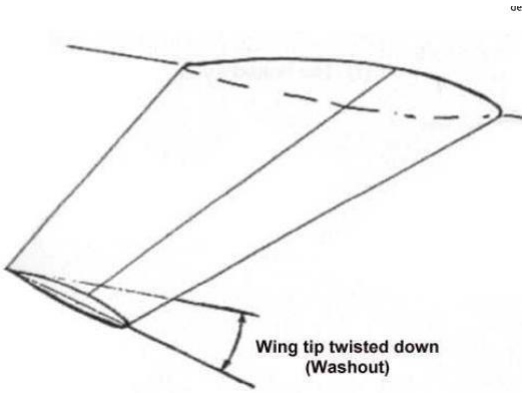

Figure 3.13: Illustration of twist

Wing twist (1)

• Wash-in: αtip > αroot

• Wash-out: αtip < αroot

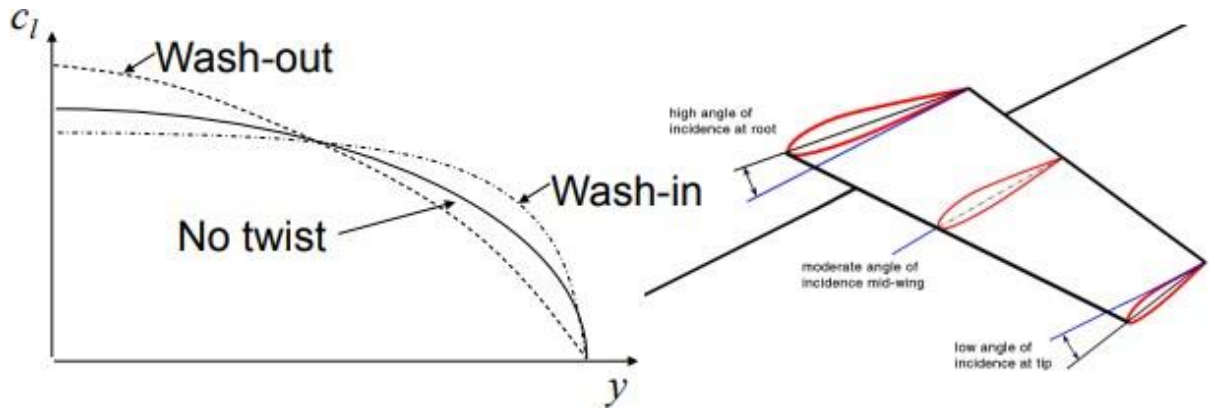

Figure 3.14: Aerodynamic effect of twist

Wings often have wash-out to reduce structural weight and improve stall characteristics.

• The point of initial stalling should be sufficiently inboard, around 0.4s from the wing root.

• This can be achieved with suitable twist. If the stall point is too far outboard, a little washout will bring it inboard.

• However, a washout of more than 5o results in an unacceptable increase in induced drag.

Tapered Wings

• Taper ratio is defined as à Reduction of the amount of lift near the wing-tip. à Tip vortex is weaker à Induced drag is smaller

• Taper also reduces structural weight

• As the chord at the root is unchanged the maximum lift is not severely affected by taper

• If the taper is not too high, the stalling characteristics are acceptable, even without twist

Effect of wing taper on lift distribution

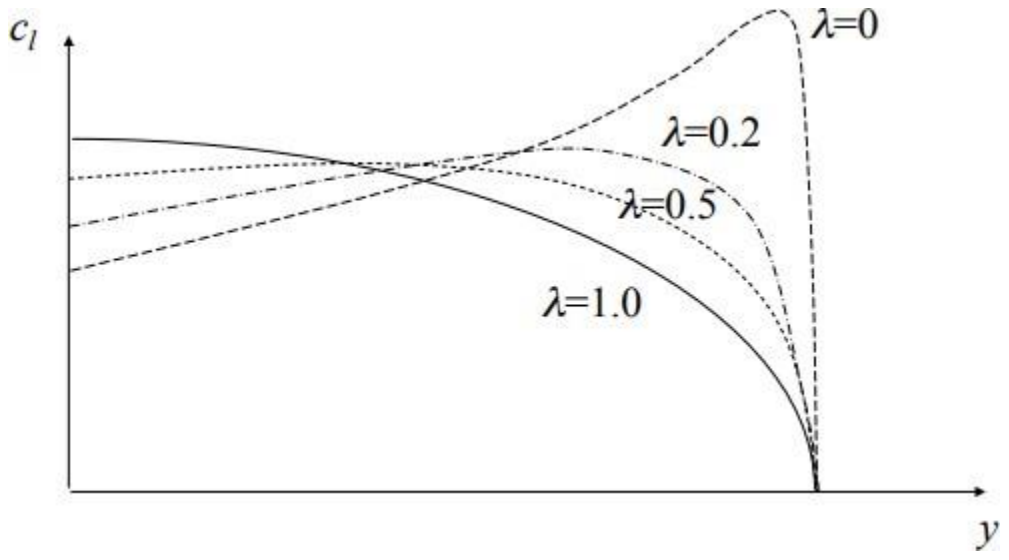

Figure 3.15: Aerodynamic effect of taper

Taper increases sectional lift coefficient

Effect of Wing Sweep

In addition to reducing airfoil thickness, aircraft designers can also raise a wing‘s M_{crit} by sweeping it either forward or aft. To understand how this works, consider the untapered, swept wing in Figure 3.16. Sweeping the wing without changing its shape increases the effective chord length. Figure 3.16 shows why this is true.

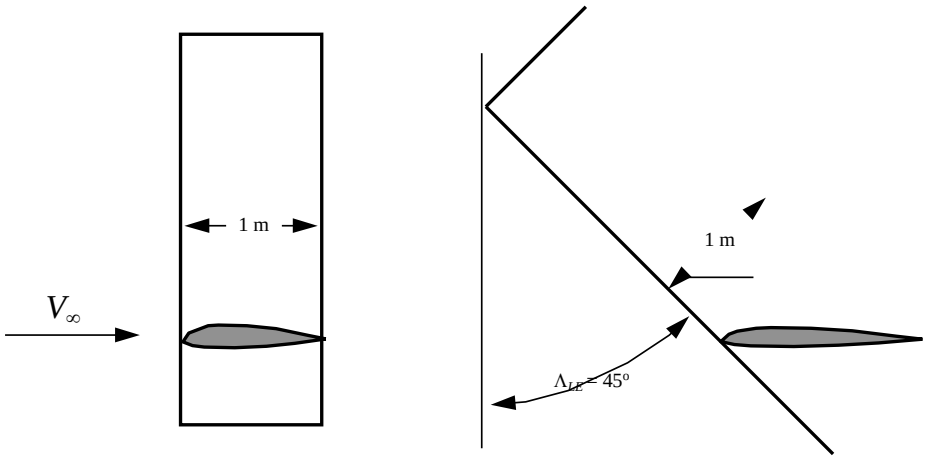

Figure 3.16: Effect of wing sweep on streamwise t/c ratio

Chord is measured in the streamwise direction, since the airfoil shape the air must flow around is a streamwise slice of the wing. From the geometry of Figure 3.16, the relationship between the chord of the unswept wing and the chord of the swept wing is:

$$c_{(swept\ wing)} = c_{(unswept\ wing)} / \cos \Lambda_{LE} \qquad (4.43)$$

so that:

$$\left(\frac{t_{max}}{c}\right)_{(swept\ wing)} = (\cos \Lambda_{LE}) \left(\frac{t_{max}}{c}\right)_{(unswept\ wing)} \quad (4.44)$$

Substituting the swept wing chord into (4.42) yields an expression for critical Mach number for swept wings:

$$M_{crit} = 1.0 - 0.065 \cos^{0.6} \Lambda_{LE} \left(100 \frac{t_{max}}{c}\right)^{0.6}$$

or, in terms of the unswept wing's M_{crit}:

$$M_{crit} = 1.0 - \cos^{0.6} \Lambda_{LE} \, (1.0 - M_{crit(unswept)}) \quad (4.45)$$

For tapered wings, the effect is modeled by using $\Lambda_{.25c}$, the sweep angle of the line connecting the quarter chord points of the wing's airfoils, and using the maximum value of $\left(\frac{t_{max}}{c}\right)$ on the wing:

$$M_{crit} = 1.0 - \cos^{0.6} \Lambda_{.25c} \, (1.0 - M_{crit(unswept)}) \quad (4.46)$$

Swept wings

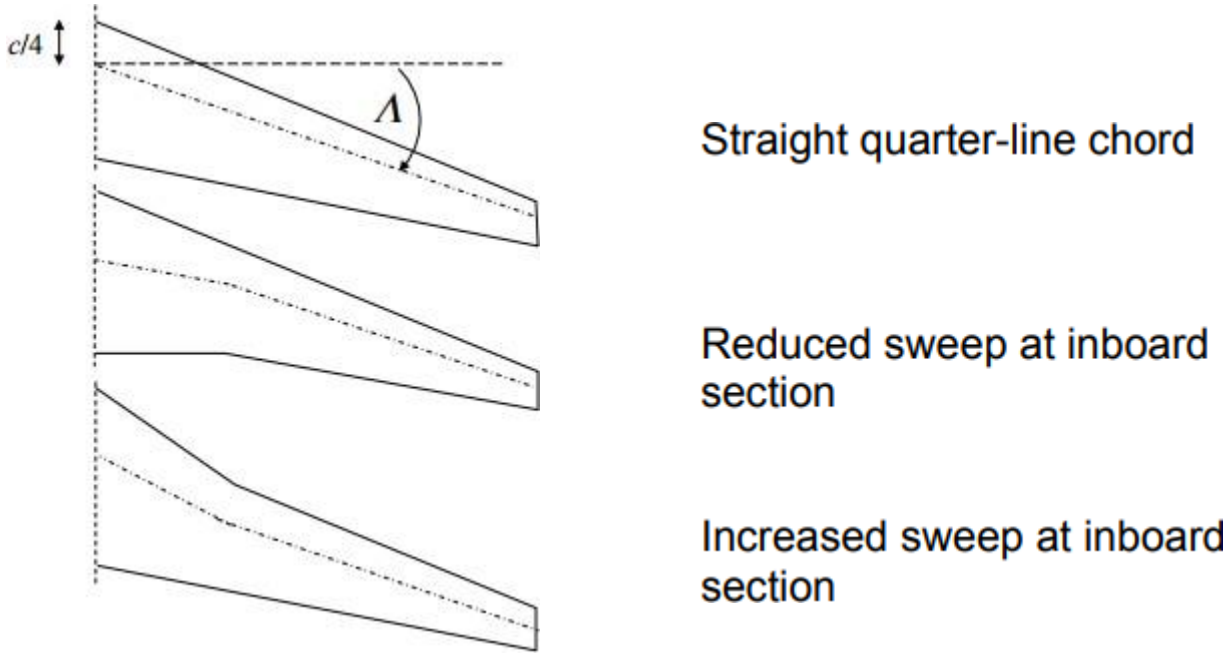

Figure 3.17: Different sweep planforms

Effect of sweep

A component of the free stream airspeed, VT is tangent to the wing. Therefore, the airspeed seen by the airfoil is only $V_{N.}$

$$V_N = V_\infty \cos\Lambda$$

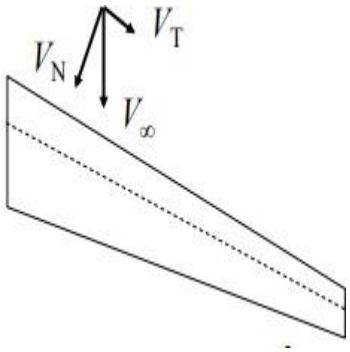

Figure 3.18: Sweepback

The effective Mach number seen by the wing‘s airfoil is Meff =M∞cosΛ à A higher V∞ is required to reach sonic conditions.

Using sweepback

• Up to M=0.65 or M=0.7 à straight wings with appropriate thickness ratio are sufficient.

• M > 0.7 à sweepback is required

• Sweep angle of 35° is rarely exceeded.

Twist Angle

If the wing tip is at a lower incidence than the wing root, the wing is said to have negative twist t) or washout. On the other hand, if the wing tip is at a higher incidence thanαor simply twist (the wing root, the wing is said to have positive twist or wash-in. The twist is usually negative; which means the wing tip angle of attack is lower than root angle of attack as sketched in figure a. This indicates that wing angle of attack is reduced along the span. The wings on a number of modern aircraft have different airfoil sections along the span, with different values of zero lift angle of attack; this is called aerodynamic twist. The wing tip airfoil section is often thinner than root airfoil section as sketched in figure b.

Sometimes, the tip and root airfoil sections have the same thickness-to-chord ratio, but the root airfoil section has higher zero-lift angle of attack (i.e. more negative) than tip airfoil section. When the tip incidence and root incidence are not the same, the twist is referred to as geometric twist. However, if the tip airfoil section and root airfoil section are not the same, the twist is referred to as aerodynamic twist. Both types of twist have advantages and disadvantages by which the designer must establish a selection that satisfies the design requirement. The application of twist is a selection as a decision

making, but the amount of twist is determined via calculations. In this section, both items will be discussed.

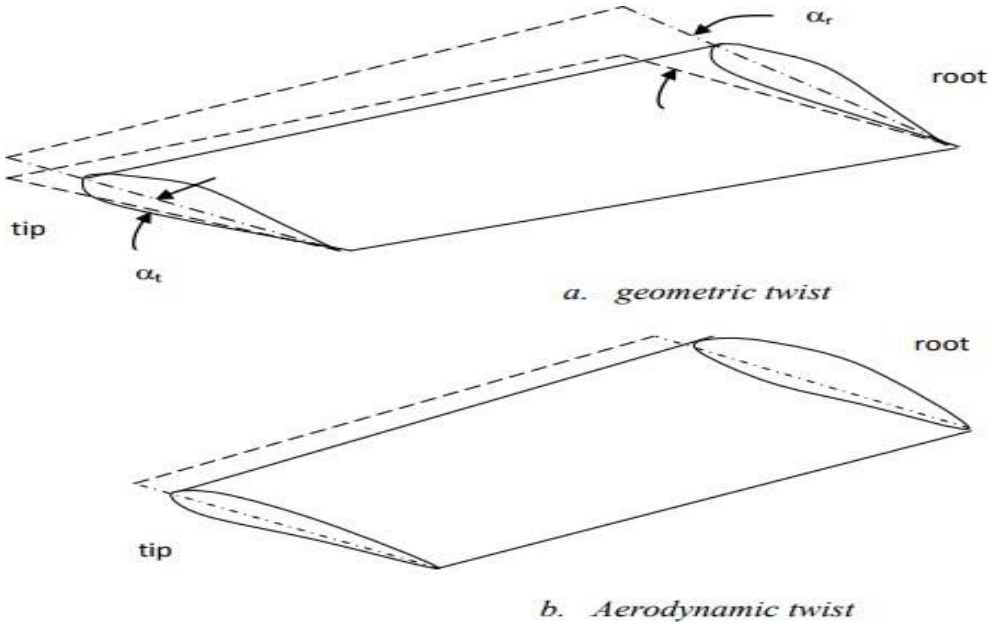

Figure 3.19: Wing twist

The Classical Vortex Lattice Method

There are many different vortex lattice schemes. In this section we describe the ―classical‖ implementation. Knowing that vortices can represent lift from our airfoil analysis, and that one approach is to place the vortex and then satisfy the boundary condition using the ―1/4 - 3/4 rule,‖ we proceed as follows:

1. Divide the planform up into a lattice of quadrilateral panels, and put a horseshoe vortex on each panel.

2. Place the bound vortex of the horseshoe vortex on the 1/4 chord element line of each panel.

3. Place the control point on the 3/4 chord point of each panel at the midpoint in the spanwise direction (sometimes the lateral panel centroid location is used) .

4. Assume a flat wake in the usual classical method.

5. Determine the strengths of each Gn required to satisfy the boundary conditions by solving a system of linear equations. The implementation is shown schematically in Fig.3.20.

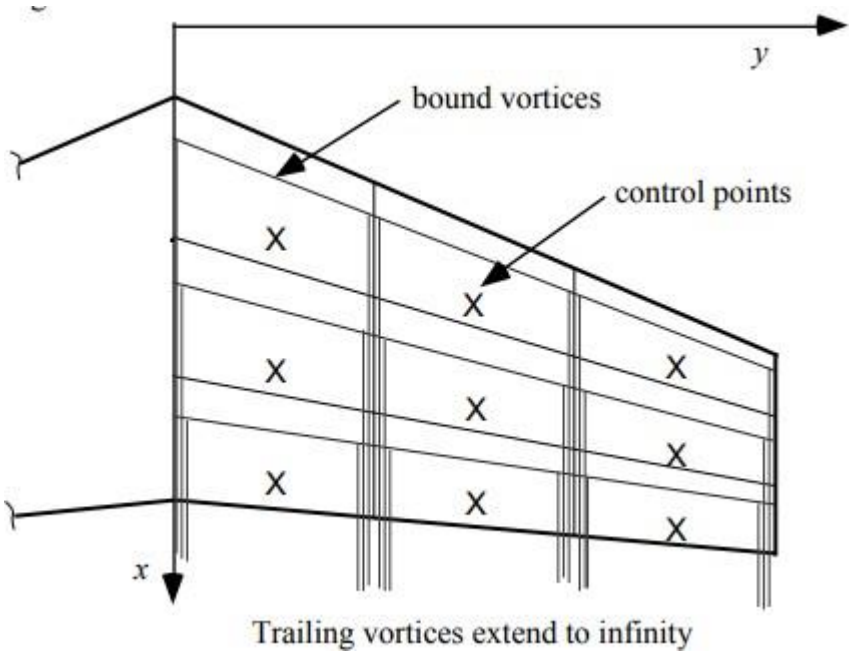

Figure 3.20: Horseshoe vortex layout for the Classical Vortex Lattice Method

Note that the lift is on the bound vortices. To understand why, consider the vector statement of the Kutta-Joukowski Theorem, F = rV ´G . Assuming the freestream velocity is the primary contributor to the velocity, the trailing vortices are parallel to the velocity vector and hence the force on the trailing vortices are zero. More accurate methods find the wake deformation required to eliminate the force in the presence of the complete induced flowfield.

Next, we derive the mathematical statement of the classical vortex lattice method described above. First, recall that the velocity induced by a single horseshoe vortex is

$Vm = C_{m,n}G_n$.

This is the velocity induced at the point m due to the nth horseshoe vortex, where $C_{m,n}$ is a vector.

Delta wings, primary and secondary vortex

Swept wings that have platforms such as shown in Fig are called delta wings. dominant aspect of this flow is the two vortices that are formed along the highly swept leading edges, and that trail downstream over the top of the wing. This vortex pattern is created by the following mechanism. The pressure on the bottom surface of the wing is higher than the pressure on the top surface.

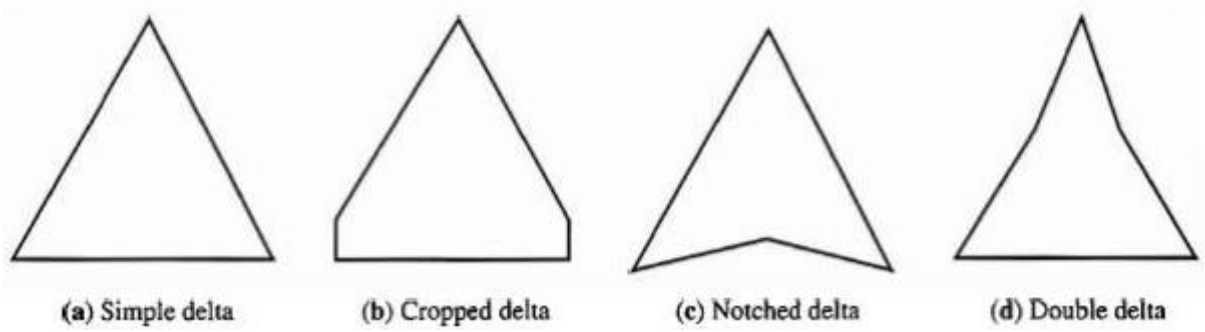

Figure 3.21: Delta wing planforms

Thus, the flow on the bottom surface in the vicinity of the leading edge tries to curl around the leading edge from the bottom to the top. If the leading edge is relatively sharp, the flow will separate along its entire length. This separated flow curls into a

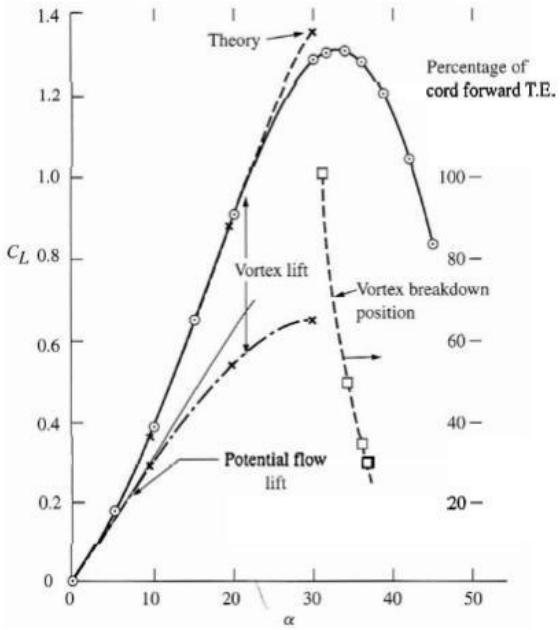

primary vortex above the wing just inboard of each leading edge. The stream surface which has separated at the leading edge loops above the wing and then reattaches along the primary attachment line. The primary vortex is contained within this loop. A secondary vortex is formed underneath the primary vortex, with its own separation line, and its own reattachment line. Unlike many separated flows in aerodynamics, the vortex pattern over a delta wing is a friendly flow in regard to the production of lift. The vortices are strong and generally stable. They are a source of high energy, relatively high vorticity flow, and the local static pressure in the vicinity of the vortices is small. Hence, the vortices create a lower pressure on the top surface than would exist if the vortices were not there. This increases the lift compared to what it would be without the vortices.

The difference between the experimental data and the potential flow lift is the vortex lift. The vortex lift is a major contributor to the overall lift; The lift slope is small, on the order of 0.05 per degree. The lift, however, continues to increase over a large range of angle of attack (the stalling angle of attack is about 35°).

The net result is a reasonable value of C_{Lmax}=1.35. The lift curve is nonlinear, in contrast to the linear variation exhibited by conventional wings for subsonic aircraft. The vortex lift is mainly responsible for this nonlinearity. The next time you have an opportunity to watch a delta-wing aircraft take off or land, for example, the televised landing of the space shuttle, note the large angle of attack of the vehicle. Also, this is why the Concorde supersonic transport, with its low-aspect-ratio deltalike wing, lands at a high angle of attack. In fact, the angle of attack is so high that the front part of the fuselage must be mechanically drooped upon landing in order for the pilots to see the runway.

Elements of lifting surface theory.

Numerical approach for three dimensional wings have extensively been developed over the last several years, especially because of the improvement of the computer processing speed which allow us to solve complex type of flow even on a personal computer.

The aerodynamic characteristics of wings are defined by their profiles and plan fonlls. The profile is a section in a plane perpendicular to the spanwise axis and the plan form is the shape of a wing in plan view. In the present thesis, only straight wings (with the sweepback angle equal to zero) are discussed The wing is placed in a uniform stream ofve1ocity Uat an angle ofincidence g.

Source Panel Method

Steps to determine the solution:

1. Write down the velocities, ui , vi , in terms of contributions from all the singularities. This includes qi g from each panel and the influence coefficients which are a function of the geometry only.
2. Find the algebraic equations defining the ‒influence‖ coefficients. To generate the system of algebraic equations:
3. Write down flow tangency conditions in terms of the velocities (N eqn‘s., N+1 unknowns).
4. Write down the Kutta condition equation to get the N+1 equation.
5. Solve the resulting linear algebraic system of equations for the qi , g .
6. Given qi , g , write down the equations for uti, the tangential velocity at each panel control point.
7. Determine the pressure distribution from Bernoulli‘s equation using the tangential velocity on each panel. We now carry out each step in detail. The algebra gets tedious, but there‘s no problem in carrying it out. As we carry out the analysis for two dimensions, consider the additional algebra required for the general three dimensional case.

Vortex panel Method

Program PANEL is an exact implementation of the analysis given in Section 4.4, and is essentially the program given by Moran.6 Other panel method programs are available in

the textbooks by Houghton and Carpenter and Kuethe and Chow.Moran‘s program includes a subroutine to generate the ordinates for the NACA 4-digit and 5-digit airfoils (see Appendix A for a description of these airfoil sections). The main drawback is the requirement for a trailing edge thickness that‘s exactly zero. To accommodate this restriction, the ordinates generated internally have been altered slightly from the official ordinates. The extension of the program to handle arbitrary airfoils is an exercise. The freestream velocity in PANEL is assumed to be unity, since the inviscid solution in coefficient form is independent of scale. PANEL‘s node points are distributed employing the widely used cosine spacing function. The equation for this spacing is given by defining the points on the thickness distribution to be placed at:

$$\frac{x_i}{c} = \frac{1}{2}\left[1 - \cos\left\{\frac{(i-1)\pi}{(N-1)}\right\}\right] \qquad i = 1, \ldots, N.$$

These locations are then altered when camber is added (see Eqns. (A-1) and (A-2) in App. A). This approach is used to provide a smoothly varying distribution of panel node points which concentrate points around the leading and trailing edges.

Vortex lattice methods

A solution for three-dimensional wings of any general form can be obtained by using a vortex lattice model. For incompressible, inviscid flow, the wing is modelled as a set of lifting panels. Each panel will contain a single horse-shoe vortex. A bound vortex is located at the panel ¼

chord position with two trailing vortex lines shed from each end.

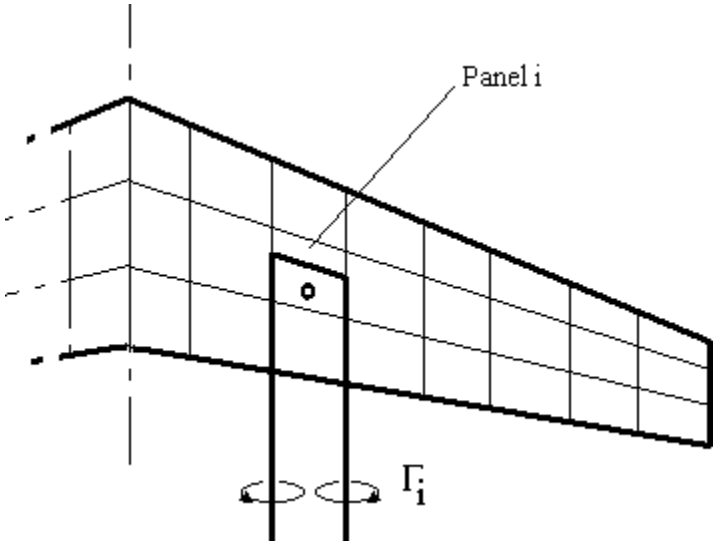

Figure 3.23: Vortex lattice structure

Both span-wise and chord-wise variation in lift can be modelled as a set of step changes from one panel to the next.

The required strength of the bound vortex on each panel will need to be calculated by applying a surface flow boundary condition. The equation used is the usual condition of zero flow normal to the surface. For each panel the condition is applied at the 3/4 chord position along the center line of the panel. The normal velocity is made up of a freestream component and an induced flow component. This induced component is a function of strengths of all vortex panels on the wing. Thus for each panel an equation can be set up which is a linear combination of the effects of the strengths of all panels. A matrix of influence coefficients is created which is multiplied by the vortex strengths and equal to a right hand side vector of freestream effects.

$$V_n = 0 = V_\infty sin(\theta) + w_i$$

$$w_i = \Sigma_{j=1}^{N} A_{ij} \Gamma_j$$

$$\Sigma_{j=1}^{N} A_{ij} \Gamma_j = -V_\infty sin(\theta)$$

The influence coefficient A_{ij} will represent the induced flow on panel i due to the vortex on panel j. If all panels are assumed to be approximately planar then this influence coefficient can be calculated as a relatively simple application of the Biot-Savart law along the three component vortex lines.

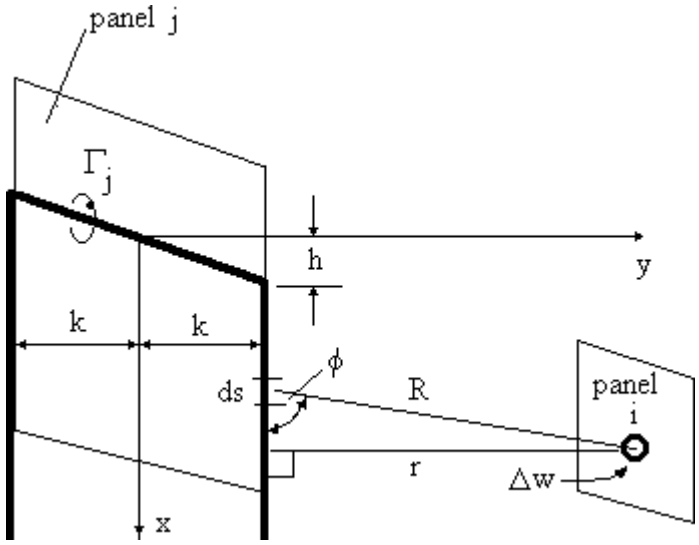

Figure 3.24: Induced velocity due to vortex lattice panel

The result of this integration leads to the following formulae for influence coefficients in general.

$$\Delta w = \frac{1}{4\pi}\frac{sin(\phi)}{r^2}\Gamma_j.ds$$

$$w_{ij} = \int \frac{1}{4\pi}\frac{sin(\phi)}{r^2}.ds.\Gamma_j = A_{ij}\Gamma_j$$

where the integer is done in three parts, the two trailing lines and the bound vortex, giving

$$A_ij = \frac{1}{4\pi}(A_{bound} + A_{left} + A_{right})$$

where

$$A_{bound} = \frac{1}{(x+h)(y-k)-(x-h)(y+k)} \cdot \left(\frac{2h(x+h)+2k(y+k)}{R_1} - \frac{2h(x-h)+2k(y-k)}{R_2} \right)$$

$$A_{left} = -\frac{1}{(y+k)} \cdot \left(1 + \frac{x+h}{R_1} \right)$$

$$A_{right} = \frac{1}{(y-k)} \cdot \left(1 + \frac{x-h}{R_2} \right)$$

$$R_1 = \sqrt{(x+h)^2 + (y+k)^2)}$$

$$R_2 = \sqrt{(x-h)^2 + (y-k)^2)}$$

The right-hand side terms for the boundary condition equations will depend upon the freestream velocity, the angle of attack for the wing and the slope of the panels due to camber effects.

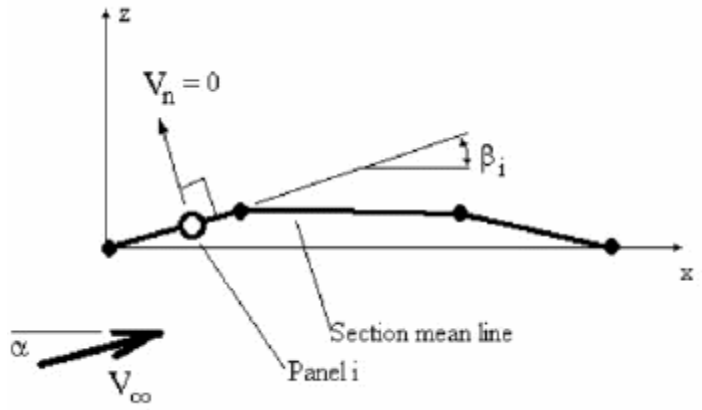

$$sin(\theta) = sin(\alpha - \beta_i) \approx \alpha - \beta_i \approx \alpha - \left(\frac{dz}{dx} \right)_i$$

Figure 3.25: Induced velocity due to vortex lattice panel

Assuming all theangles are small. a solution for the strength of the vortex lines on each panel is found by solving the matrix of equations.

The lift coefficient for the wing at a given angle of attack will be obtained by integrating the panel lift distribution. The lift on a particular panel can be found using the Kutta Law.

$$L_i = \rho V_\infty \Gamma_i 2k$$

which is the lift of panel i.

Therefore lift of wing is the sum of all panel lifts,

$$L = \Sigma_{i=1}^{N} L_i$$

The downwash velocity induced at on a panel can be calculated once the strength of the wing loading is known. The variation between local flow angles for the panel and the freestream velocity can be found. A consequence of this downwash flow is that the direction of action of each panel's lift vector is rotated relative to the freestream direction. The local lift vectors are rotated backward and hence give rise to a lift induced drag. By integrating the component of panel lift coefficient that acts parallel to the freestream across the span then the induced drag coefficient can be found.

$$D_i = \rho V_\infty \Gamma_i sin(\alpha_i)$$

which is the drag from panel *i*.

Therefore the lift induced drag of the wing is

$$D_{induced} = \Sigma_{i=1}^{N} D_i$$

The induced flow angle (α_i) represents a rotation of the lift vector backward and must be calculated from the velocities induced on the bound vortex of the panel by other panels and the freestream.

Pitching moment about the wing root leading edge can be calculated by summing the panel lift multiplied by a moment arm which extends in the x-direction from the leading edge of the wing to the centre of the bound vortex for the panel

UNIT-IV

FLOW PAST NON-LIFTING BODIES AND INTERFERENCE EFFECTS

INTRODUCTION

In the previous chapter, we studied the lifting-line theory to understand the aerodynamic lift and (induced) drag characteristics of an isolated finite wing. In this chapter, we extend our study to the flow around the fuselage. While the main function of the wing is to provide lift, the main function of the fuselage is to provide space for the payload (passengers/cargo). The fuselage is a slender body of revolution, which offers low drag. However, the lift contributed by the fuselage is small compared to that of the wings. So, the fuselage is relatively a non-lifting body.

After gaining insight into the aerodynamic characteristics of the fuselage, we shall take a look at the junction flow between the wing and the fuselage, which involves the interference effects between the two bodies. We shall also briefly note some features of the effect of the flow from propeller on the wing and tail located downstream. A few aspects of the flow over the entire airplane are also studied.

FLOW PAST NON-LIFTING BODIES

Similar to the finite wing which was modeled as a lifting line of vortices, the flow over the non-lifting fuselage can also be studied using the method of singularities. However, due to the non-lifting nature of the flow, here we use singularities which are sources or doublets. We study the aerodynamics of the flow over the fuselage by considering it as a slender body of revolution as shown in figure 4.1.

In the process of applying the method of singularities to study the aerodynamic characteristics of potential flow over the fuselage, it should be noted that the limitations

of the panel methods apply as usual, namely the flow considered is incompressible (and consequently low-subsonic), inviscid and irrotational.

Slender body theory

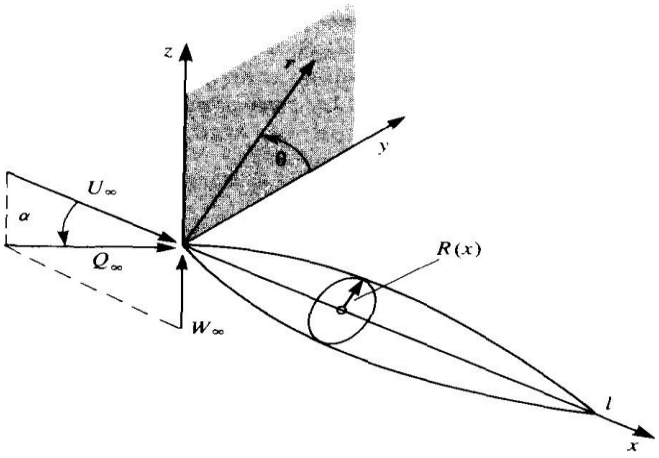

Fig 4.1: Slender body nomenclature (Ref: Low Speed Aerodynamics, Katz and Plotkin, Mc-Graw Hill, Inc., 1991)

Assumptions for formulating as a slender body are:

(a) Low slenderness ratio, $\frac{R(x)}{l}$<<1

(b) Small angle of attack, α<<1

(c) Small ratio of body radius to length, , $|\frac{dR\ x}{dx}|$<<1

Since the flow over the slender body is depicted in the cylindrical coordinate system in the above figure, we consider the Laplace equation for potential flow in cylindrical coordinates to understand the flow over the slender body (like the fuselage):

$$\nabla^2\Phi = \frac{\partial^2\Phi}{\partial x^2} + \frac{\partial^2\Phi}{\partial r^2} + \frac{1}{r}\frac{\partial\Phi}{\partial r} + \frac{1}{r^2}\frac{\partial^2\Phi}{\partial\theta^2} = 0 \qquad (4.1)$$

Note that in the above equation (4.1), $r = \overline{y^2 + z^2}$

We also note from figure 4.1 that the freestream velocity Q_∞ can be resolved into its components as:

$$\begin{aligned}\mathbf{Q}_\infty &= U_\infty \mathbf{e}_x + W_\infty \mathbf{e}_z \\ &= Q_\infty[\cos\alpha\,\mathbf{e}_x + \sin\alpha(\sin\theta\,\mathbf{e}_r + \cos\theta\,\mathbf{e}_\theta)] \\ &\approx Q_\infty[\mathbf{e}_x + \alpha(\sin\theta\,\mathbf{e}_r + \cos\theta\,\mathbf{e}_\theta)]\end{aligned} \tag{4.2}$$

While solving (4.1), the boundary condition to be satisfied, is obtained from the solid wall boundary condition at the surface of the body:

$$\mathbf{Q}.\mathbf{n} = 0 \tag{4.3}$$

Let the surface of the body in figure 4.1 be represented by

$$F \equiv r - R(x) = 0 \tag{4.4}$$

Then the direction of the normal vector at the surface, **n**, is given by the gradient of the surface, namely ∇F

So, the boundary condition (4.3) can be $\nabla\Phi^* \cdot \nabla F = 0$, rewritten as:

(4.5)

Expanding (4.5) in cylindrical coordinates gives:

$$\frac{\partial\Phi}{\partial r} + Q_\infty\alpha\sin\theta - \left[\frac{\partial\Phi}{\partial x} + Q_\infty\right]\frac{dR(x)}{dx} = 0 \qquad \text{for } r = R(x)$$

(4.6)

In (4.6), neglecting products of derivatives (which are small), we get

$$\frac{\partial \Phi}{\partial r}(x, R, \theta) = Q_\infty R'(x) - Q_\infty \alpha \sin\theta \tag{4.7}$$

$$= \frac{\partial \emptyset_a (x,R,\theta)}{\partial r} + \frac{\partial \emptyset_t (x,R,\theta)}{\partial r} \tag{4.8}$$

In (4.8), we have used the superposition principle to split the linear potential function $\emptyset$ into two functions $\emptyset_a$ and $\emptyset_t$, which denote the potential functions for the axisymmetric longitudinal flow and transverse flow components over the slender body. Equation (4.8) represents the overall boundary condition, which in turn can be viewed as the superposition of the boundary conditions for the individual axisymmetric longitudinal and transverse flows.

This shows that the potential flow over a slender body can be studies separately as the axisymmetric longitudinal flow and transverse flow, and then the overall solution can be obtained simply by adding up the two potential flow solutions. We now undertake the study of the two potential flows

Axisymmetric longitudinal flow past the slender body (for evaluation of $\emptyset_a$):

Since the axisymmetric longitudinal flow is symmetric w.r.t. θ, the Laplace equation (4.1) for this case becomes:

$$\frac{\partial^2 \Phi}{\partial x^2} + \frac{\partial^2 \Phi}{\partial r^2} + \frac{1}{r}\frac{\partial \Phi}{\partial r} = 0 \tag{4.9}$$

This has the corresponding component of the boundary condition from (4.7) as

$$\frac{\partial \Phi}{\partial r}(x, R, \theta) = Q_\infty R'(x) \tag{4.10}$$

As we discussed earlier, this symmetric flow over the slender body can be considered as non-lifting. So, we obtain solutions for the flow by modeling a distribution of sources of strength $\sigma(x)$ along the body axis. This distribution is shown in figures 4.2 and 4.3.

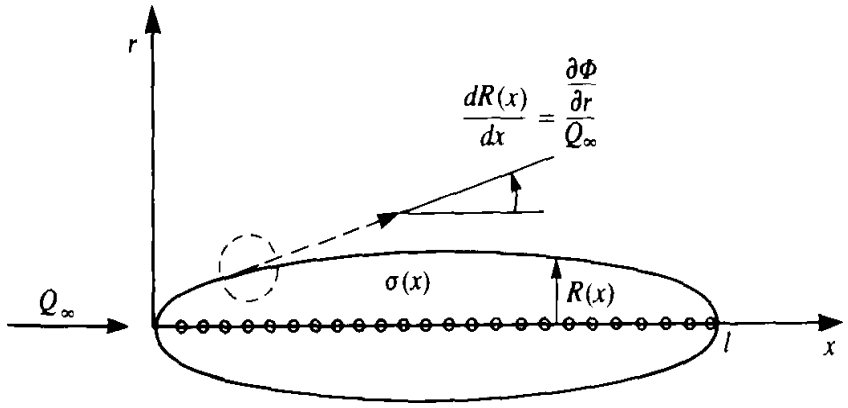

Fig 4.2: Source distribution along *x*-axis (Ref: Low Speed Aerodynamics, Katz and Plotkin,
Mc-Graw Hill, Inc., 1991)

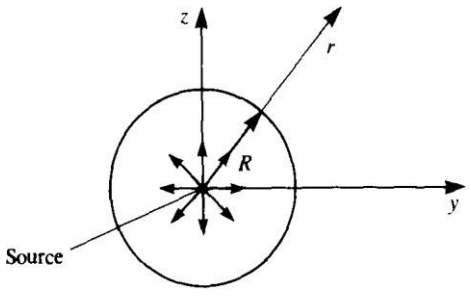

Fig 4.3: Cross-sectional view of the source distribution (Ref: Low Speed Aerodynamics, Katz and Plotkin, Mc-Graw Hill, Inc., 1991)

Using the potential flow theory learnt in Chapter 1, we obtain the solution for the Laplace equation (4.9) that also satisfies the boundary condition (4.10), as follows:

$$\Phi(r, x) = \frac{-Q_\infty}{4\pi} \int_0^l \frac{S'(x_0)\, dx_0}{\sqrt{(x - x_0)^2 + r^2}}$$

$$q_r(r, x) = \frac{\partial \Phi}{\partial r} = \frac{Q_\infty}{4\pi} \int_0^l \frac{S'(x_0) r\, dx_0}{[(x - x_0)^2 + r^2]^{3/2}}$$

$$q_x(r, x) = \frac{\partial \Phi}{\partial x} = \frac{Q_\infty}{4\pi} \int_0^l \frac{S'(x_0)(x - x_0)\, dx_0}{[(x - x_0)^2 + r^2]^{3/2}} \tag{4.11}$$

In the above expressions, $\boldsymbol{S(x)}$ is the body cross-sectional area, i.e., $\boldsymbol{S(x) = \pi R^2(x)}$

Next, we solve for the transverse flow past the slender body.

Transverse flow past the slender body (for evaluation of $\emptyset_t$):

We note that the transverse flow passes over the cylindrical cross-section (namely *y*-*z* plane in fig. 4.1) of the slender body. So, we use the distribution of doublets (which is suitable for the flow over a cylinder, as studied in chapter 1.). We again consider the Laplace equation (4.1):

$$\nabla^2 \Phi = \frac{\partial^2 \Phi}{\partial x^2} + \frac{\partial^2 \Phi}{\partial r^2} + \frac{1}{r}\frac{\partial \Phi}{\partial r} + \frac{1}{r^2}\frac{\partial^2 \Phi}{\partial \theta^2} = 0 \tag{4.12}$$

This has the corresponding component of the boundary condition from (4.7) as

$$\frac{\partial \Phi}{\partial r}(x, R, \theta) = -Q_\infty \alpha \sin\theta \tag{4.13}$$

As discussed above, this flow over the slender body is modeled by a distribution of doublets of strength $\mu(x)$ along the body axis. This distribution is shown in figure 4.4

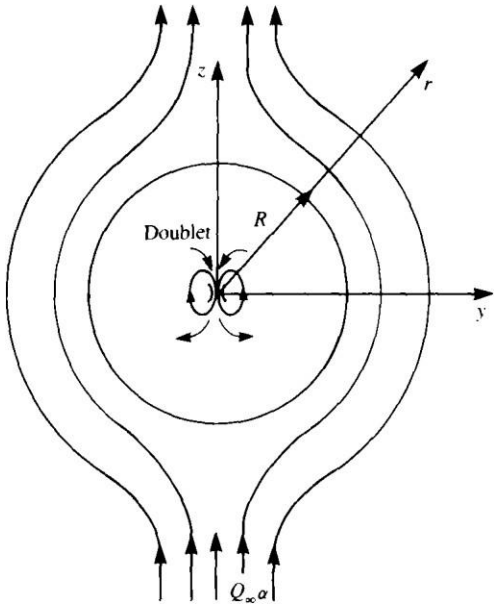

Fig 4.3: Crossflow model using doublet distribution along the *x*-axis and pointing in the z-direction (Ref: Low Speed Aerodynamics, Katz and Plotkin, Mc-Graw Hill, Inc., 1991)

Again, using the potential flow theory learnt in Chapter 1, we obtain the solution for the Laplace equation (4.12) that also satisfies the boundary condition (4.13), as follows:

$$\Phi(r,\ \theta,\ x) = Q_\infty \alpha R^2 \frac{\sin\theta}{r}$$

$$q_r(r,\ \theta,\ x) = -Q_\infty \alpha R^2 \frac{\sin\theta}{r^2}$$

$$q_\theta(r,\ \theta,\ x) = Q_\infty \alpha R^2 \frac{\cos\theta}{r^2}$$

$$q_x(r,\ \theta,\ x) = \frac{\partial \Phi}{\partial x} = 2Q_\infty \alpha R R' \frac{\sin\theta}{r} \qquad (4.14)$$

Complete solution for flow past the slender body:

We obtain the complete solution for the flow past the slender body by summing up the expressions for the velocity potential and the respective perturbation velocities in equations (4.11) and (4.14).

The pressure coefficient C_p can then be obtained as:

$$C_p = 1 - \frac{q^2}{Q_\infty^2} = -\frac{2q_x}{Q_\infty} - \frac{2\alpha}{Q_\infty}(q_r \sin\theta + q_\theta \cos\theta) - \frac{q_r^2 + q_\theta^2 + q_x^2}{Q_\infty^2} \tag{4.15}$$

Substituting the expressions from (4.11) and (4.14) in (4.15) and performing the required algebra, we obtain

$$C_p = -\frac{2q_{xA}}{Q_\infty} - (R')^2 - 4\alpha R' \sin\theta + \alpha^2(1 - 4\cos^2\theta)$$

where, as obtained by Karamcheti (*Principles of Aerodynamics*, 1980)

$$q_{xA} = \frac{Q_\infty}{2\pi} S''(x) \ln\frac{r}{2} + \frac{Q_\infty}{4\pi}\int_0^l S'''(x_0) \ln|x - x_0|\, dx_0 \tag{4.16}$$

Using the above coefficient of pressure, the distribution of pressure and the resultant component forces can be obtained. The resulting expressions for the distribution of the component forces are given below:

$$\frac{dF_x}{dx} = \left\{ p_\infty - \tfrac{1}{2}\rho Q_\infty^2 \left[\alpha^2 + \frac{q_{xA}}{Q_\infty} + (R')^2 \right] \right\} S'$$

$$\frac{dF_y}{dx} = 0$$

$$\frac{dF_z}{dx} = \rho Q_\infty^2 \alpha S' \qquad (4.17)$$

Based on the above results, following conclusions can be drawn:

(i) The side force distribution is zero and therefore the side force is also zero.

(ii) The normal force distribution is proportional to the angle of attack and the rate of change of cross-sectional area. In fact, this can also become zero if the body‘s ends are pointed.

(iii) The axial force can also become zero if the body‘s ends are pointed (Ref: Ward G.N., *Linearized theory of steady high-speed flow*, Cambridge University Press, 1955)

(iv) For pointed slender bodies, there is no lift and pressure drag, but there is an aerodynamic pitching moment.

WING-BODY INTERACTION

The aerodynamic coefficients of the major components of the airplane - wing, fuselage, empennage - are quite well established through theory and systematic measurements. The inviscid flow aerodynamics of the wing was treated thoroughly in earlier chapters. The findings established there apply accordingly to the empennage (vertical stabilizer and rudder, and horizontal stabilizer and elevator). The aerodynamics of the fuselage was the subject of the previous section. When these individual parts are assembled into a complete airplane, however, their interaction (interference) plays a very important role in the formation of aerodynamic forces. In many cases these interference effects are of the same order of magnitude as the contributions of the individual parts to the aerodynamic

forces of the airplane as a whole. For this reason, consideration of these interactions is indispensable to the study of the aerodynamics of the airplane. The physical processes behind the aerodynamics of the interactions are, of course, much harder to conceive than those of the aerodynamics of the individual parts. Consequently, the theoretical study of the interference problem has been attacked much later and is, even today, not yet established to the extent of that of the individual parts. The theory of interference aerodynamics is available to a large extent for inviscid flow only.

Most important of the numerous interference effects among the various airplane components are the interactions between the wing and the fuselage and between the wing and the empennage. The interference between the wing and the fuselage is felt mainly in a changed lift distribution over these parts. The effect of the wing on the empennage, on the other hand, lies mainly in a changed incident flow direction of the empennage caused by the induced velocity field of the wing.

Here, we mainly study the interaction between the flow over the junction between the wing and fuselage.

Wing-fuselage interference effects

When putting together a wing and a fuselage, a flow about the wing-fuselage system results, with the fuselage lying in the flow field of the wing and the wing in the flow field of the fuselage. Thus, an aerodynamic interference exists between the fuselage and the wing, in that the presence of the fuselage changes the flow about the wing and the presence of the wing changes the flow about the fuselage.

Consider the flow field of a wing-fuselage system at subsonic velocity in symmetric, incident flow (angle of sideslip = 0). Figure 4.4a shows the flow about the fuselage as affected by the wing. Along the fuselage axis, additive velocities normal to the fuselage

axis are induced by the wing, which are directed upward before the wing and downward behind it. In the range of the wing-fuselage penetration, the flow is parallel to the wing chord, corresponding to a constant downwash velocity along the wing chord. The fuselage is therefore in a curved flow with an angle-of-attack distribution $\alpha(x)$ varying along the fuselage axis as shown in Fig. 4.4a. This angle-of-attack distribution, induced by the wing, shows that the fuselage is subjected to an additive nose-up pitching moment.

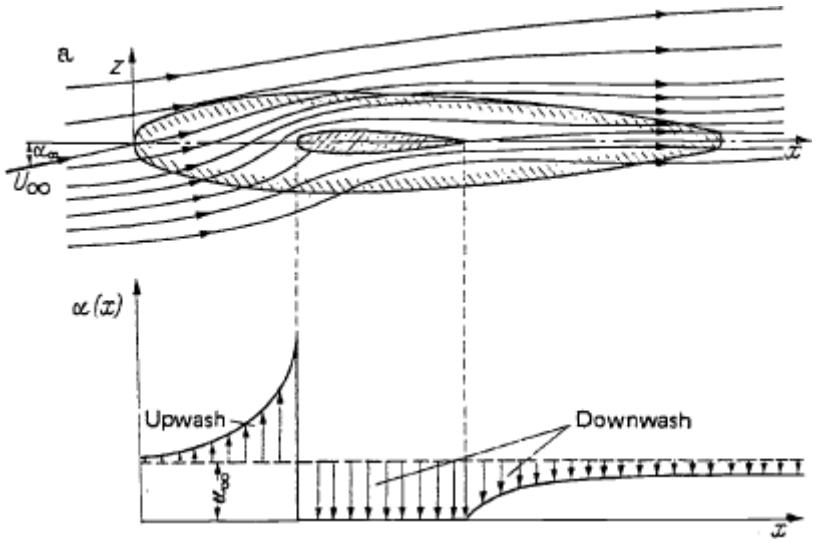

Fig 4.4: Symmetric flow about a wing-fuselage system (schematic) (a) Flow in the airplane plane of symmetry and AOA distribution $\alpha(x)$ on the fuselage axis

The effect of the fuselage on the flow about the wing is sketched in Fig. 4.4b. The component of the incident flow velocity normal to the fuselage axis $U_\infty \sin\alpha_\infty \approx U_\infty \alpha_\infty$, generates additive upwash velocities in the vicinity of the fuselage. The effect on the wing of these induced velocities normal to the plane of the wing is equivalent to an additive symmetric angle-of-attack distribution over the wing span (twist angle).

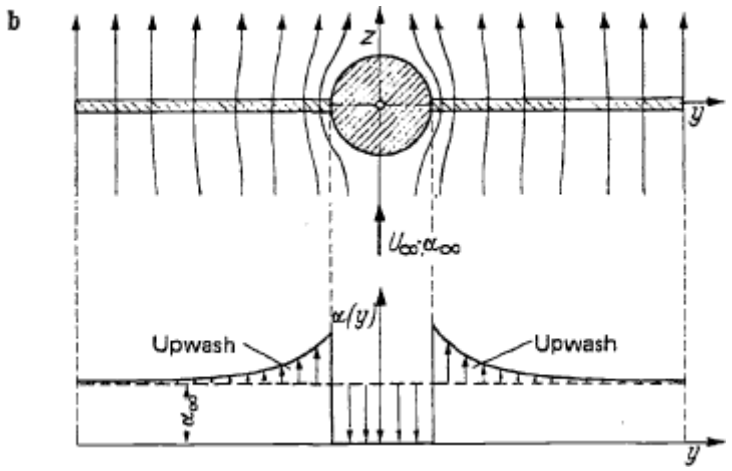

Fig 4.4: Symmetric flow about a wing-fuselage system (schematic) (b) Flow in a plane normal to the fuselage axis and angle-of-attack distribution $\alpha(y)$ over the wing span. (Ref: Aerodynamics of the airplane, Schlichting and Truckenbrodt, Mc-Graw Hill, Inc., 1979)

Next, consider the flow field of a wing-fuselage system at subsonic velocity in asymmetric, incident flow (angle of sideslip $\neq 0$), as shown in figure 4.5a.The flow about the wing-fuselage system with the angle of sideslip can be thought to be divided into an incident flow parallel to the plane of symmetry, of velocity $U_\infty \cos\beta \approx U_\infty$and an incident flow normal to the plane of symmetry, of velocity $U_\infty \sin\beta \approx U_\infty \beta$.

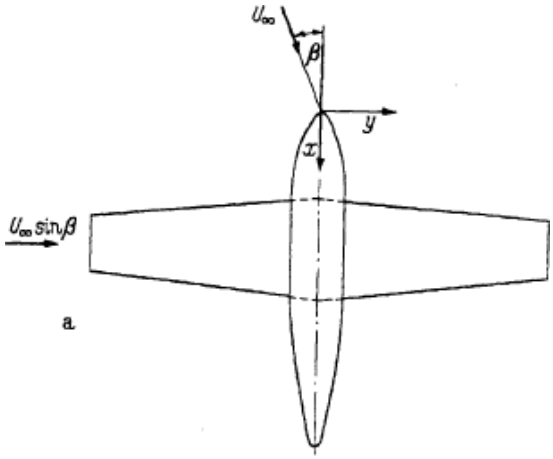

Fig 4.5: Asymmetric flow about a wing-fuselage system (schematic) (a) Wing planform (Ref: Aerodynamics of the airplane, Schlichting and Truckenbrodt, Mc-Graw Hill, Inc., 1979)

The latter component of the incident flow generates a cross flow over the fuselage as illustrated in Fig. 4.5b, c, and d for a high-wing, a mid-wing, and a low-wing system, respectively. This cross flow over the fuselage results in an additive antimetric distribution of the normal velocities along the span that is equivalent to an antimetric angle-of-attack distribution α(y). The lift distributions over the wing span generated by this angle-of-attack distribution have reversed signs for high-wing and low-wing airplanes. The rolling moment (rolling moment due to sideslip), as affected by this antimetric lift distribution, is zero for the mid-wing airplane, positive for the high-wing airplane, and negative for the low-wing airplane.

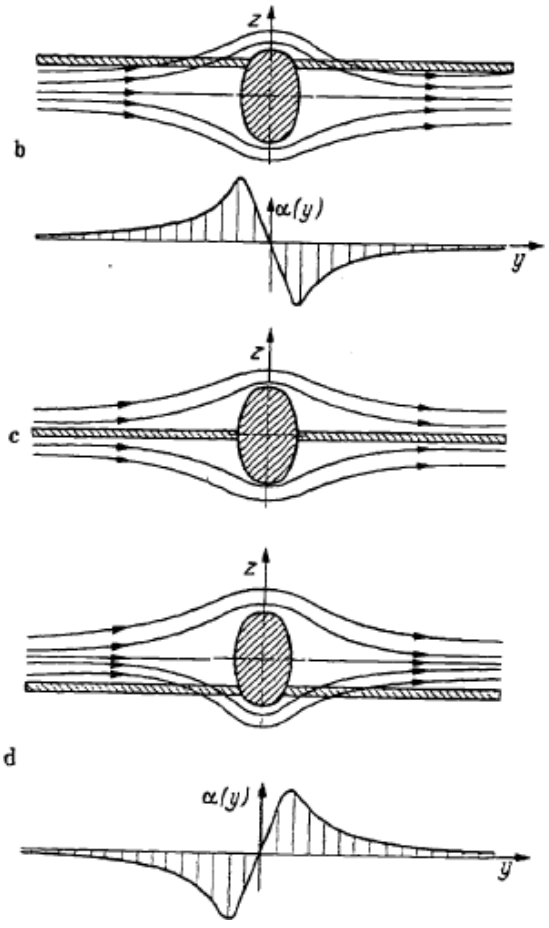

Fig 4.5: Asymmetric flow about a wing-fuselage system (schematic) (b) High-wing airplane with AOA distribution α(*y*) (c) Mid-wing airplane (d) Low-wing airplane with

AOA distribution $\alpha(y)$ (Ref: Aerodynamics of the airplane, Schlichting and Truckenbrodt, Mc-Graw Hill, Inc., 1979)

Effects of propeller stream on the wing/tail downstream

Experimental studies showed that when the wing/tail was under the effect of the slipstream (jet) from a propeller whose axis was fixed in the direction of the undisturbed wind, the rotation and the dynamic pressure changes in the jet resulted in a nonsymmetrical variation in the lift. Study of the downwash relations led to the result that the two portions into which the jet is divided by the wing/tail did not again reunite behind the wing/tail but that each portion experienced a lateral deviation in the direction of the jet rotation.

FLOW OVER WHOLE AIRPLANE

Aircraft lift coefficient

A complete aircraft will frequently generate significantly more lift than its wing alone. An estimate of a whole aircraft‘s lift can be made by summing the lift contributions of its various lifting surfaces. This method is suitable for use in the early conceptual phase of design.

$$C_{L\alpha\ (whole\ aircraft)} = C_{L\alpha\ (wing)} + C_{L\alpha\ (horizontal\ tail)}$$

Aircraft drag coefficient

A single representative coefficient of drag expression for the complete aircraft may be given by:

$$C_D = C_{D_{0L}} + \frac{C_L^2}{\pi AR\, e}$$

where: C_{DOL} = zero-lift drag coefficient, parasite drag coefficient

e = Oswald (aircraft) efficiency factor

AR = Aspect ratio of the wing

UNIT-V
BOUNDARY LAYER THEORY

Introduction to boundary layer

Displacement Thickness is an alternative definition stating that the boundary layer represents a deficit in mass flow compared to inviscid flow with slip at the wall. The flow velocity will then increase rapidly within the boundary layer, governed by the boundary layer equations. Laminar boundary layers can be loosely classified according to their structure and the circumstances under which they are created. The thin shear layer which develops on an oscillating body is an example of a Stokes boundary layer, while the Blasius boundary layer refers to the well-known similarity solution near an attached flat plate held in an oncoming unidirectional flow and Falkner–Skan boundary layer, a generalization of Blasius profile. When a fluid rotates and viscous forces are balanced by the Coriolis effect (rather than convective inertia), an Ekman layer forms. In the theory of heat transfer, a thermal boundary layer occurs. A surface can have multiple types of boundary layer simultaneously. The viscous nature of airflow reduces the local velocities on a surface and is responsible for skin friction. The layer of air over the wing's surface that is slowed down or stopped by viscosity is the boundary layer. There are two different types of boundary layer flow: laminar and turbulent.

Laminar boundary layer

The laminar boundary is a very smooth flow, while the turbulent boundary layer contains swirls or "eddies." The laminar flow creates less skin friction drag than the turbulent flow, but is less stable. Boundary layer flow over a wing surface begins as a smooth laminar flow.

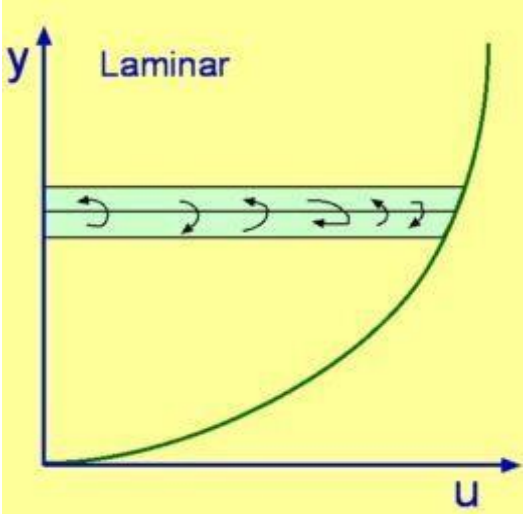

Figure 5.1: Illustration of the laminar boundary layer

Turbulent boundary layer

A turbulent boundary layer on the other hand is marked by mixing across several layers of it. The mixing is now on a macroscopic scale. Packets of fluid may be seen moving across. Thus there is an exchange of mass, momentum and energy on a much bigger scale compared to a laminar boundary layer. A turbulent boundary layer forms only at larger Reynolds numbers. The scale of mixing cannot be handled by molecular viscosity alone. Those calculating turbulent flow rely on what is called Turbulence Viscosity or Eddy Viscosity, which has no exact expression. It has to be modeled. Several models have been developed for the purpose.

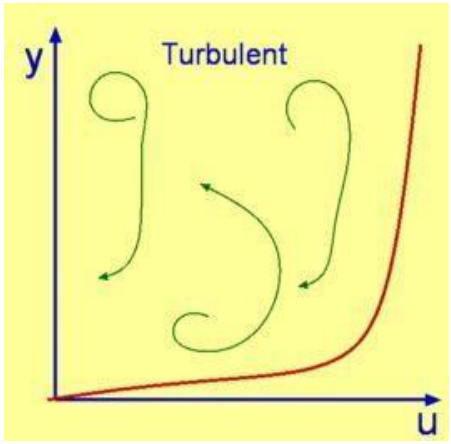

;

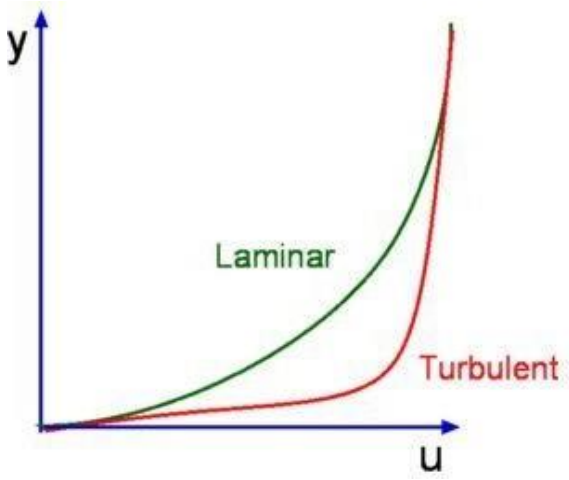

Figure 5.2: Illustration of the turbulent boundary layer and conceptual difference in velocity profiles in the two layers

Transition

The process of a laminar flow becoming turbulent is known as laminar-turbulent transition. This is an extraordinarily complicated process which at present is not fully understood. However, as the result of many decades of intensive research, certain features have become gradually clear, and it is known that the process proceeds through a series of stages. "Transitional flow" can refer to transition in either direction that is laminar-turbulent transitional or turbulent-laminar transitional flow.

Figure 5.3: Illustration of the transition from laminar to turbulent regimes

Boundary layer on flat plate

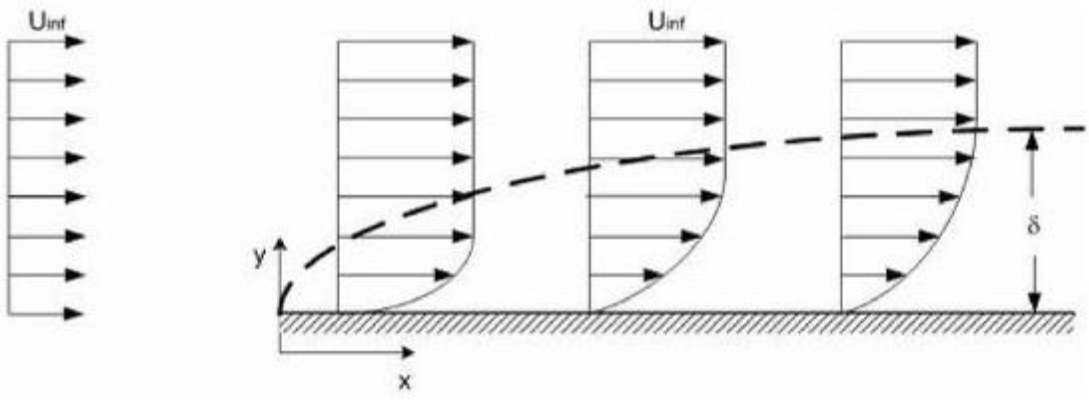

Figure 5.4: Development of boundary layer

Consider a stationary body with a fluid flowing around it, like the semi-infinite flat plate with air flowing over the top of the plate (assume the flow and the plate extends to infinity in the positive/negative direction perpendicular to the (x-y plane). At the solid walls of the body the fluid satisfies a no-slip boundary condition and has zero velocity, but as you move away from the wall, the velocity of the flow asymptotically approaches the free stream mean velocity. Therefore, it is impossible to define a sharp point at which the boundary layer becomes the free stream, yet this layer has a well-defined characteristic thickness. The parameters below provide a useful definition of this characteristic, measurable thickness. Also included in this boundary layer description are some parameters useful in describing the shape of the boundary layer. The boundary layer thickness, δ, is the distance across a boundary layer from the wall to a point where the flow velocity has essentially reached the 'free stream' velocity, uo. This distance is defined normal to the wall. It is customarily defined as the point y where:

$$u(y)=0.99u_o$$

at a point on the wall x. For laminar boundary layers over a flat plate, the Blasius solution to the flow governing equation.

Displacement thickness

The displacement thickness, δ* or δ1 is the distance by which a surface would have to be moved in the direction perpendicular to its normal vector away from the reference plane in an inviscid fluid stream of velocity uo to give the same flow rate as occurs between the surface and the reference plane in a real fluid. In practical aerodynamics, the displacement thickness essentially modifies the shape of a body immersed in a fluid to allow an inviscid solution. It is commonly used in aerodynamics to overcome the difficulty inherent in the fact that the fluid velocity in the boundary layer approaches asymptotically to the free stream value as distance from the wall increases at any given location.

The definition of the displacement thickness for compressible flow is based on mass flow rate:

- Since $u/U_\infty \to 0.99, as \quad y \to \infty$, it is customary to select the boundary layer thickness δ as that point where u/U_∞ **approaches 0.99.**
- u/U_∞ **reaches 0.99 at η= 5.0** and we can write $\delta \Big/ \sqrt{\left(\frac{\nu x}{U_\infty}\right)} \approx 5.0$

$$or \quad \delta \approx 5.0\sqrt{\left(\frac{\nu x}{U_\infty}\right)} = \frac{5.0x}{\sqrt{\mathrm{Re}_x}}$$

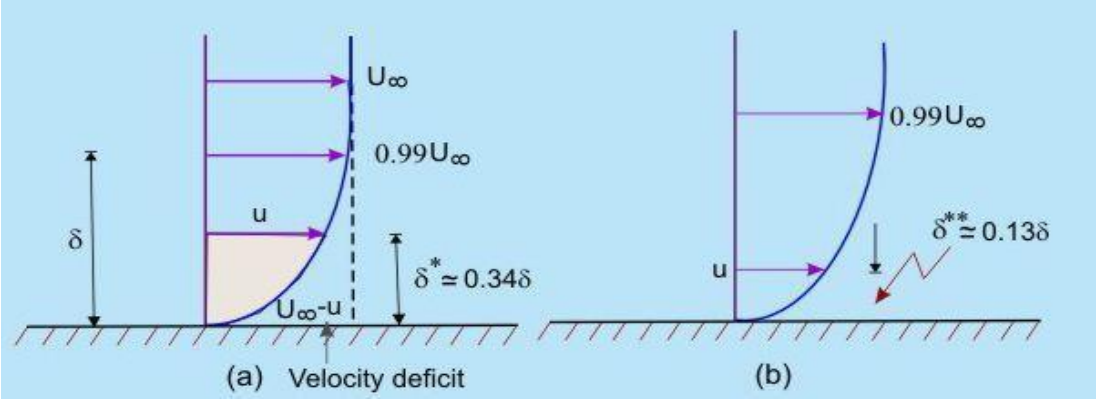

Figure 5.5: Velocity profile in boundary layer over a flat plate

- **Displacement thickness** (δ^*) **:** It is defined as the distance by which the external potential flow is displaced outwards due to the decrease in velocity in the boundary layer.

$$U_\infty \delta^* = \int_0^\infty (U_\infty - u)dy$$

$$\delta^* = \int_0^\infty \left(1 - \frac{u}{U_\infty}\right)dy$$

$$dy = \delta d\eta = \sqrt{\frac{\nu x}{U_\infty}}d\eta$$

$$\delta^* = \sqrt{\frac{\nu x}{U_\infty}}\int_0^\infty (1 - f')d\eta = \sqrt{\frac{\nu x}{U_\infty}}\lim_{\eta\to\infty}[\eta - f(\eta)]$$

$$\delta^* = 1.7208\sqrt{\frac{\nu x}{U_\infty}} = \frac{1.7208x}{\sqrt{\mathrm{Re}_x}}$$

Following the analogy of the displacement thickness, a momentum thickness may be defined.

Momentum thickness (δ^{**}): It is defined as the loss of momentum in the boundary layer as compared with that of potential flow. Thus

$$\rho U_\infty^2 \delta^{**} = \int_0^\infty \rho u(U_\infty - u)dy$$

$$\delta^{**} = \int_0^\infty \frac{u}{U_\infty}\left(1 - \frac{u}{U_\infty}\right)dy$$

With the substitution of (u/U_∞) and η from Eg. (28.21a) and (28.19), we can evaluate numerically the value of δ^{**} for a flat plate as

$$\delta^{**} = \sqrt{\frac{\nu x}{U_\infty}}\int_0^\infty f'(1 - f')d\eta$$

$$or \quad \delta^{**} = 0.664\sqrt{\frac{\nu x}{U_\infty}} = \frac{0.664x}{\sqrt{\mathrm{Re}_x}}$$

The relationships between $\delta, \delta^* and \delta^{**}$ have been shown

Momentum and Energy thickness

- To employ boundary layer concepts in real engineering designs, we need approximate methods that would quickly lead to an answer even if the accuracy is somewhat less.
- Karman and Pohlhausen devised a simplified method by satisfying only the boundary conditions of the boundary layer flow rather than satisfying Prandtl's differential equations for each and every particle within the boundary layer. We shall discuss this method herein.

$$\int_0^\delta \left(u\frac{\partial u}{\partial x} + v\frac{\partial u}{\partial y}\right)dy = \int_0^\delta \left(-\frac{1}{\rho}\frac{\partial p}{\partial x} + \nu\frac{\partial^2 u}{\partial y^2}\right)dy$$

$$\int_0^{\delta} u\frac{\partial u}{\partial x}dy + \int_0^{\delta} v\frac{\partial u}{\partial y}dy = \int_0^{\delta} -\frac{1}{\rho}\frac{\partial p}{\partial x}dy + \int_0^{\delta} \nu\frac{\partial^2 u}{\partial y^2}dy$$

- The second term of the left hand side can be expanded as

$$\int_0^{\delta} v\frac{\partial u}{\partial y}dy = [vu]_0^{\delta} - \int_0^{\delta} u\frac{\partial v}{\partial y}dy$$

$$\int_0^{\delta} v\frac{\partial u}{\partial y}dy = U_{\infty}v_{\delta} + \int_0^{\delta} u\frac{\partial u}{\partial x}dy \left(\sin ce\ \frac{\partial u}{\partial x} = -\frac{\partial v}{\partial y}\right)$$

Substituting the relation between $\frac{\partial p}{\partial x}$ and the free stream velocity U_{∞} for the inviscid zone in we get

$$\int_0^{\delta} 2u\frac{\partial u}{\partial x}dy - U_{\infty}\int_0^{\delta}\frac{\partial u}{\partial x}dy - \int_0^{\delta} U_{\infty}\frac{dU_{\infty}}{dx}dy = -\left(\frac{\mu\left.\frac{\partial u}{\partial y}\right|_{y=0}}{\rho}\right)$$

$$\int_0^{\delta}\left(2u\frac{\partial u}{\partial x} - U_{\infty}\frac{\partial u}{\partial x} - U_{\infty}\frac{dU_{\infty}}{dx}\right)dy = -\frac{\tau_w}{\rho}$$

$$\int_0^{\delta}\frac{\partial}{\partial x}[u(U_{\infty}-u)]dy + \frac{dU_{\infty}}{dx}\int_0^{\delta}(U_{\infty}-u)dy = \frac{\tau_w}{\rho}$$

$$\int_0^{\delta}\frac{\partial}{\partial x}[u(U_{\infty}-u)]dy + \frac{dU_{\infty}}{dx}\int_0^{\delta}(U_{\infty}-u)dy = \frac{\tau_w}{\rho}$$

$$\frac{d}{dx}\int_0^{\delta}[u(U_{\infty}-u)]dy + \frac{dU_{\infty}}{dx}\int_0^{\delta}(U_{\infty}-u)dy = \frac{\tau_w}{\rho}$$

- Since the integrals vanish outside the boundary layer, we are allowed to increase the integration limit to infinity (i.e $\delta = \infty$.)

$$\frac{d}{dx}\left[U_\infty^2 \delta^{**}\right] + \delta^* U_\infty \frac{dU_\infty}{dx} = \frac{\tau_w}{\rho}$$

$$\delta^* = \int_0^\delta \left(1 - \frac{u}{U_\infty}\right) dy$$

$$\delta^{**} = \int_0^\delta \frac{u}{U_\infty}\left(1 - \frac{u}{U_\infty}\right) dy$$

Effect of Curvature

- It has been observed that the **flow is reversed at the vicinity of the wall** under certain conditions.
- The phenomenon is termed as **separation of boundary layer**.
- Separation takes place **due to excessive momentum loss near the wall in a boundary layer trying to move downstream against increasing pressure, i.e.,** $\frac{dp}{dx} > 0$ **, which is called *adverse pressure gradient.***
- Figure 29.2 shows the flow past a circular cylinder, in an infinite medium.
    1. Up to $\theta = 90^\circ$, the flow area is like a constricted passage and the flow behaviour is like that of a nozzle.
    2. Beyond $\theta = 90^\circ$ the flow area is diverged, therefore, the flow behaviour is much similar to a diffuser

    This dictates the inviscid pressure distribution on the cylinder which is shown by a firm line in Fig. 29.2.

    Here

p_∞ **: pressure in the free stream**

U_∞ **: velocity in the free stream and**

ρ ***:*** **is the local pressure on the cylinder.**

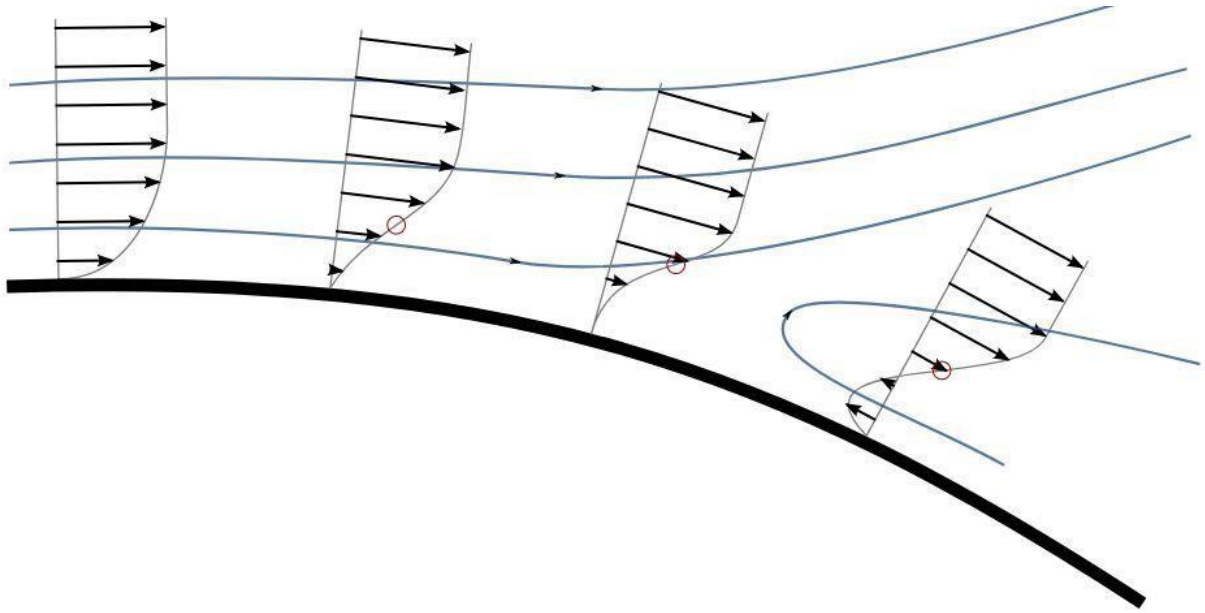

Figure 5.6: Flow reversal due to adverse pressure gradient

Temperature boundary layer.

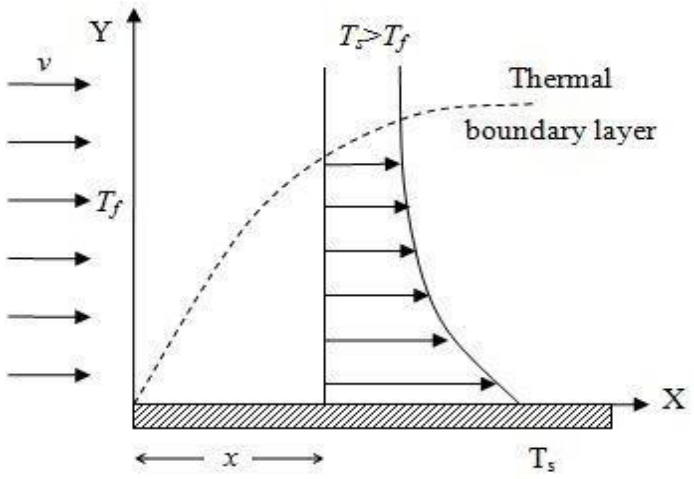

Figure 5.7: Illustration of temperature boundary layer

If $T_s > T_f$, the fluid temperature approaches asymptotically and the temperature profile at a distance x is shown in fig.4.3. However, a thermal boundary may be defined (similar to velocity boundary) as the distance from the surface to the point where the temperature is within 1% of the free stream fluid temperature (T_f). Outside the thermal boundary layer the fluid is assumed to be a heat sink at a uniform temperature of T_f. The thermal boundary layer is generally not coincident with the velocity boundary layer, although it is certainly dependant on it. That is, the velocity, boundary layer thickness, the variation of velocity, whether the flow is laminar or turbulent etc are all the factors which determine the temperature variation in the thermal boundary layer. The thermal boundary layer and velocity boundary layer are related by the Prandtl number, $Pr = \frac{\nu}{\alpha}$; where $\nu \left(= \frac{\mu}{\rho}\right)$ is called the momentum diffusivity and $\alpha\left(= \frac{\kappa}{\rho C_p}\right)$ is called the thermal diffusivity; is less than unity, the momentum boundary layer (or velocity boundary layer) remains within the thermal boundary layer. If $P_r > 1$, the boundary layers will be reversed as shown in the fig. The thermal boundary layer and velocity boundary layer coincides at $P_r = 1$.

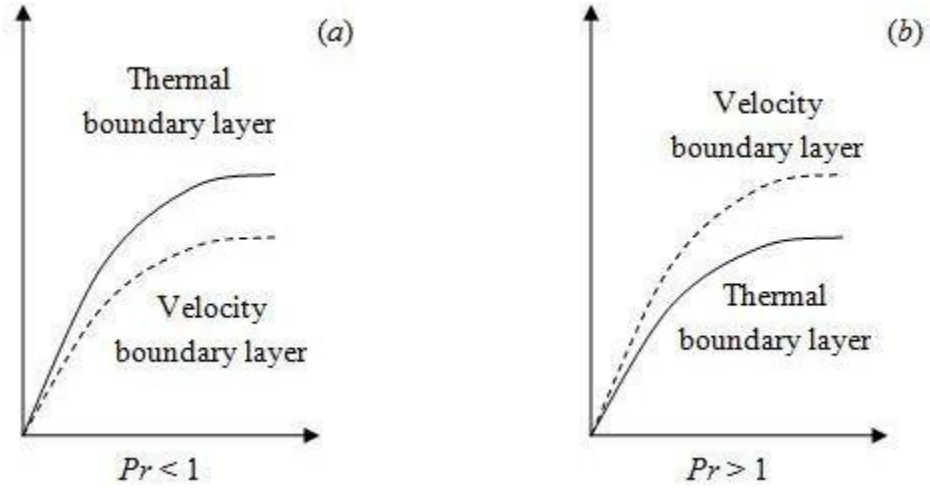

Figure 5.8: Thermal and velocity boundary layers

The above boundary layer theory will be helpful to understand the heat transfer in the process. Through the boundary layers heat transfer is covered in a separate chapter, but the detailed derivation and development of all the relationships having engineering importance for the prediction of forced convection heat transfer coefficient is beyond the scope of the course. The reader may consult any standard fluid mechanics and heat transfer books for detailed knowledge. The purpose of this chapter is to present a collection of the most useful of the existing relations for the most frequently encountered cases of forced convection.